Department of Precision and Microsystems Engineering

Microscale Hot Forming of PEEK

M. Rings

Report no : 2024.060
Coach : H. M. Bilyalova MSc
Professor : Dr. ir. Marcel Tichem
Specialisation : High-Tech Engineering
Type of report : MSc Thesis
Date : 19-08-2024

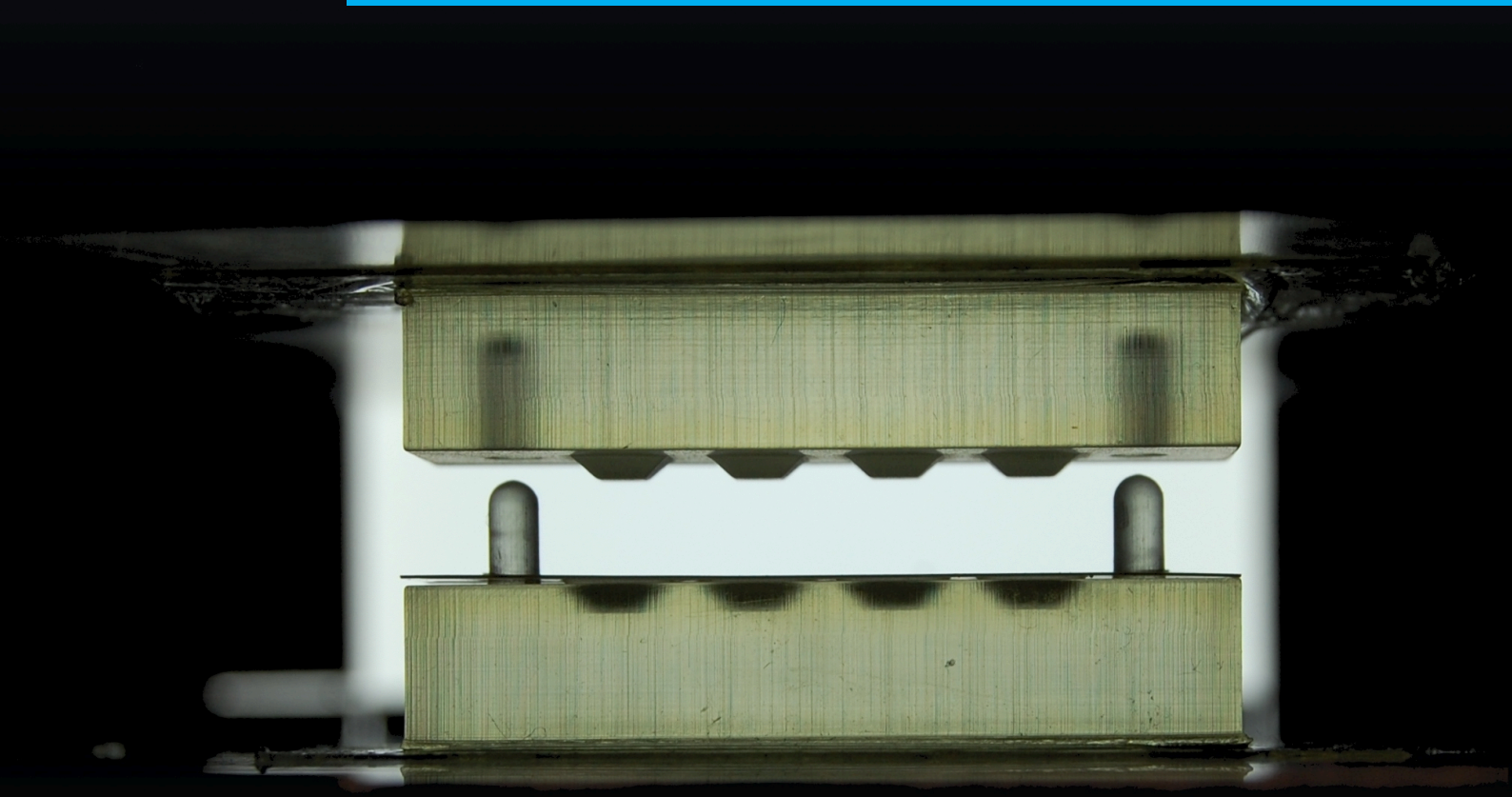

TU Delft Delft University of Technology

Challenge the future

Microscale Hot Forming of PEEK

by

M. Rings

to obtain the degree of Master of Science
at the Delft University of Technology,
to be defended publicly on Tuesday August 27th, 2024 at 14:30.

Project duration:	July, 2023 – August, 2024	
Thesis committee:	Dr. ir. M. Tichem,	TU Delft
	H. M. Bilyalova MSc,	TU Delft
	Dr. ir. J. F. L. Goosen,	TU Delft

An electronic version of this thesis is available at http://repository.tudelft.nl/.

TU Delft

Abstract

This research successfully establishes a proof of concept for the hot forming of PEEK sheets using resin-printed polymer molds.

Mechanical metamaterials, through their architected inner structures, offer unique properties that enable unparalleled functionalities. In the MECOMOS project, a novel manufacturing method is proposed to fabricate a multi-stable 3-DoF PEEK metamaterial that enables tip, tilt, and z-translation. The method involves forming PEEK layers to create the geometries of the unit cells, followed by joining these formed layers to produce a monolithic metamaterial [1].

In this research, a new forming method, hot forming, is developed and analyzed for shaping these layers. This method creates microscale features in PEEK sheets by implementing the process steps of hot embossing into matched die thermoforming.

Polymer molds with various geometries, including rounded cylinders, blocks and trapezoids, are successfully resin printed. Key variables influencing the mold output in resin printing include the cleaning procedure, post-curing, and layer thickness. The smallest printable features measure 400 x 400 x 100 µm, the printing errors range from 40 to 150 µm and are predominantly independent of feature size.

The proof of concept for the hot forming process reveals its strong potential as a manufacturing method. The forming parameters are highly forgiving, with a broad range of process parameters still yielding high replication quality. The suitable forming temperature spans from 100 to 150°C, and pressing forces between 750 and 3000 N prove effective.

Contents

Acronyms

CAD	Computer-aided design
DoF	Degrees of Freedom
FDM	Fused Deposistion Modeling
MECOMOS	Mechanical Metamaterials for Compact Motion Systems
PEEK	Polyether Ether Ketone
SLA	Stereolithography
UV	Ultraviolet

Acknowledgements

I would like to thank multiple people for their help throughout my thesis journey.

First and foremost, Marcel for his guidance throughout the entire course of this research, and Hava for providing me with lots of insight into the different forming methods, helping me shape the research. The achievements presented in this thesis would not have been possible without both of your help. The PME lab technicians for their invaluable support in the assembly of the setup. Their flexibility was crucial for the completion of the setup. Ward for providing his tensile testing data and Pradnya for sputtercoating the samples, enabling the analysis of the mold samples. Everyone present during the MECOMOS meetings for the interesting discussions resulting in new perspectives on the topic. The MSE and IWM lab technicians, for letting me use their equipment and their willingness to help throughout the project. And last, but certainly not least, I would like to thank all my friends and family for their continuous support during this journey.

I truly appreciate each of you, and I hope you find as much enjoyment in reading this report as I did in writing it.

1 Introduction

1.1. Motivation

The Mechanical Metamaterials for Compact Motion Systems (MECOMOS) project focuses on the development of next-generation microscale precision motion components for high-tech systems. Mechanical metamaterials, through their architected inner structures, offer unique properties that enable unparalleled functionalities. One major advantage of integrating motion functionality within material structures is the significant reduction in the volume required for motion solutions. This reduction is particularly important for high-tech systems operating at the micro- and nanoscale, where functional density and complexity are critical. The potential to achieve a large range of motion with reduced volume is a compelling factor in advancing precision motion components in micro- and nanotechnology [1].

The design of unit structures within these materials is critical to unlocking their full potential. Below is an example of a prototype of a mechanical metamaterial. This prototype features a multistable 3-DoF metamaterial that facilitates tip, tilt, and z-translation. The unit cells are composed of hemispheres with beam elements, and layers of these hemispheres are stacked to form the metamaterial, enabling the movement [2].

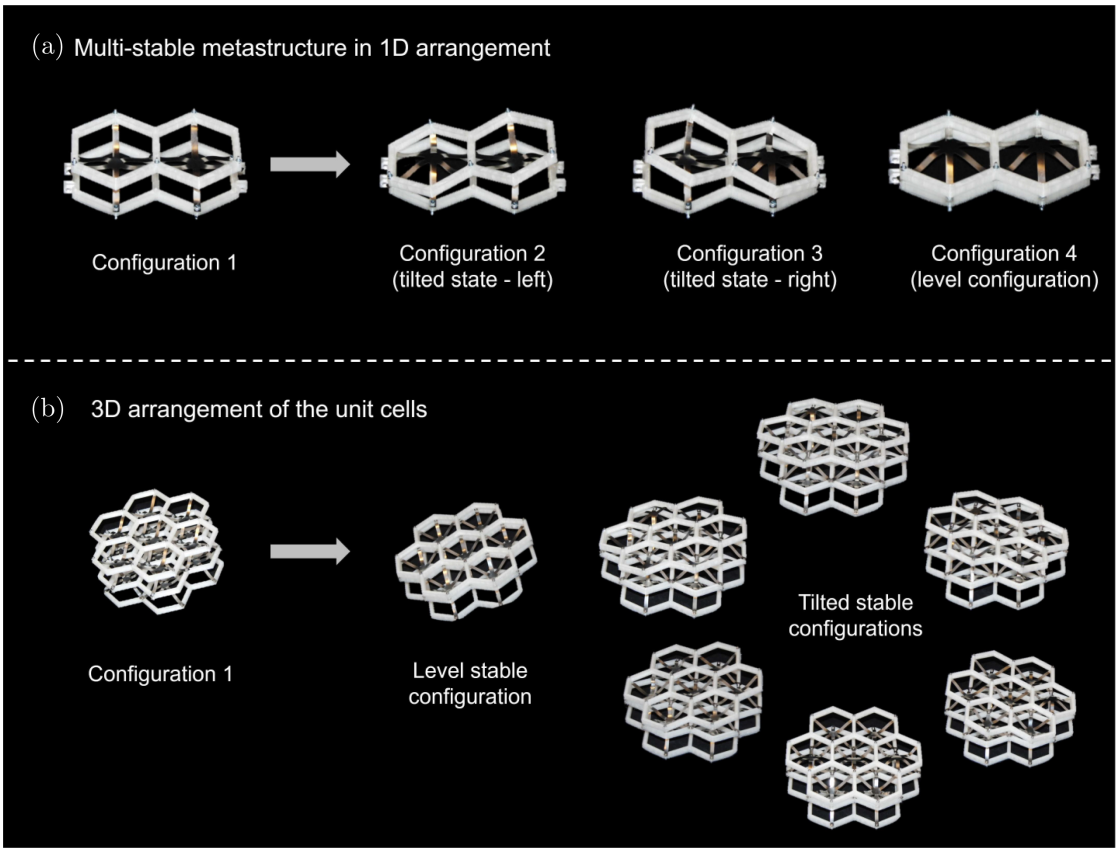

Figure 1.1: Prototype of a multi-stable 3-DoF metamaterial [3].

In the proposed manufacturing approach multiple layers are first formed, to create the geometries of the unit cells, followed by joining these formed layers to transform this prototype into a monolithic metamaterial. This research focuses solely on the first part: the forming of the layers. A new forming method, hot forming, is developed and analysed to determine its feasibility for implementation in the manufacturing of the monolithic metamaterial with submillimeter unit structures.

The metamaterial is made out of Polyether Ether Ketone (PEEK) as it is a high-performance thermoplastic that is frequently used in demanding engineering applications. PEEK has proven to be suitable for components that must retain excellent mechanical and chemical resistance properties at high temperatures. It offers significant value by producing lightweight, durable parts capable of withstanding especially challenging operating conditions [4, 5].

For the forming of the PEEK layers, the goal is to maximize repeatability and develop an easily adjustable process to maintain flexibility in altering the geometry and dimensions of the features. This research is entirely experimental, marking the first phase in researching the potential of the hot forming method.

1.2. State of the art

For the development of our new forming method, two conventional forming techniques are considered, thermoforming and double sided hot embossing.

Thermoforming

In thermoforming, a polymer sheet is heated to its glass transition temperature and then pressed onto one mold, or between two molds to replicate their shape. The features on the molds are generally larger than the substrate thickness, deforming the entire substrate. The molds are not heated, causing the substrate to cool rapidly upon full contact. For this research only matched die thermoforming is considered, wherein the heated substrate is compressed between corresponding positive and negative molds, as visualised in Fig. 1.2. This technique ensures control over the replication quality on both sides of the substrate [6–8].

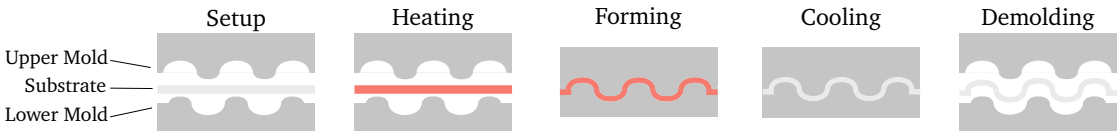

Figure 1.2: Schematic overview of the thermoforming process steps.

Double sided Hot Embossing

In hot embossing, a substrate is placed between two textured molds that are heated to the glass transition temperature of the substrate. The molds are then pressed onto the substrate, texturing its surface, as shown in Fig. 1.3. Unlike thermoforming, which forms the entire substrate, hot embossing only textures the surface [9–11].

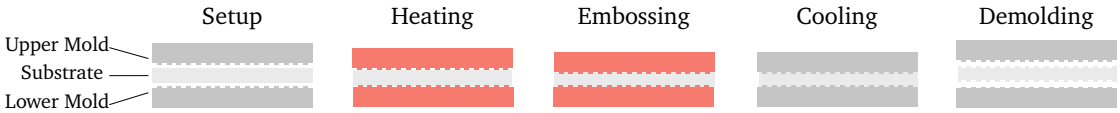

Figure 1.3: Schematic overview of the hot embossing process steps.

1.3. Problem statement

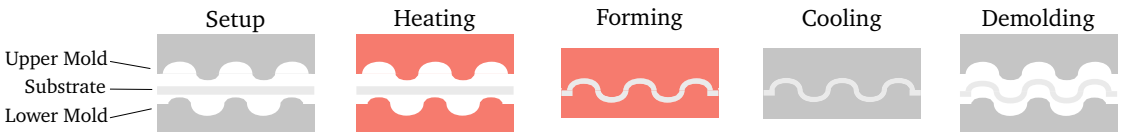

Figure 1.4: Schematic overview of the hot forming process with heating plates.

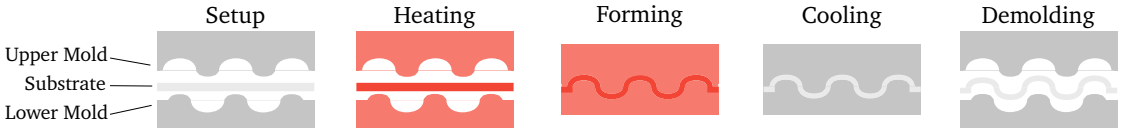

Figure 1.5: Schematic overview of the hot forming process with the heating chamber.

To form the layers, which can eventually be stacked to create the metamaterial, a new forming method, hot forming, is developed in this research. The hot forming process aims to improve the resolution of thermoforming by combining the process steps of hot embossing with the matched molds used in thermoforming. This gives hot forming the

potential to achieve the high precision of hot embossing while forming the entire substrate as done in thermoforming.

In the hot forming process, two matching positive and negative molds are heated until the glass transition temperature of the substrate. The polymer sheet is then placed between the molds. Followed by the pressing of the molds onto each other.

The heating of the molds ensures that the substrates maintains its forming temperature while in contact with the molds. This allows for the substrate to flow into any small cavities, making that all small details can be replicated with this technique.

The amount of time that the molds are pressed onto each other, the pressing time, must be long enough to allow for the material to flow into all small cavities.

After the pressing is done, the molds should be cooled, followed by the separation of the molds and the substrate is removed from the molds.

The main difference between thermoforming and hot forming is that in thermoforming only the substrate is heated. This causes the substrate to cool down after being in full contact with the molds. After the substrate is cooled to below its glass transition temperature, it won't be able to deform. Consequently, during the thermoforming process, the substrate has a limited time to deform, leading to reduced resolution. The shorter time frame restricts the substrate's ability to flow into small crevices, thereby preventing the accurate replication of those fine details.

The molds used for this research will be 3D printed with a SLA printer. While the main objectives for molds in forming techniques include maximum precision and tensile strength, this research is still in the prototype phase, therefore precision and accuracy will be compromised to achieve more design flexibility.

Two different setups are considered in this research. In the first setup the two molds are heated by two heating plates. The substrate is then placed between the two heated molds, where it will only take over the temperature once in full contact with the molds. In the second setup the molds and the substrate are placed in a closed chamber that is kept at the forming temperature. This setup ensures that not only the molds but also the substrate is uniformly heated. The primary advantage of this setup is that the substrate is consistently maintained near the glass transition temperature. It is expected that this setup will allow for a more uniform flow, as now the substrate will be at the forming temperature from the beginning, and not only when in contact with the molds. The schematics of both setups are visualised in Fig. 1.4 and Fig. 1.5. A comparison of all manufacturing techniques considered in this chapter are visualised in Fig. 1.6.

The objective of this research is to develop a proof of concept for hot forming of PEEK sheets using resin printed molds.

To help reaching this overarching research objective, several subquestions are defined:

- Can we resin print molds that are suitable for the hot forming process?
  - What are the requirements for molds in hot forming?
  - What are the size limits of resin printing when looking at these requirements?
- What is the replication quality of the hot forming process?
  - Which process parameters influence the replication quality?

  - What are dimensional limits of hot forming?
- Does the hot forming process affect the PEEK material properties?
  - Is it possible to hot form without affecting the PEEK material properties?

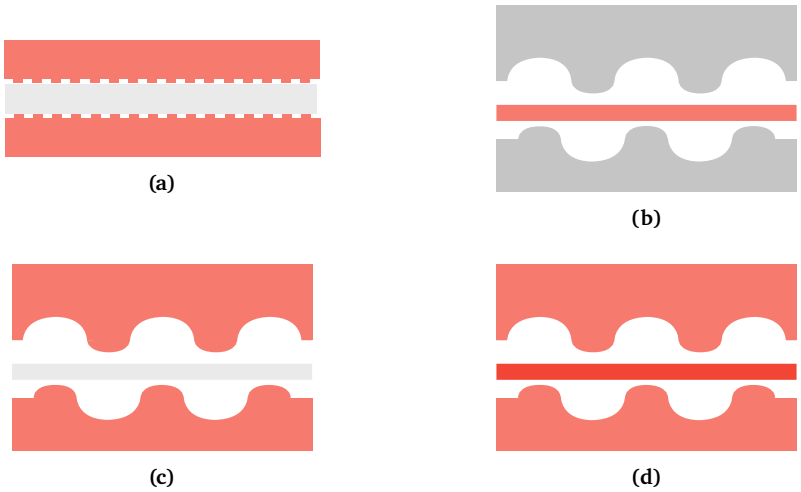

Figure 1.6: Overview of the heating step for all methods. Hot embossing (a), thermoforming (b), hot forming with heating plates (c) and hot forming with heating chamber (d).

1.4. Outline

This report is divided into two main parts: in Ch. 2, test prints are manufactured using SLA resin printing, subsequently they are measured and characterised, to find optimal dimensions for matching positive and negative molds. Ch. 3 details the proof of concept for hot forming of PEEK sheets using the resin printed molds. Finally, conclusions and recommendations for further research are discussed in Ch. 4.

2

Mold Manufacturing

This chapter aims to determine whether it is possible to resin print polymer molds that can be implemented into the hot forming process. First, the objectives for the molds are defined. Subsequently, the materials and methods are elaborated on, detailing the process steps, all relevant variables, materials, and the designs, alongside with the rationale behind these choices. Experimental results and measurements will be presented thereafter. Following this, the feasibility of using resin printed molds for the process will be evaluated. Finally, the manufacturing strategy for the molds used in the next chapter will be presented.

2.1. Mold Objectives

The aim of this chapter is to investigate whether it is possible to 3D resin print molds that are suitable for the hot forming process. Test samples will be printed and evaluated based on the most critical requirements for molds used in the given process. The primary requirements for these molds are: print accuracy, repeatability, surface roughness, tensile strength, and hardness.

Maximizing print accuracy is crucial, as it ensures significant control over the design of the process output. Similarly, enhancing repeatability is essential, as it allows for design modifications to offset any inaccuracies by addressing the discrepancies between the design and the final product. Achieving low surface roughness is essential to prevent demolding issues. Finally, maximizing the tensile strength and hardness of the resin material is necessary to ensure that the molds do not deform or fail during the process.

2.2. Variables in SLA printing of molds

This section will begin by elaborating on the variables involved in mold printing and their influence on both the printing process and the resulting printed molds.

The variables involved in the resin printing of molds can be grouped into two categories: the independent variables and the dependent variables. The independent variables, which can be adjusted during the printing process, include exposure time, cleaning procedure, post-curing, layer thickness, and anti-aliasing. The dependent variables, influenced by the independent variables, comprise printing accuracy, repeatability, surface roughness, tensile strength, and hardness [12–14].

An overview of all variables is provided in Tab. 2.1. The independent (adjustable) variables are represented on the vertical axis, whereas dependent variables are positioned on the horizontal axis. A single star denotes a weak relationship between the corresponding variables, while two stars indicate a strong relationship.

	Printing accuracy	Repeatability	Surface roughness	Tensile strength	Hardness
Exposure time	★★		★	★★	★★
Cleaning procedure	★★	★★	★★	★	★
Post curing	★			★★	★★
Layer thickness	★★		★★		
Anti-aliasing	★★	★★	★★		

Table 2.1: Overview of the variables involved in mold printing, and their interrelationships. A single star denotes a weak relationship between the variables, whereas two stars indicate a strong relationship.

SLA resin printing

In Stereolithography (SLA) resin printing, 3D objects are fabricated layer by layer by solidifying UV-curable resin. This solidification is achieved by exposing the resin to a laser light, as shown in Fig. 2.1. After the laser has cured one layer, the platform moves upward, allowing a new layer of uncured resin to flow beneath the mold. This layer is then cured, continuing the cycle. The area to be cured varies for each layer, so the laser selectively exposes the resin according to the required area. Resin that is not exposed to the laser remains in its original uncured, liquid form [12–14].

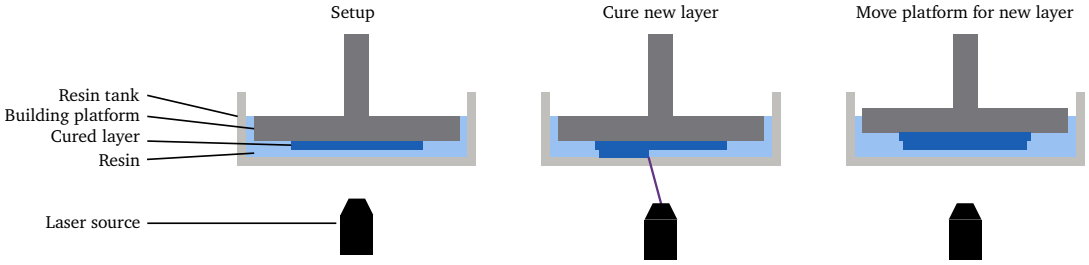

Figure 2.1: Schematic overview of SLA resin printing.

Exposure time

Exposure time is the duration that the resin is exposed to UV light for curing. It impacts the printed part significantly. Overexposure, where layers are exposed longer than necessary, causes the UV light to bleed into surrounding areas, curing a larger area and resulting in bulkier features than intended. Underexposure, where the layers aren't exposed long enough, leads to smaller or unstable features, as semi-cured resin is easily deformed during handling or even dissolved during cleaning. Thus, exposure time affects not only printing accuracy but also surface roughness. Additionally, it is a fundamental property of UV curable resin that the duration of exposure to UV light will change the tensile strength and hardness [12–14].

Layer thickness

In resin printing the objects are created layer by layer, the thickness of each layer significantly impacts the printed parts. Decreasing the layer thickness enhances the ability to reproduce finer details, thereby improving overall printing accuracy and surface roughness.

Anti-aliasing

The aim of anti-aliasing in resin printing is to minimize the visible layering on the surface of printed parts, and thereby enhancing surface smoothness. In anti-aliasing a predetermined amount of voxels at the surface are partially cured. These semi-cured voxels maintain softness and flatten as a consequence, resulting in a smoother surface texture. Cured and uncured voxels, can be seen as black and white respectively, by introducing varying gray levels, semi-cured voxels are defined, increasing the number and intensity of gray voxels enhances the overall smoothness of the molds. The effect of anti-aliasing is visualised in Fig. 2.2, applied to a sloped line.

Anti-aliasing significantly affects the accuracy of printing curved surfaces, as it promotes smoother transitions. Correspondingly, it reduces surface roughness. However, repeatability is compromised due to variability in how semi-cured voxels react during each print cycle. Particularly during the cleaning process, semi-cured voxels can deform or even dissolve differently between prints.

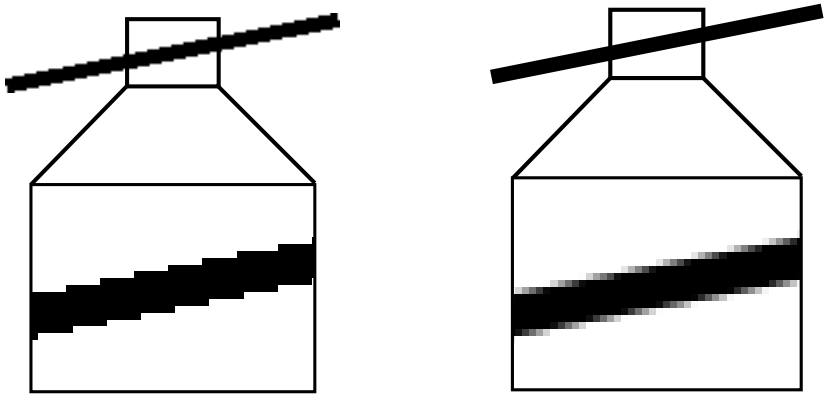

(a) (b)

Figure 2.2: A sloped line, pixelized without (a) and with (b) anti-aliasing.

Cleaning

The first step in post-processing resin prints is cleaning, a critical step aimed at removing residual uncured resin from the printed mold. This is essential for preserving the intended dimensions and intricate details of the print. The cleaning procedure impacts resin printing of molds in two ways, the duration of the cleaning and the method of cleaning. Generally, cleaning involves submerging the 3D resin printed mold in a solvent that dissolves uncured resin residues from its surface. Prolonged exposure to the solvent can initiate reactions with the cured resin, leading to reduced mechanical properties such as tensile strength and hardness. Furthermore, the cleaning method can intensify the cleansing process, potentially damaging the molds.

A conventional cleaning approach involves a two-stage bath technique, comprising a preliminary rinse in a 'dirty' solvent followed by a more meticulous cleanse in a 'clean' solvent, both carried out using automated machines that agitate the liquid for a predetermined duration. In cases where this two-stage technique proves inadequate for cleaning the molds, an ultrasonic cleaner may be employed as an additional or alternative measure. This device generates ultrasonic waves that produce imploding bubbles, effectively removing contaminants, including those in the minute crevices of the molds. However, the thoroughness of this cleaning method increases the mold's exposure to the solvent, thereby increasing the risk of (semi-)cured resin reacting with the solvent.

Overall, the cleaning process significantly influences various aspects of resin printing, including printing accuracy, repeatability, surface roughness, tensile strength, and hardness of the mold. Careful consideration of the cleaning methods is therefore crucial to maintaining the desired quality and functional properties of the molds [12, 14].

Post curing

Following printing and cleaning, the next step for resin printing polymer molds is post-curing to improve their mechanical properties. Post-curing involves exposing the now-clean molds to UV light for a specified duration.

During printing, the resin cures to its initial 'green' state, where some polymer connections remain incompletely formed. Post-curing the molds with additional UV-light enhances the polymer structure by strengthening bonds, and thereby improving mechanical attributes such as strength, stiffness, and resistance to temperature. In some cases, elevated temperatures are applied during post-curing, accelerating the process and enabling more thorough bond formation, leading to enhancements in material properties beyond those achievable through UV light alone.

While at the post curing step, the mold no longer contains any uncured resin for the UV-light to bleed into, the post curing process can still have an small effect on the accuracy of the molds. The increased number of bonds pulls the material together more tightly, causing (minor) shrinkage. Additionally, surface roughness may be affected due to semi-cured voxels potentially completing their curing process and deforming in unintended ways. However, the primary effect of post-curing lies in significantly enhancing the tensile strength and hardness of the molds. The additional UV exposure enables the molds to achieve their optimal mechanical performance characteristics [12, 14].

Print accuracy

The print accuracy refers to the degree of similarity between the intended design and the actual printed mold. Perfect print accuracy is achieved when the printed mold precisely

matches the design. This dependent variable is influenced by all previously mentioned independent variables, ie. exposure time, layer thickness, anti-aliasing, cleaning, and post-curing.

Repeatability
Repeatability is measured by comparing the difference between identically manufactured features of the same design, both within a single mold and across different molds. Repeatability is primarily influenced by the cleaning procedure and anti-aliasing.

Surface roughness
Surface roughness is crucial for molds used in hot forming, as a lower surface roughness reduces the chance of demolding issues. Many independent variables affect the surface roughness of the mold, including exposure time, cleaning, layer thickness and anti-aliasing.

Tensile strength
Tensile strength is a critical factor in the performance of molds, as higher tensile strength reduces the likelihood of deformation during pressing. The curing process forms bonds within the resin, offering its mechanical properties, and thereby making exposure time and post-curing procedures crucial determinants of tensile strength. Additionally, the cleaning procedure influences tensile strength, as excessive exposure to solvents can cause undesirable reactions with the cured resin, leading to a reduction in tensile strength.

Hardness
The hardness is important in mold manufacturing as higher hardness enhances durability. It improves surface quality by reducing sensitivity to damage, such as scratches. Similar to tensile strength, hardness is influenced by exposure time, cleaning procedures, and post-curing processes due to their impact on the mechanical properties of UV curable resins.

2.3. Materials and Methods

This section will begin by elaborating on the variables of mold printing that are considered in this research. Next, the test samples that will be used to explore the possibilities of mold printing are discussed. Followed by the process steps of the resin printing strategy, along with the the materials used during the process will be detailed. Finally, the methods employed to evaluate the quality of the results will be presented.

2.3.1. Selected variables

Tab. 2.2 indicates which variables will be modified and which dependent variables will be measured to improve the print quality of the test samples.

	Printing accuracy	Repeatability	Surface roughness	Tensile strength	Hardness
Exposure time	★★		★	★★	★★
Cleaning procedure	★★	★★	★★	★	★
Post curing	★			★★	★★
Layer thickness	★★		★★		
Anti-aliasing	★★	★★	★★		

Table 2.2: Overview of the variables involved in mold printing, and their interrelationships. A single star denotes a weak relationship between the variables, whereas two stars indicate a strong relationship. The green stars indicate the variables investigated in this chapter.

2.3.2. Test samples

To explore the possibilities of mold printing, different test samples are developed. In this section these test samples are discussed. The designs are presented together with the intended objectives of the corresponding analysis.

Design Blocks Size Reduction

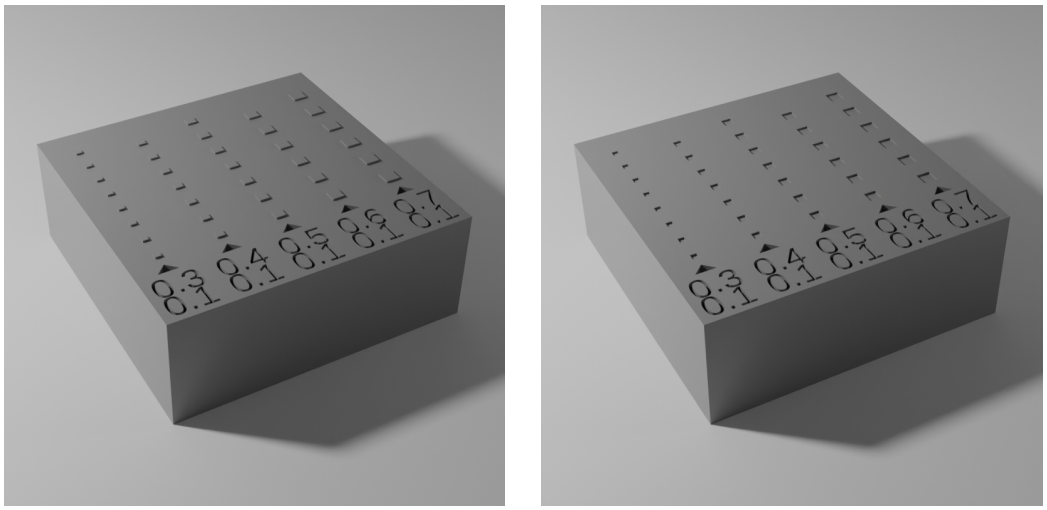

(a) **(b)**

Figure 2.3: Design of the test prints used to analyse the smallest block-shaped features: (a) positive and (b) negative test print.

The objective of this test sample is to identify the smallest feature for which a consistent print output can be achieved. During the hot forming experiments, will be researched whether it is possible to form the smallest printable geometry, thereby concluding whether the hot forming process or the resin printing is the limiting factor in terms of size.

Using blocks for this objective offers several advantages. First, the minimal size of resin printing is primarily determined by rounded and angled walls. Since a block does

not incorporate these features, it avoids limitations associated with voxel stacking needed to create arches, allowing for straightforward vertical stacking of voxels.

Secondly, the simplicity of block geometry facilitates a more straightforward and reliable analysis. When analysed under a microscope, it is easy to assess printing accuracy by evaluating whether a surface is flat or not. In contrast, curved designs complicate the determination of whether the output curve matches the desired specifications.

Design Cylinders with Varying Aspect Ratio

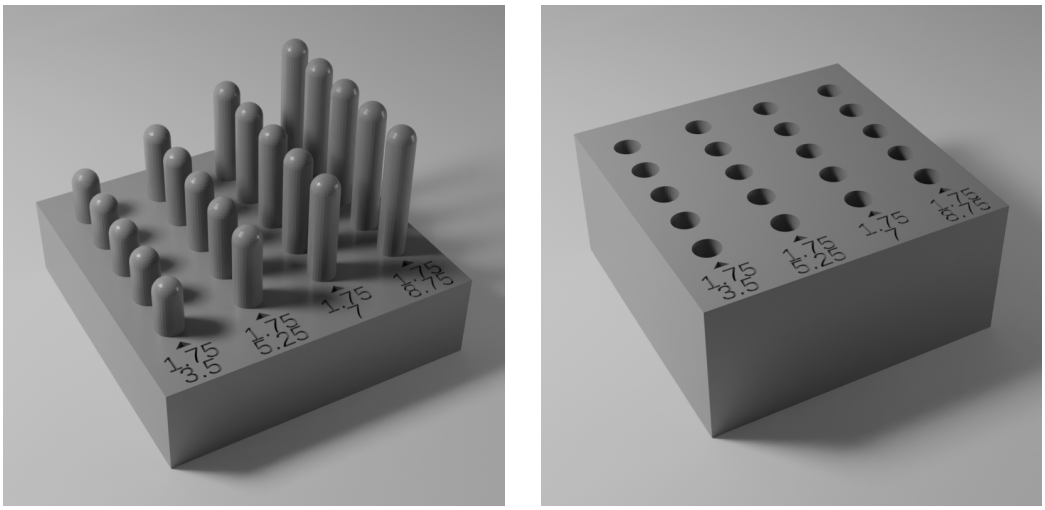

(a) **(b)**

Figure 2.4: Design of the test prints used to analyse the cylindrical features: (a) positive and (b) negative test print.

For this test print the objective is to analyze cylindrical features with varying aspect ratios. The aim will be to investigate the stretching limits of the substrate material during hot forming. Using features with increasing aspect ratios, the effect of stretch increments is researched. The cylinders are rounded at the top to reduce stress concentrations during hot forming.

Because in resin printing voxels are stacked on top of each other, it is impossible to perfectly replicate an arched surface. However, due to time constraints, this geometrical deviation will not be investigated, any differences compared to the design roundness will not be considered.

For this test sample, aspect ratios of 1:2, 1:3, 1:4, and 1:5 will be tested. To achieve these aspect ratio's, the width is kept constant and the height is increased. The goal is to use the minimal possible width to reduce the size of the test print and minimize the size of the features, the test samples are shown in Figs. 2.4a and 2.4b.

The minimal width of the cylinders is constrained by the negative features. If the width is too small, the solvent will not be able to penetrate into the feature, leaving uncured resin residue, reducing the depth of the feature, and resulting in a loss of detail. The minimal width is determined by printing negative features with varying widths, all having an aspect ratio of 1:5. The widths range from 1 mm to 2 mm, with the goal of identifying the smallest width that can be completely cleaned, a CAD render of the test sample is shown in fig. 2.5.

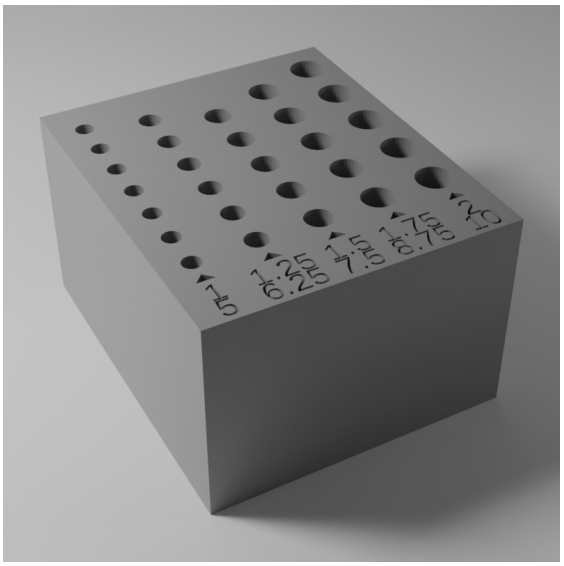

Figure 2.5: Test print with an increasing width for the cylindrical features with an aspect ratio of 1:5.

Design Trapezoids 2x2x1 mm

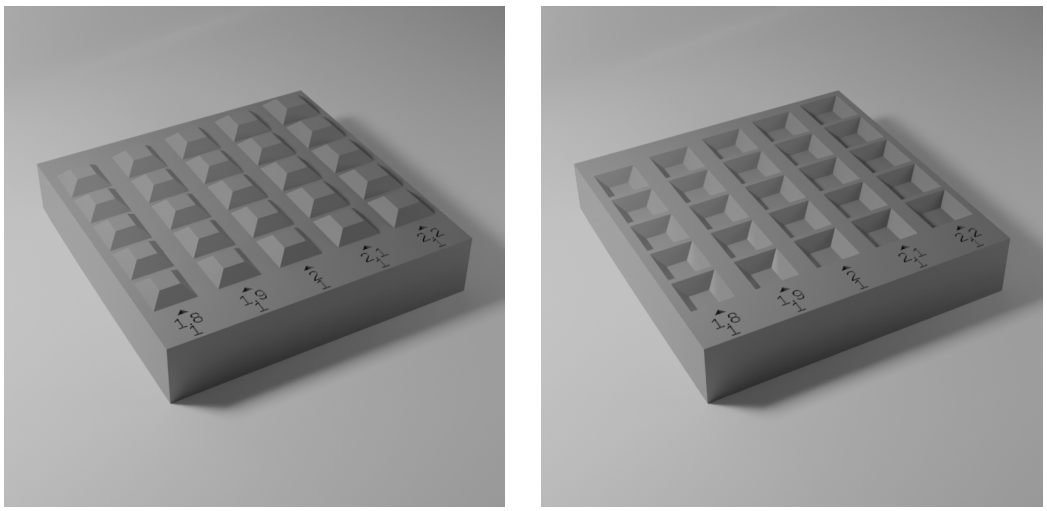

(a) **(b)**

Figure 2.6: Design of the test prints used to analyse the 2x2x1 mm trapezoidal features: (a) positive and (b) negative test print.

The objective of this test sample is to find out how accurate a print can be made of a trapezoid with a 2x2 mm top area and a height of 1 mm. This geometry is chosen as it is a simplified unit cell of the MECOMOS metamaterial. As this research represents an initial step in the manufacturing of the metamaterial, the feature geometry does not need to be functional in terms of buckling performance. The features only need to approximate the final geometry sufficiently to allow for a realistic assessment of whether resin molds can be suitable for joining the layers to create the metamaterial. A top area of 2x2 mm is chosen as that is the current limit in joining the layers to create the metamaterial [15].

Without any manufacturing tolerances, the negative mold should be Δx wider than the positive mold, where Δx is given by the following formula:

$$\Delta x = t \cdot \tan(0.5 \cdot \theta) \tag{2.1}$$

This formula can be derived from Fig. 2.7, with t being the substrate thickness and θ being the trapezoid angle. Using Eq. (2.1), it is possible to create a uniform thickness between the molds. However with resin printing it's expected that there will be some error in printing accuracy, meaning that it is most likely that the positive and the negative won't fit on top of each other if they are designed perfectly according to this relationship. To determine the required adjustments, the positive and negative features are tested for widths ranging from 1800 µm to 2200 µm in steps of 100 µm, to ensure that the features align properly and create uniform spacing for the substrate during the hot forming process.

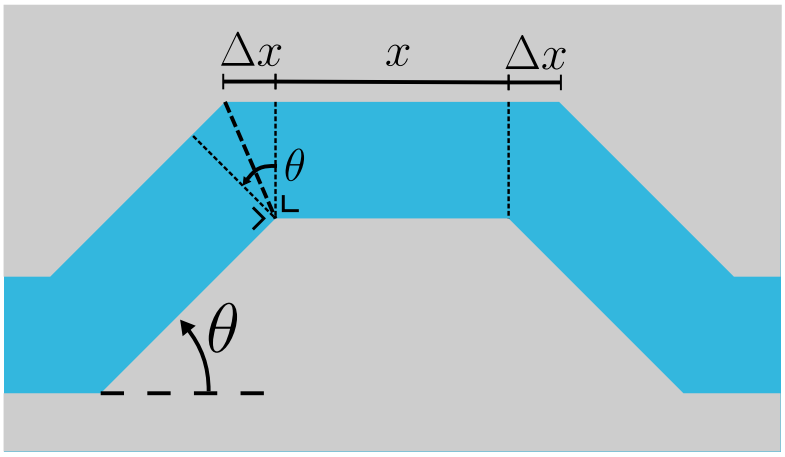

Figure 2.7: Derivation of the relationship between trapezoid angle θ, substrate thickness t and the corresponding additional width for the negative mold Δx.

Design Trapezoids Size Reduction

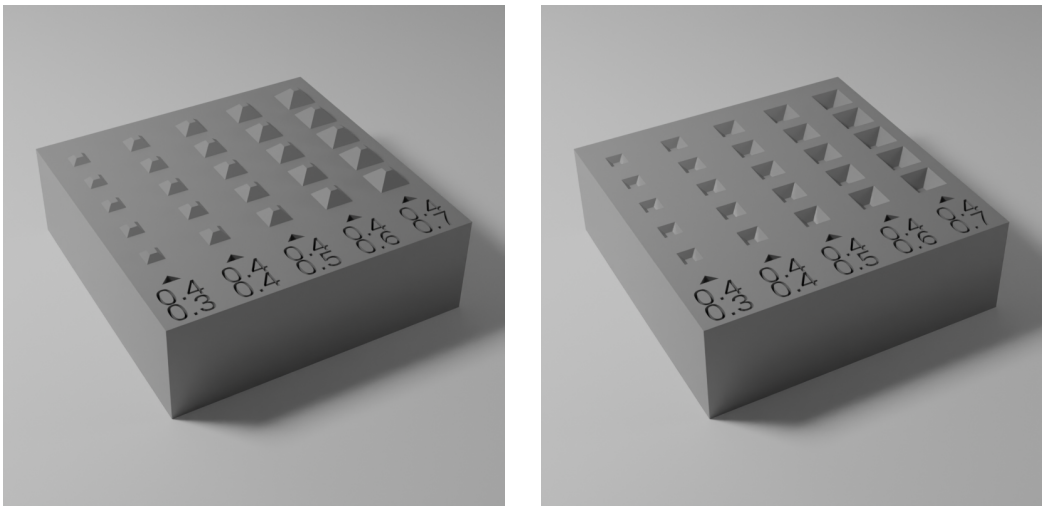

(a) **(b)**

Figure 2.8: Design of the test prints used to analyse the smallest trapezoidal features: (a) positive and (b) negative test print.

The objective of this test sample is to determine the smallest trapezoids that can be produced through resin printing. A goal further down the line is to reduce the feature size of the metamaterial. Therefore, it is crucial to identify the size limits for resin printing trapezoids, with consistent output dimensions.

To identify the smallest trapezoids, a both positive and negative features are tested for heights ranging from 300 µm to 700 µm in increments of 100 µm. The width of the top area of the trapezoids is based on the results of the smallest printable width determined in Section 2.4.2.

Resin Dog Bones

The last test samples discussed in this section are the dog bones used for the tensile tests. The dog bones correspond to the ASTM D638-22 norm for a Standard Test Method for Tensile Properties of Plastics [16]. A render of the dog bone is visualised in Fig. 2.9.

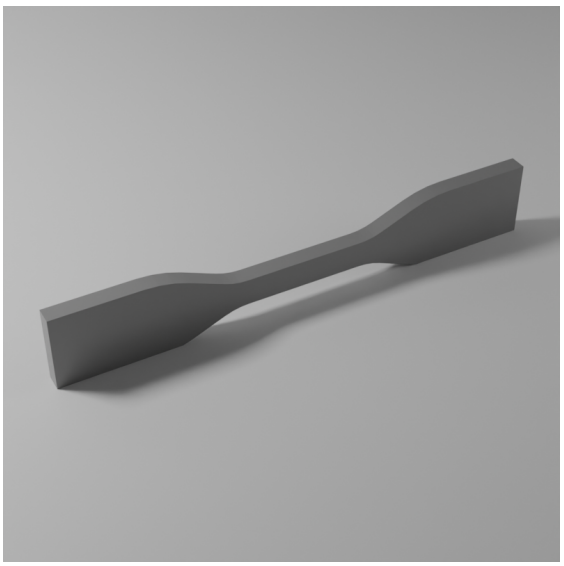

Figure 2.9: Render of the dog bone model used for resin printing.

2.3.3. Mold manufacturing steps

The mold printing process considered in this research comprises five steps: designing the molds, slicing the design into a format compatible with the 3D resin printer, printing the molds, cleaning the molds, and finally, post-curing the molds to attain their final mechanical properties.

Design

OpenSCAD is utilized for the design phase of this research. This is a free, open-source and script-only 3D CAD modeller. The primary advantage of using a script-based modeller is the ease with which feature sizes can be adjusted, which is useful when adjusting the size of the positive and negative features to make them compatible with each other. The scripts used for this research can be found in the Appendix C.

Slicing & printing
Slicing is performed using the Preform software, the designated slicer for Formlabs resin printers. The Formlabs 3 printer was selected because of its consistent output, a result of Preform's restricted adjustability, which only permits changes to layer thickness. Although this limits control over variables like anti-aliasing, it ensures optimal exposure time. Adjusting exposure time in other printers is challenging due to environmental variables such as temperature, leading in most cases to suboptimal prints.

Cleaning
The cleaning process consists of a two-step washing system with two Form Wash machines. These automated machines agitate isopropanol for a predetermined amount of time. The molds are first rinsed for 2 minutes in a bath with contaminated isopropanol, followed by a 2-minute wash in a second bath with clean isopropanol for a more thorough cleanse. Given the small-scale of the features, the molds are subsequently cleaned in a Sonorex Ultrasonic cleaner. There, the molds are placed for 5 minutes, dried with an air compressor, followed by an additional interval in the cleaner as needed.

Post curing
Once cleaned, the molds are post-cured in the Form Cure for 120 minutes at 80°C. This high temperature and extended curing time are necessary to attain the exceptional mechanical properties of the Formlabs High Temperature resin.

(a) (b) (c) (d)

Figure 2.10: Equipment used in mold manufacturing: (a) Formlabs Form 3, (b) Formlab Form Wash, (c) Sonorex Ultrasonic cleaner and (d) Formlabs Form Cure.

2.3.4. Materials

The resin used for the molds is Formlabs High Temperature Resin, selected for its superior mechanical properties. Although Formlabs has not disclosed the composition of the resin, the provided datasheet specifies a heat deflection temperature of 238°C and a tensile strength of 58 MPa following post-curing.

2.3.5. Measurements

This section details the measurements conducted to assess and quantify the results of the printing process. The first measurements are carried out with the Keyence Digital Micro-

scope VHX-6000. This instrument is employed to measure the width, height, and base angle of each feature, aiming to gain insight into both the printing accuracy, how closely the print aligns with the design, and the repeatability, the consistency of similar features across the same and different molds. Each feature is printed 5 times across 3 distinct test samples. The width, height, and base angle are measured to calculate the averages along with the absolute error values for each feature. Although these measurements may not offer the precision of a continuous 3D method, they provide a reliable indication of printing quality. Fig. 2.11 presents two examples illustrating how the printing quality of a block-shaped feature can be assessed using these four measurements.

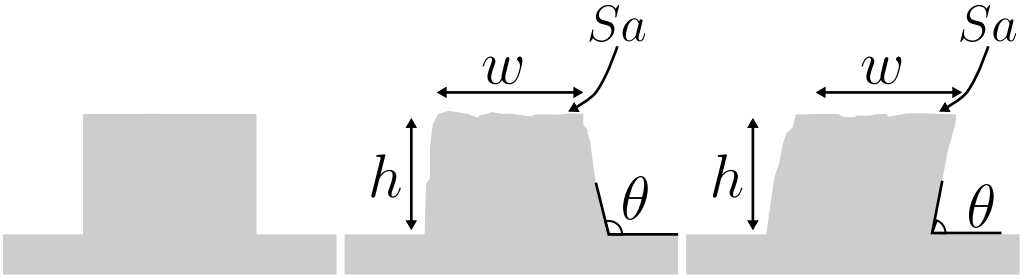

(a) Block Shape **(b)** Block Shape **(c)** Block Shape

Figure 2.11

The second type of measurement performed with the Keyence microscope focuses on assessing surface roughness. A 200x200 µm area is selected at the midpoint of each flat surface to quantify the surface roughness in µm. This is determined by measuring the height differential between each point and the arithmetic mean of the surface height, and implementing both in the following integral [17]:

$$\mathrm{Sa} = \frac{1}{A} \iint_A |Z(x,y)| \; dx\, dy \tag{2.2}$$

To assess the results, the measured values will be compared to Tab. 2.3, which includes standard values for surface roughness for different types of manufacturing techniques.

Manufacturing process	Surface roughness, Sa (µm)
FDM 3D printing	3.1
Drilling	1.6
Milling	0.8
Turning	0.4
Grinding	0.1
Lapping	0.1

Table 2.3: Surface roughness chart by manufacturing technique [18].

In order to remove undesired reflections, resulting in interference, gold sputtering is carried out using the JEOL JFC-1300 Auto Sputter Coater, with a current of 20 mA for 30 seconds.

Additionally, tensile tests are conducted using a Zwick Roell Z005 Allround testing machine with a temperature chamber. These tests are carried out at both room temperature and 143°C, which corresponds to the operating temperature of the hot forming process. The machine is configured to apply a pulling rate of $2\,\mathrm{mm\,s^{-1}}$, halting and returning to its starting point upon an 80% reduction in force.

2.4. Results and Discussion

This section shows the results of the test prints for each geometry. First the results of the cylindrical features and the blocks are shown, to determine the limitations and possibilities of SLA mold printing. These results are then implemented into a simplified design of the unit cells of the MECOMOS metamaterial, to find out if hot forming is suitable for the manufacturing of the metamaterial. Lastly, the results of the tensile tests of the mold material are discussed.

2.4.1. Results Cylinders with Varying Aspect Ratio's

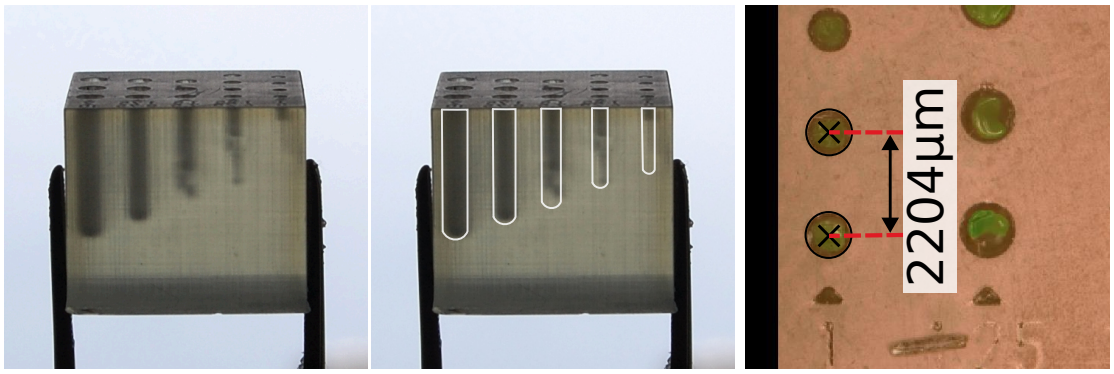

(a) (b) (c)

Figure 2.12: (a): Picture of the negative test sample with increasing width for the 1:5 cylindrical features. (b): Indicators show the intended dimensions. (c): example of a distance measurement between two features.

Before the cylinders with varying aspect ratios are tested, a preliminary test is done to determine the minimal width suitable to analyse the different aspect ratios. The minimal width of the cylinders is limited by the negative features. If the width is too small the solvent won't be able to penetrate into the feature. This leaves the uncured resin inside, reducing the depth of the feature and resulting in loss of details on the features. Moreover, in the ultrasonic cleaner, narrow features limit the space available for cavitation bubbles to form, grow, and collapse, which in turn reduce the cleaning effectiveness. The minimum width is determined by printing negative features with varying widths and a consistent aspect ratio of 1:5. The resulting test print, featuring rounded cylinders with widths ranging from 1000 to 2000 µm, demonstrated that a width of 1750 µm is the minimum for which a negative feature with an aspect ratio of 1:5 can be effectively cleaned. In the 1500 µm feature a resin layer is still visible in the test print, just as for the 1250 µm feature. For the the 1000 µm feature the solvent almost couldn't penetrate the feature at all. The test print is shown in Fig. 2.12a. The same test print is used to analyse the

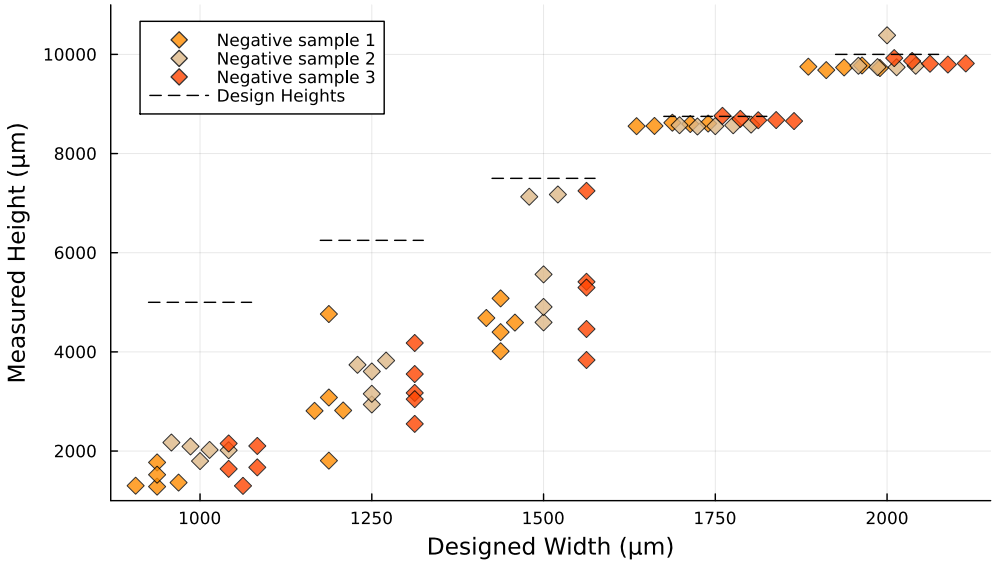

Figure 2.13: Measured height for each of the design widths for the negative test print of the 1:5 cylindrical features.

error of the XY-position of the features. The results showed that the XY-errors ranged between 4 to 25 µm. This means that the position errors are a factor 10 to 50 smaller than the width tolerances. Indicating that the position have a small effect whether the matching molds will fit onto each other, compared to the effect of the size of the feature. Due to time limitations the errors of the XY-position of the features therefore won't be considered in the following sections.

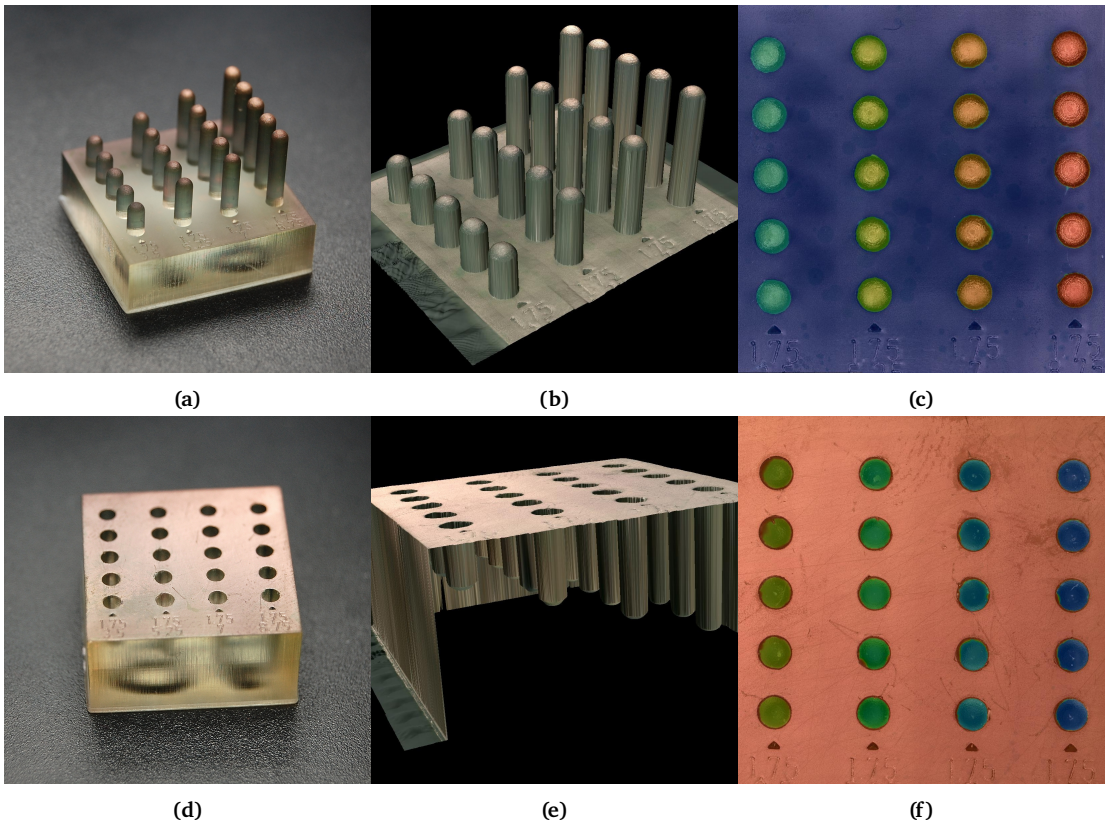

Figure 2.14: For both positive and negative test prints: Picture of the test print (a, d), microscope image of the print (b, e), height map of the test print (c, f).

The images of the test prints show that the test prints closely resemble the design, with straight rounded cylinders. The print lines are only visible for the curved surface of the rounded tops. The vertical walls don't show any printing lines. The colors on the height maps range from blue to red, indicating the height of the measured points. For the positive test prints the base is blue as this is the lowest point and the positive pins increase gradually to red for the increasing heights of the features. The height maps show a sharp transition from blue to red, confirming that the test prints closely match the design.

The images reveal small bumps on some features, which are actually very thin resin flakes formed during the cleaning process. These flakes appear elongated in the images because they block the view as the microscope scans from the top, making it seem as though the particles extend to the bottom of the feature. However, images taken with the Dino Lite microscope clearly show that these are very thin dust-like flakes that will not interfere when the positive and negative molds are pressed together. For the positive features, it is evident that they are completely clean, in contrast to the negative features which show a small amount of resin residue.

Print accuracy

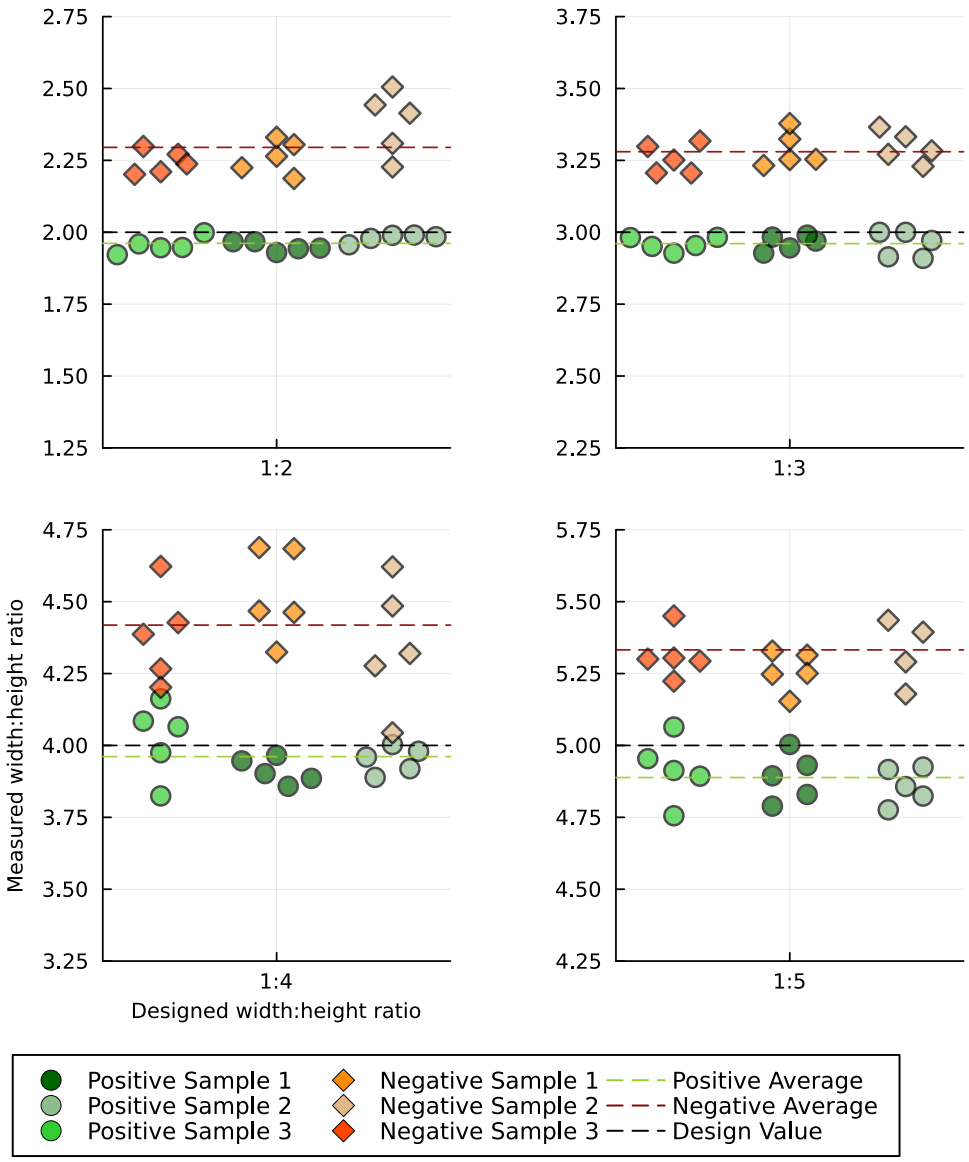

Figure 2.15: Beeswarm plot of the aspect ratio measurements for the rounded cylinders with an intended aspect ratio of 1;2, 1:3, 1:4, and 1:5.

The results of the width and height measurements are presented by plotting the aspect ratios of the test features. This approach is utilized because these features will serve as a basis for determining the maximum achievable stretch in the hot forming process. Consequently, the specific dimensions of the features are not critical, provided that their widths remain relatively consistent.

The measurements of the height and the width of the features indicate that the aspect ratios are accurate for the positive features, however the accuracy decreases slightly for increasing aspect ratios.

For the positive features, the 1:2 aspect ratio resulted in an average height ratio of 1:1.96, an error of 0.04. 1:5 gave an average height ratio of 1:4.89, resulting in an error of 0.11. Where the negative features resulted in height ratio's of 1:2.26 and 1:5.32 for

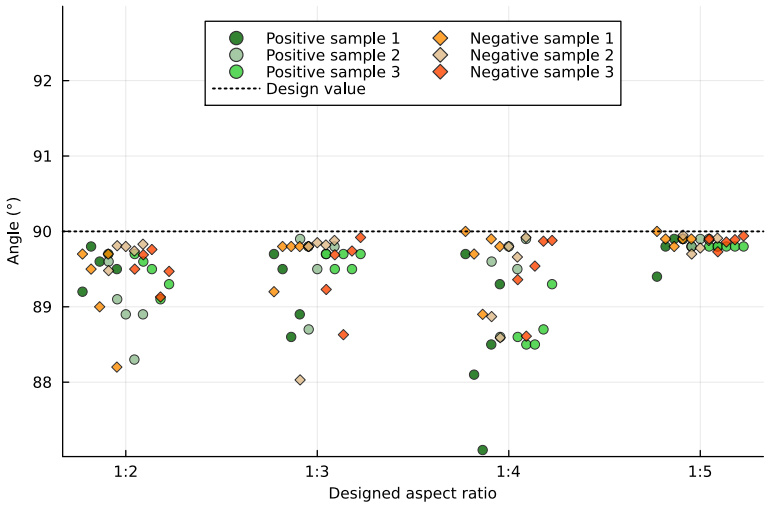

Figure 2.16: Measured angle of the printed cylinders.

1:2 and 1:5, respectively.

The aspect ratio for the negative features is consistently higher across all measured ratios. This difference arises from the fact that the measured width of the negative features is significantly smaller than the designed width. The average measured width of the negative features is 1560 µm, which is considerably less than the intended width of 1750 µm. In contrast, the average width of the positive features is 1737 µm.

The insufficient width of the negative features can be attributed to overexposure during the printing process. Overexposure results in an extended exposure time per layer, causing adjacent voxels to cure and thus enlarging the cured area. Consequently, this leads to the negative features being smaller than their designed dimensions. For each layer, during the printing process, the exposed area is larger for the negative test prints as for the positive test prints, therefore the effect of bleeding becomes larger.

The measured angles confirm that the features are relatively straight, there an error of only 3 degrees is measured for the angle at the base of the cylindrical test features, Fig. 2.16.

Given that the aspect ratios of the positive features closely align with the design specifications and primarily influence the substrate's stretch, it isn't necessary to adjust design dimensions of the positive cylinders to improve print accuracy. However, adjustments are necessary for the negative features. To compensate for the substrate's thickness and improve print accuracy, the width of the negative features should be increased by 400 µm, and an additional 200 µm should be added to the height of the negative features relative to the positive features Appendix A.1.

2.4.2. Results Smallest Blocks

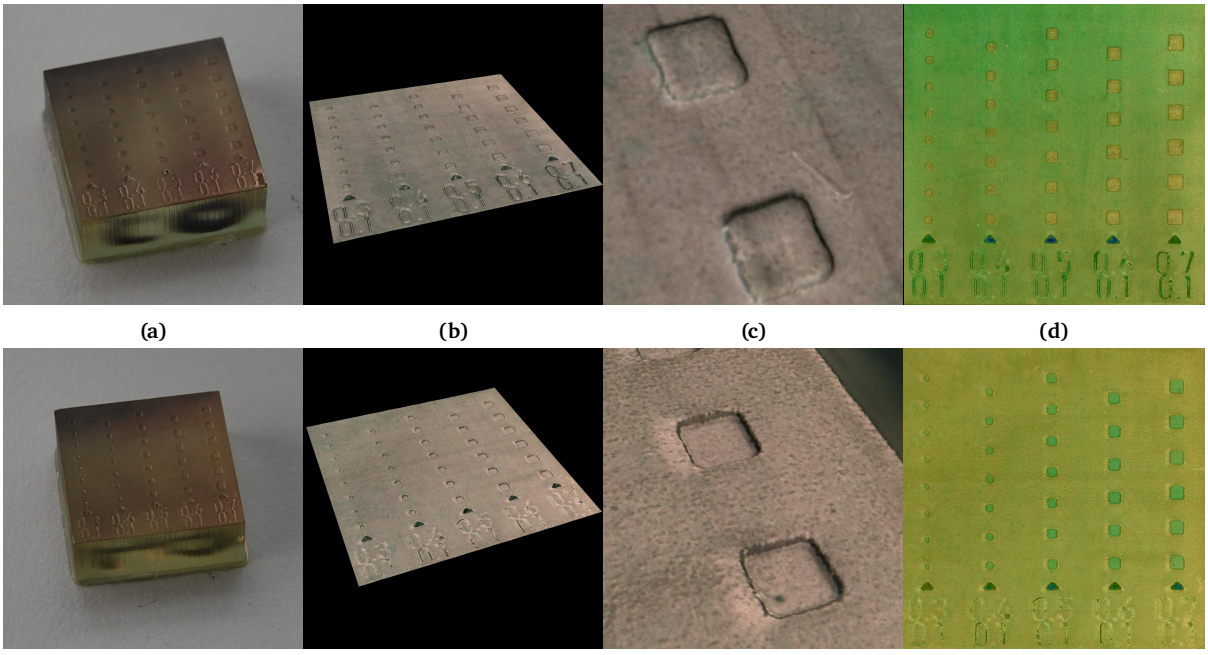

(a) (b) (c) (d)

(e) (f) (g) (h)

Figure 2.17: For both positive and negative test prints: Picture of the test print (a, e), microscope image of the print (b, f), detail of a single feature (c, g), height map of the test print (d, h).

In both the positive and negative test prints, all blocks have rounded corners. The blocks with a 300 µm width, in both cases, lose their square shape due to the small feature size and corner rounding. A design width of at least 400 µm is required for positive blocks to consistently reproduce a square shape. Although the 400 µm block in the negative test print fails to maintain a square shape, the negative blocks must be larger to accommodate the positive feature. Consequently, the 400 µm positive block is considered the smallest suitable option. The graphs in the following section are used to determine the appropriate dimensions for the corresponding negative block.

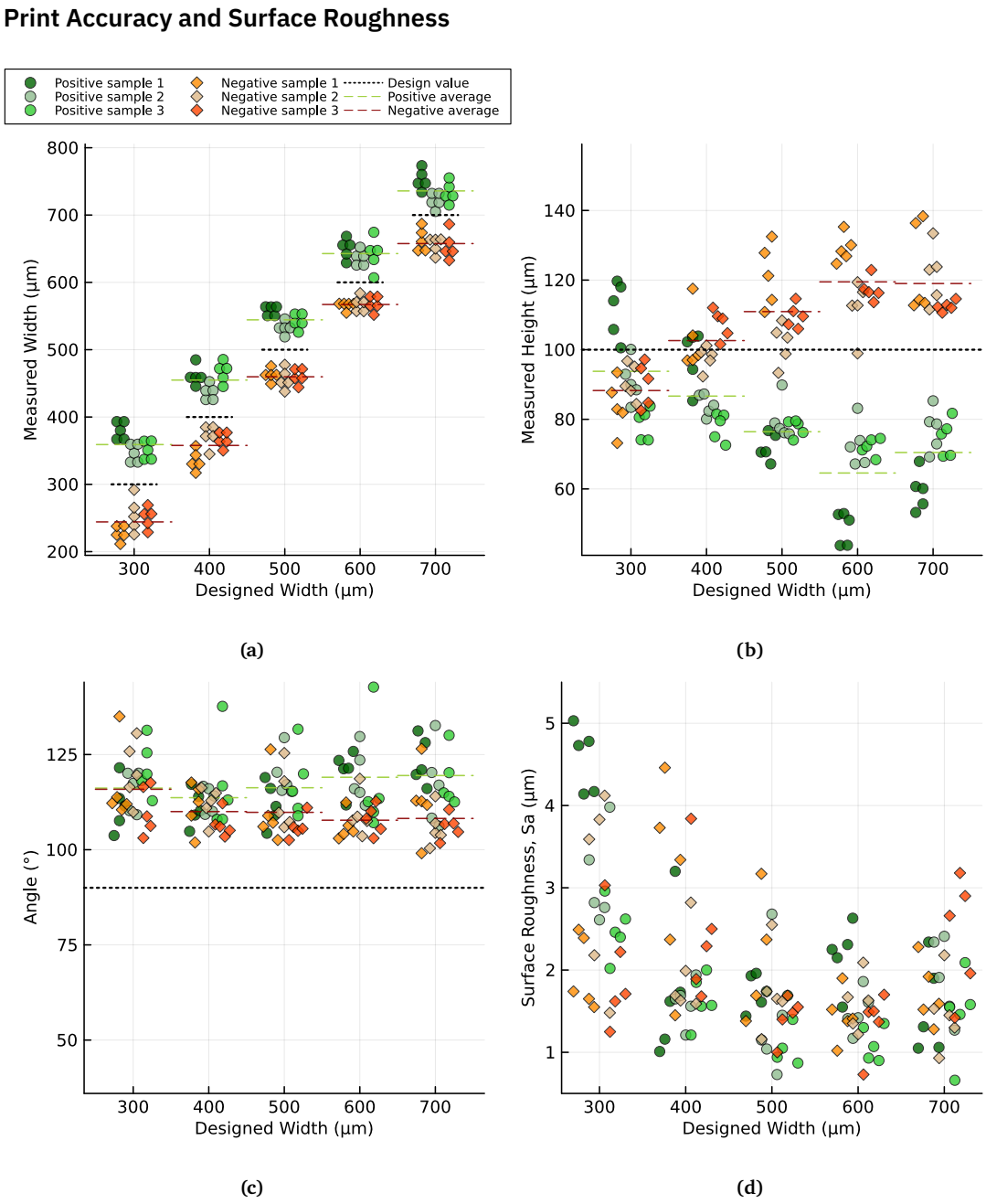

Figure 2.18: Various measurements of the test prints: (b) height, (a) width, (c) base angle and (d) Sa surface roughness.

The block width measurements are closely clustered. Analysis of the images reveal that a design width of 400 µm is the minimum required to preserve a square shape. From the measurements the appropriate design width for the negative features is determined to fit the positive features. The positive blocks with a 400 µm design width are found to be up to 100 µm larger than intended, likely due to resin bleeding during the printing process. To ensure proper fit, the design width for the negative features should be set at 600 µm. Height measurements show an error margin of up to 40 µm, which represents a significant 40% deviation for a 100 µm design height. To accommodate this, the design height of the negative features should be 100 µm greater than that of the positive features,

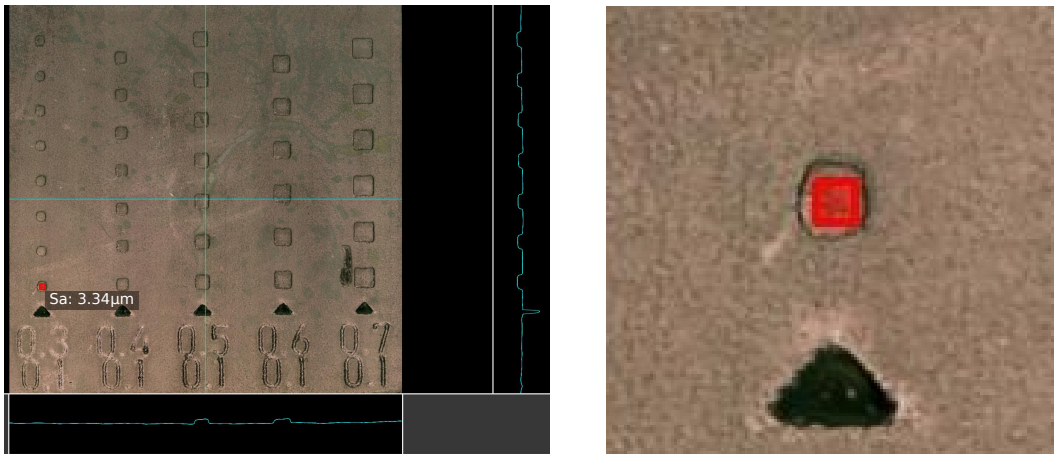

(a) **(b)**

Figure 2.19: Surface roughness measurement of a feature: (a) measurement Sa surface roughness, (b) close-up of the area used for calculation.

meaning a 200 µm design height for the negative features when the positive features are 100 µm. The base angle measurements for both positive and negative features are uniformly distributed across all design widths but are generally larger than the intended 90 degrees, indicating the challenge of achieving precise angles at this scale. Surface roughness measurements, conducted over a 200 x 200 µm area, are less accurate for the 300 µm blocks due to edge rounding, which affects the measurement, as shown in Fig. 2.19. The estimated surface roughness ranges between 0.5 µm and 3.5 µm, comparable to the roughness typically observed in turning, milling, drilling, and Fused Deposistion Modeling (FDM) 3D printing. This wide range makes it difficult to draw conclusions from the roughness measurements [18].

2.4.3. Results Trapezoids 2x2x1 mm

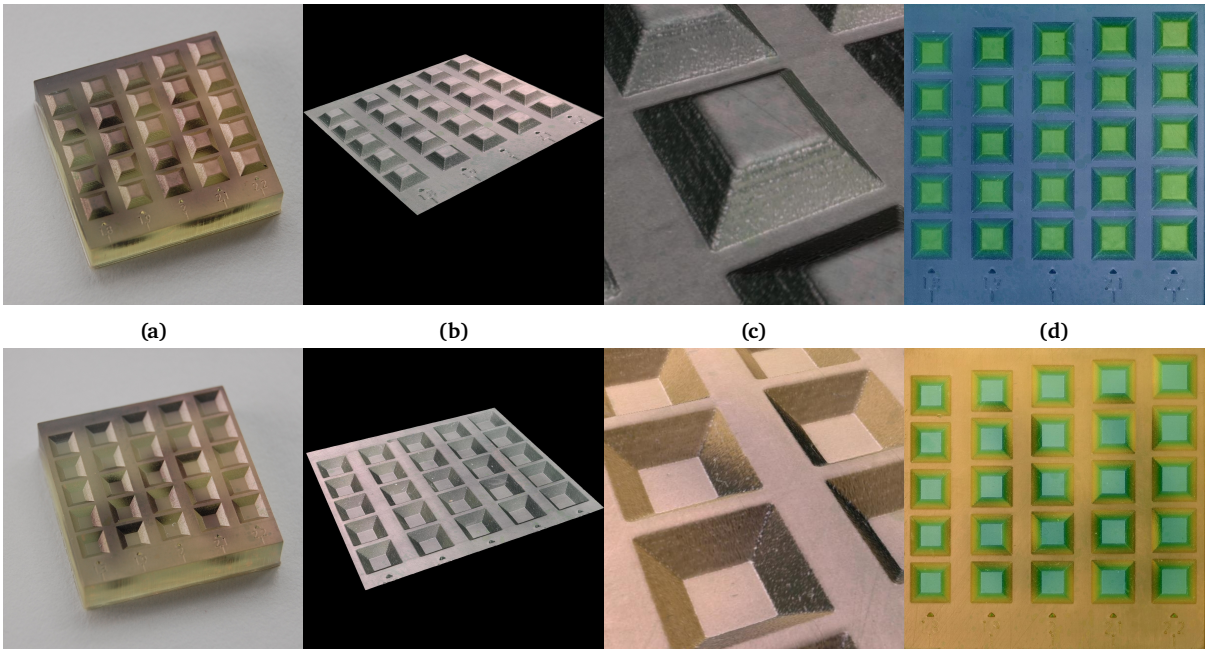

Figure 2.20: For both positive and negative test prints: Picture of the test print (a, e), microscope image of the print (b, f), detail of a single feature (c, g), height map of the print (d, h)

The printing quality of the 2x2x1 mm trapezoids is very high. The edges are again rounded off, but because the large size of the features this rounding can be neglected. The side walls seem to match the 45 degrees very well and the printing lines don't seem to negatively influence the quality of the prints.

Print Accuracy and Surface Roughness

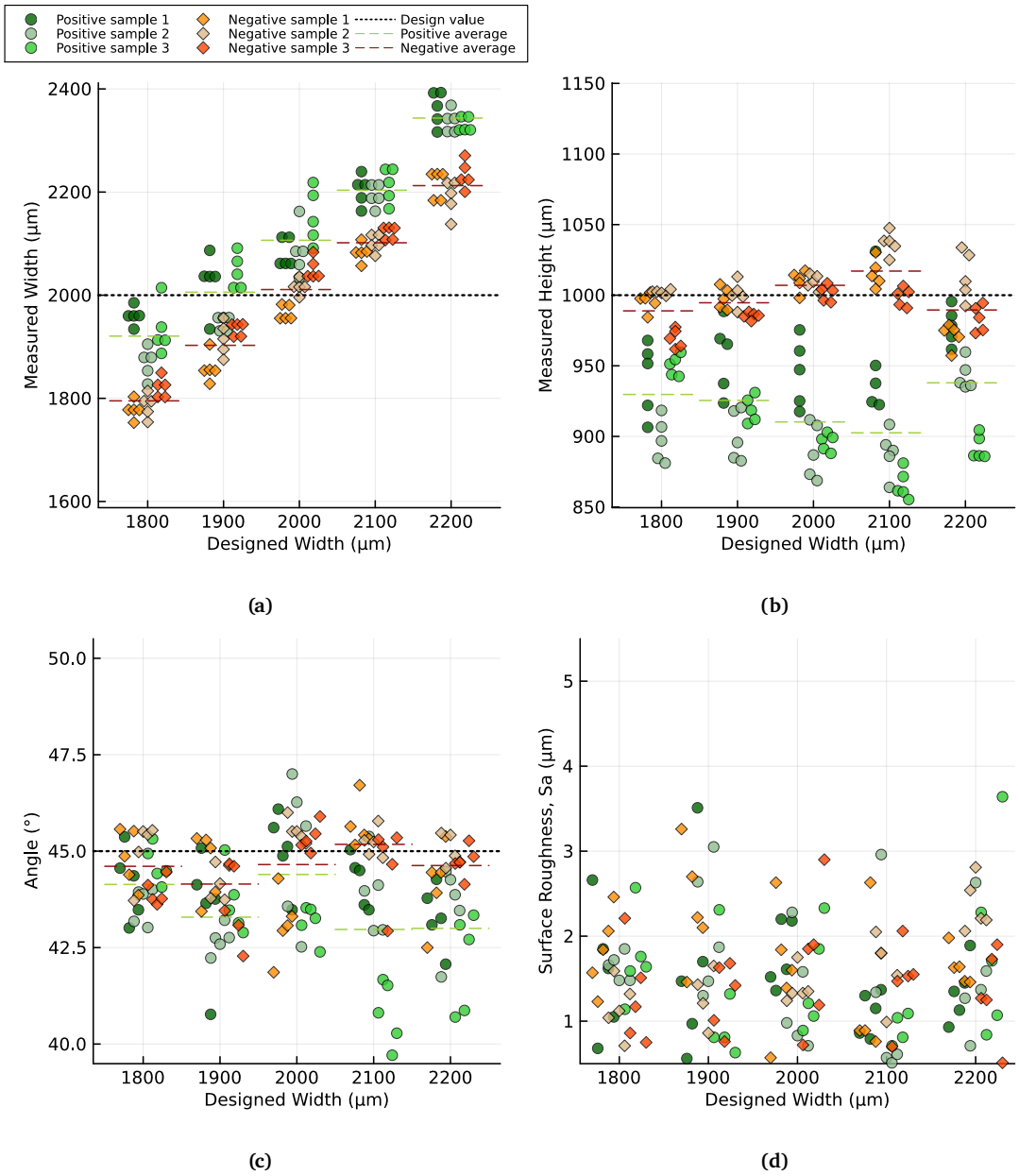

Figure 2.21: Various measurements of the test prints: (b) height, (a) width, (c) base angle and (d) Sa surface roughness.

The goal of performing these measurements is to find the design dimensions to in the end achieve 2x2x1 mm trapezoids. This means that the negative features should be 2x2x1 mm and the positive features should consistently fit inside the negative features. The negative features seem to match both the design width and height very well. The average lays quite closely to all design dimensions with an error of only 100 µm, which is negligiable compared to the design width and height. The positive features have a bigger width and a smaller height than designed. To make the positive and negative feature fit into each other an difference of W = 200 µm should be considered. For the height a difference of H = 100 µm should be sufficient. The errors in the angles are

again uniformly distributed across all dimensions for both the positive and the negative features. With the maximum error being only 5 degrees, this deviation is negligible in the context of mold manufacturing. The surface roughness again lays between 0.5 and 3 µm. Meaning that it corresponds to manufacturing techniques such as turning, milling, drilling and FDM 3D printing Tab. 2.3.

2.4.4. Results Smallest Trapezoids

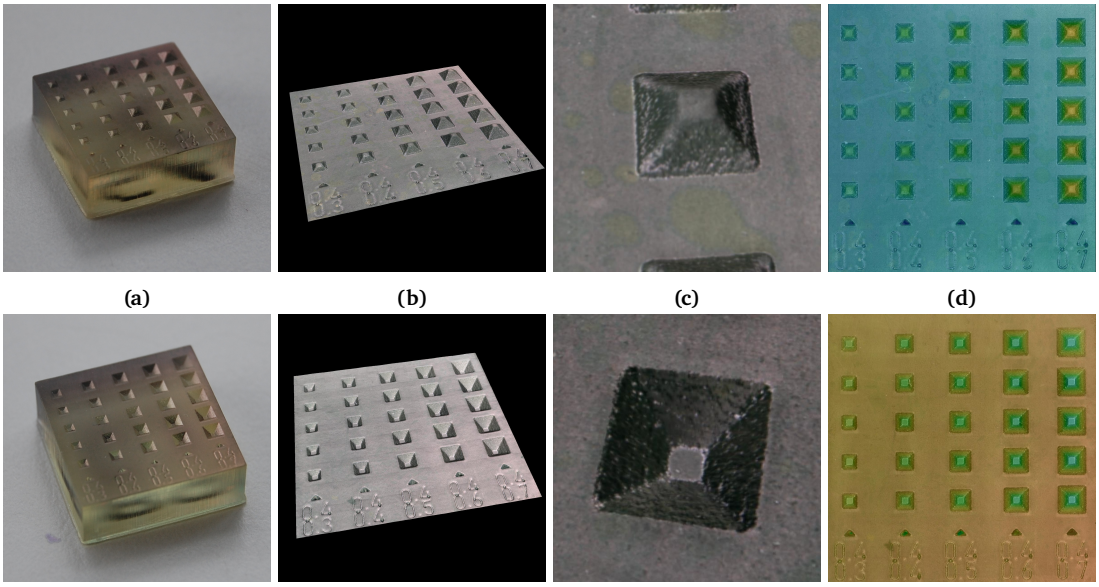

Figure 2.22: For both positive and negative test prints: Picture of the test print (a, e), microscope image of the print (b, f), microscope detail of a single feature (c, g) and height map of the test print (d, h)

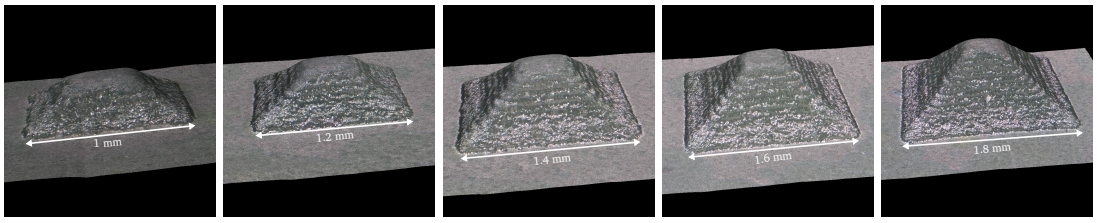

Figure 2.23: Close-up of each of the five feature sizes.

The same minimum width as for the blocks (W = 400 µm) is taken as a starting point for the smallest trapezoid. The design height is the only parameter that it varied across the different test features. A design height of H = 400 µm is the minimum height at which positive features can be printed into a trapezoidal shape. However, the printing lines are highly visible due to the small scale of the features. Despite achieving the trapezoidal shape, the angle of the positive features appears to be lower than intended, which should be taken into consideration when using this dimension in mold printing. Negative features, on the other hand, seem to align more closely with the intended design dimensions.

Print Accuracy and Surface Roughness

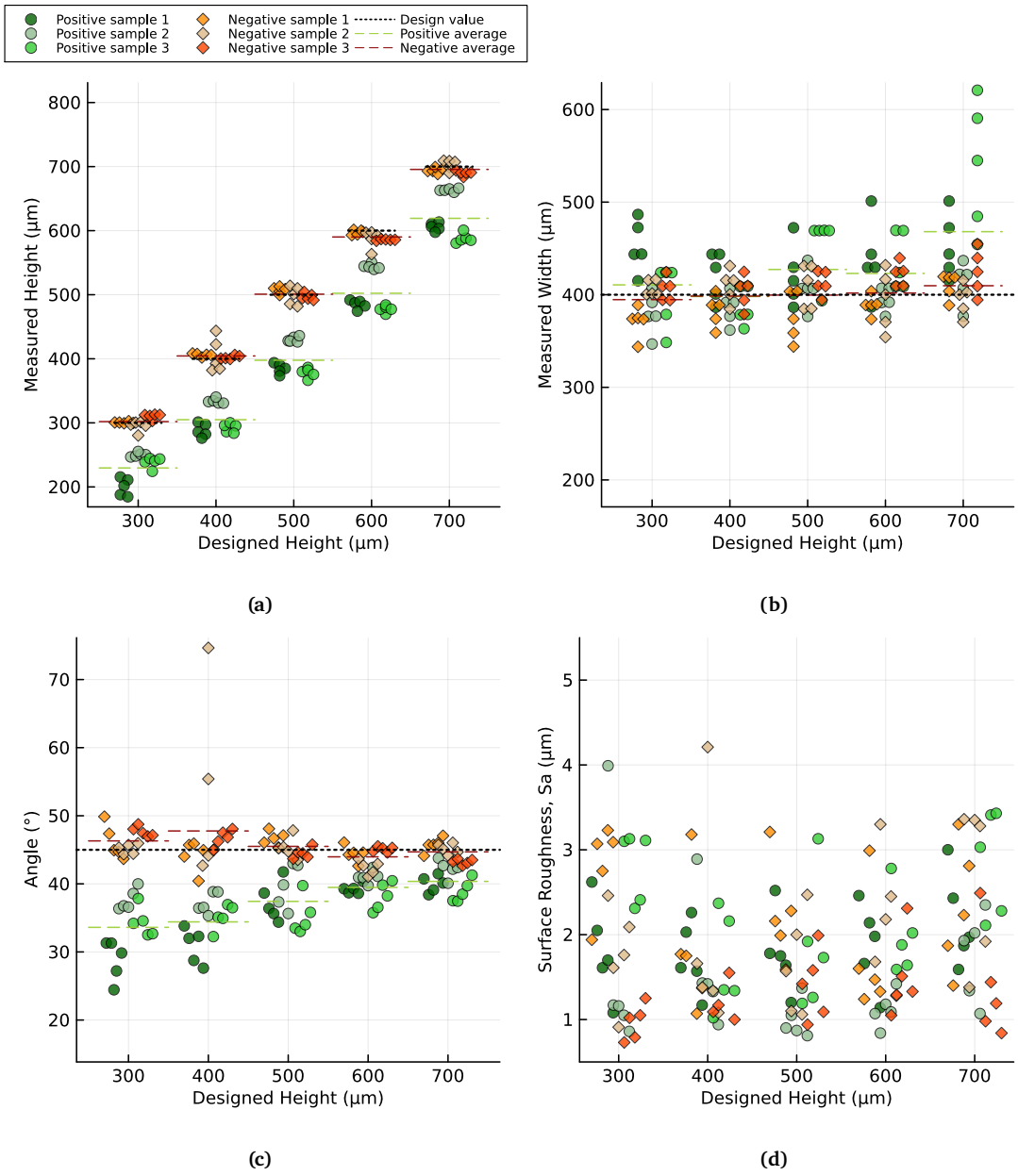

Figure 2.24: Various measurements of the test prints: (a) height, (b) width, (c) base angle and (d) Sa surface roughness

For the positive features, a minimum design height of H = 400 µm is printed into a trapezoidal shape. However the rounding effect, that is visible for all geometries, takes up such a substantial part of the features, that the positive features turn out to be less tall than designed. Due to the same reason the resulting angle is 10 to 15 degrees lower than specified. In contrast, the negative trapezoids match the intended design more closely in terms of width, height, and angle. This means that for small features the rounding effect overshadows the bleeding effect. Due to the reduced angle observed in the positive features, the width of the negative features should be slightly increased, with an additional 100 µm expected to be sufficient. No tolerances appear to be necessary for the height.

2.4.5. Results Tensile Strength Resin

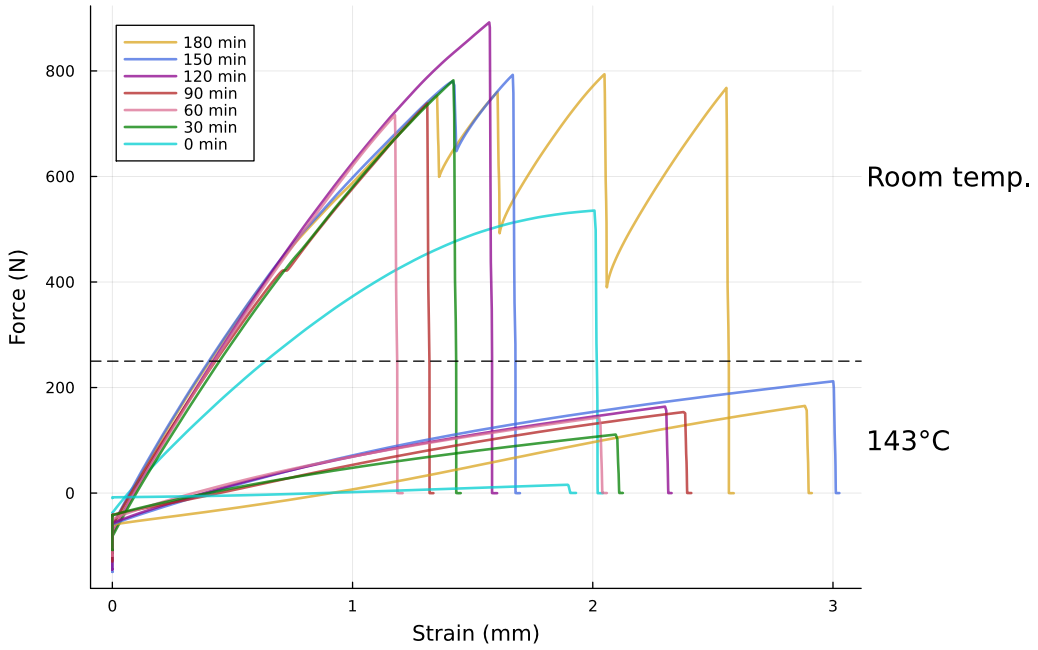

Figure 2.25: Results of the tensile test of the mold material, with post-curing times ranging from 0 to 180 minutes.

To research the effect of post-curing on the tensile strength of the mold material, tensile tests were conducted both at room temperature and at 143°C, which corresponds to the operating temperature of the hot forming process.

In the tensile test graphs, most measurement lines start at a negative force value. This anomaly is attributed to limitations in the testing setup. During the tightening of the bolts, the clamps tend to move slightly towards each other, compressing the test sample and causing the sample to 'push outwards' from the beginning. Since the tensile testing machine is programmed to control the position, it maintains this initial position by pushing instead of pulling, resulting in a negative force reading. Consequently, the initial strain measurements are inaccurate, as the sample is not yet being stretched from the start. However, this phenomenon does not affect the accuracy of the tensile strengths.

The graph indicates a substantial decrease in tensile strength, approximately by a factor of four, when the temperature increases from room temperature to 143°C. This reduction is likely due to the increased mobility of the polymer chains at higher temperatures.

At room temperature, post-curing for 120 minutes yields the highest tensile strength. This superior performance is likely due to the formation of additional bonds during the extended post-curing period. Conversely, post-curing for both 150 and 180 minutes results in lower tensile strength, with the samples exhibiting multiple small cracks during testing, leading to sharp local drops in force. Next to increased tensile strength, the additional bonds also cause increased hardness, the small cracks indicate that those samples are more brittle compared to shorter post curing durations. At 143°C, the sample with a post-curing time of 150 minutes achieves the highest tensile strength.

2.5. Conclusion Mold Manufacturing

This chapter successfully resin printed various molds with diverse geometries, including rounded cylinders, blocks and trapezoids, suitable for hot forming.

Key variables influencing the mold output in resin printing include the cleaning procedure, post-curing, and layer thickness. The four most critical requirements for molds were analysed for the different feature designs, including printing accuracy, repeatability, surface roughness and tensile strength. Rounded cylinders were printed with the goal to achieve features with an aspect ratio of 1:2, 1:3, 1:4, and 1:5. The error in accuracy ranged from 20 to 150 µm for the widths and 50 to 125 µm for the height of the features, the repeatability gave a difference of 20 µm and 125 µm, between different prints and within a single print respectively, and the base angles gave a maximum error of 3 degrees. Blocks with dimensions of 400x400x100 µm, proved to be the smallest printable features, and gave a printing accuracy of 40 µm. For the smallest trapezoids the same width and depth dimensions were used as for the blocks, the height however increased to 400 µm, to accommodate for the sloped walls. Finally, for 2x2x1 mm trapezoids an accuracy of 50 µm was achieved, a repeatability of 75 µm and an error in base angle of approximately 2 degrees.

Overall, the error value in printing accuracy, ranging from 20 to 150 µm, has proven to be for the biggest part size-independent. For the features smaller than 500 µm, the errors constitute a significant portion of the dimensions. The primary source of this error was attributed to bleeding during the printing process, which caused positive features to be larger than their negative counterparts. However, in the case of the smallest features analyzed, negative features were found to be larger than positive ones due to significant edge rounding effects that caused the positive features to be smaller than designed. Although the relatively significant error in small features diminishes precision, the issue is effectively offset by the high repeatability between different prints. These findings, however, are closely linked to the printer and resin used, and variations in results may occur with different equipment and materials.

The surface roughness results exhibited a wide range, from values similar to turned parts to those of FDM 3D-printed parts, making it difficult to draw definitive conclusions about the surface roughness of resin-printed molds. The tensile strength of the resin material was found to be four times lower at the hot forming temperature compared to room temperature, measuring 52 MPa and 13 MPa, respectively. An extension of the post-curing time from 120 to 150 minutes resulted in a 3 MPa increase in tensile strength, an increment considered negligible.

2.6. Chosen strategy

In this section the manufacturing strategy is discussed for the molds that are used for the hot forming experiments in the next chapter. For each mold design the dimensions are explained together with any modifications from the cleaning recipe discussed in Section 2.3.3.

	Width			Height		
Feature	Objective (µm)	Positive Features (µm)	Negative Features (µm)	Objective (µm)	Positive Features (µm)	Negative Features (µm)
Cylinder with 1:2 aspect ratio	1750	1550	2150	3500	3400	3700
Cylinder with 1:3 aspect ratio	1750	1550	2150	5250	5150	5450
Cylinder with 1:4 aspect ratio	1750	1550	2150	7000	6900	7200
Cylinder with 1:5 aspect ratio	1750	1550	2150	8750	8650	8950
Smallest blocks	400	400	600	100	100	300
Trapezoids 2x2 mm	2000	1800	2000	1000	900	1100
Trapezoids 4x4 mm uniform thickness	4000	3800	4000	2000	1900	2100
Trapezoids 4x4 mm non-uniform thickness	3700	3800	3700	2000	1900	2100
Smallest trapezoids	400	400	600	400	400	600

Table 2.4: The feature design dimensions for the molds used for hot forming in Ch. 3.

In Tab. 2.4 the design dimensions are depicted for the molds that are used for the hot forming process. For the cylindrical features, both the design width and height are increased compared to the results from Appendix A.1. Tolerances of W = 400 µm and H = 200 µm show friction when pressing the molds onto each other. Therefore the difference in width and height between the positive and negative features is increased to respectively 600 µm and 300 µm. Furthermore, to improve the ease of cleaning of the negative features, a small cleaning tool will be printed, to help removing the uncured resin from the negative cylindrical features. The tool is inserted into the negative features, to press out the majority of the uncured resin. This enables the solvent to more easily enter the features are remove the last resin residues sticking to the walls. Since the cleaning tool is printed from the same resin, it is unlikely to damage the features due to their equivalent hardness The cleaning tool is shown in Fig. 2.26.

In contrary to what was found in Section 2.4, after printing the molds for the blocks and the trapezoids, a design height difference of 100 µm didn't prove to be enough for the positive and negative molds to fit well onto each other. Therefore a height difference of 200 µm is chosen for these features.

The OpenSCAD molds designs that are used for the hot forming process in the next chapter are depicted in Appendix B. The OpenSCAD code can be found in Appendix C.2

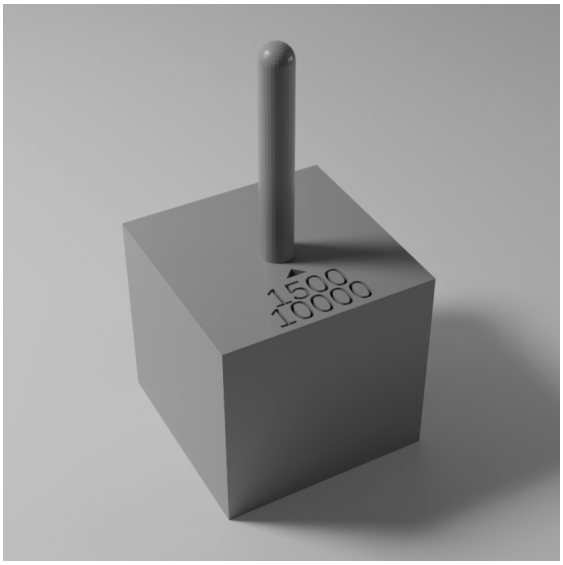

Figure 2.26: Render of the cleaning tool used for the negative cylindrical features.

3

Hot Forming

In the previous chapter, molds suitable for the hot forming process were resin printed. In this chapter the hot forming experiments are performed to develop a proof of concept for hot forming Polyether Ether Ketone (PEEK) sheets with resin printed polymer molds. The objectives for the hot forming process are first defined, followed by an explanation of the process steps, an overview of all parameters involved, and a detailed description of the measurements performed to quantify the results. Subsequently, the results are presented, and a conclusion is drawn regarding the feasibility of the hot forming process.

3.1. Hot forming objectives

The focus of this chapter lays on testing the hot forming process to determine its possibilities, this knowledge will then be applied to test the accuracy in replicating trapezoids, a simplified design of the metamaterial features. Lastly, the effects of the hot forming process on the material properties of the substrates is researched.

In the first step, the process parameters necessary to replicate a structure using this manufacturing method are researched. Subsequently, the size limitations will be examined to determine if the smallest feature that can be resin printed can also be formed. Additionally, the maximum stretch that can be applied to the PEEK substrates will be assessed. Both aspects are crucial for the metamaterial: the goal is to reduce the size of the metamaterial, which is primarily limited by the size of its features. Investigating the feasibility of manufacturing the smallest printable feature aids in estimating the potential size reduction of the metamaterial. Moreover, in the final metamaterial design, the sides

must buckle, which can be achieved by designing a thickness variation within the feature to predict the buckling location upon applying force. Researching the maximum stretch helps identify how thin the material can be made and if these thin sections introduce any issues, such as demolding problems. Understanding the limits of thickness variation informs the achievable range of thickness differences.

After finding the hot forming possibilities, simplified features of the metamaterial will be formed. The first objective is to assess the replication accuracy of the dimensions currently at the limit within the stacking area. Subsequently, the possible size reduction of this simplified model will be researched using the smallest printable feature size. Furthermore, a non-uniform thickness within a single substrate feature will also be attempted.

Lastly, the chapter explores whether the process influences the PEEK material properties. This will be investigated by performing tensile tests on the PEEK sheets, under various conditions and heat treatments, to observe potential effects on PEEK during and after hot forming.

3.2. Materials and Methods

3.2.1. Process steps

Two hot forming setups will be considered in this research. One setup with heating plates and one configuration using a heating chamber. Both processes consists of four steps: heating, forming, cooling and demolding.

Setup with heating plates

In the first step the molds are heated before the hot molds are pressed onto each other forming the substrate placed in between. In this configuration, the substrate is heated only when in direct contact with both molds, resulting in a very short heating time. Theoretically, the molds should be cooled down to a temperature well below the glass transition temperature, to prevent substrate deformation during removal. However, due to the low thermal capacity of the thin sheet, it is assumed that cooling the molds is not necessary. As soon as the PEEK sheet loses contact with the molds, it will cool instantly, removing the risk of deformation during demolding.

Setup with heating chamber

In this configuration, the molds are placed in a closed chamber that is kept at the forming temperature. This setup ensures that not only the molds but also the substrate is uniformly heated. The primary advantage of this setup is that the substrate is consistently maintained near the glass transition temperature.

3.2.2. Variables in Hot Forming

This section explains all process parameters and output variables relevant in hot forming

Forming Temperature

The forming temperature is the temperature required to shape the substrate. For this process, the forming temperature is set at the glass transition temperature (T_g) of PEEK, which is 143°C. While the range of feasible temperatures is relatively broad, excessively

high temperatures can alter the material properties of the PEEK substrate, whereas temperatures that are too low result in the substrate retaining its elasticity, causing it to rebound after the forming force is removed. For this application, maintaining the integrity of the PEEK substrate's material properties and achieving high replication quality are critical to ensuring that the layers fit perfectly and that the metamaterial behaves as expected.

Forming Force

The forming force is the pressure applied to press the two molds together. Once the substrate reaches its glass transition temperature, a small force is sufficient to plastically deform the material. However, in the open configuration, sufficient contact is required for effective heat transfer from the molds to the substrate, potentially necessitating a higher forming force than in the closed setup. The upper limit of the forming force is constrained by the structural limits of the molds, which can fail if the force is too high.

Settling Time

The settling time, applicable only to the closed configuration, is the duration for which the temperature is maintained constant after reaching the forming temperature and before applying the pressing force. This period allows all components in the heated chamber to uniformly reach the forming temperature. If the settling time is too short, there may be a discrepancy between the sensor reading and the actual temperature of the molds and substrate. In this research a constant settling time of 2 minutes is used to ensure uniform heat distribution.

Pressing Time

The pressing time is the duration for which the molds are pressed together. Insufficient pressing time does not allow the material to flow adequately, resulting in less defined corners and lower resolution of small-scale features.

Substrate Thickness

Substrate thickness influences the hot forming process as thinner sheets retain more elasticity and thicker sheets limit the size of the features. A general guideline is that the feature width should be a factor of the substrate thickness to ensure effective pressing into the feature geometry and to avoid transitioning into hot embossing [10]. In this research a substrate thickness of 125 µm is used for the hot forming experiments.

Replication Quality

Replication quality assesses how accurately the molds are reproduced during the hot forming process. This can be evaluated by checking for detailed replication, such as the sharpness of edges and dimensions like feature height and width. For this research the replication quality is only assessed by visual inspection.

Tensile Strength

Tensile strength is a critical variable of the hot forming process, particularly for the PEEK substrate used in this research. High forming temperatures may cause the substrate material to transition from a semi-crystalline to an amorphous state, resulting in changes to its crystal structure, increased opacity, and altered mechanical properties.

Repeatability

Repeatability is a crucial factor, for achieving the final goal of developing a metamaterial that meets industry standards. However, given the difficulties in accurately measuring substrate thickness variations, it is impractical to prioritize this aspect in this research.

3.2.3. Materials

The 125 µm PEEK sheets that are used in the hot forming process have the following specifications.

Material property	Value
Density	1.26 to 1.32 g/cm^3
Maximum Operating Temperature	+200 °C
Thermal Conductivity	0.25 W/mK
Dielectric Strength	190 kV

Table 3.1: Material properties of the PEEK sheets used in the hot forming process [19].

3.2.4. Experiments

In this section the hot forming experiments are explained. Three different geometries are researched to find the dimensional limits of hot forming. First, rounded cylinders are employed to identify the maximum stretch achievable through hot forming. Subsequently, blocks are used to assess the minimum feature size that is feasible within the hot forming process. Lastly, trapezoids are examined, as they represent a simplified design of the unit cells in the metamaterial shown in Fig. 1.1. The findings of this analysis are used to assess the suitability of hot forming for manufacturing the metamaterial.

Maximum Stretch in Hot Forming

In the first experiments cylindrical features are formed find the largest stretch is that can be achieved with hot forming. Rounded cylinders with increasing aspect ratios are used to find the limits of the process. It is expected that the substrate will start to tear and/or wrinkle at the limit. The experiments will be performed with both heating plate and the heating chamber setups. The setup with the heating plates is expected to have a lower maximum stretch due to the uneven temperature distribution from the heating plates across the molds and substrate. The tops of the rounded cylinders are expected to be cooler than the bases of the pins, potentially causing the substrate to cool below its formable range. In contract, in the heating chamber all components are kept at the hot forming temperature, ensuring that the substrate remains within the forming range, which should yield a higher maximum stretch.

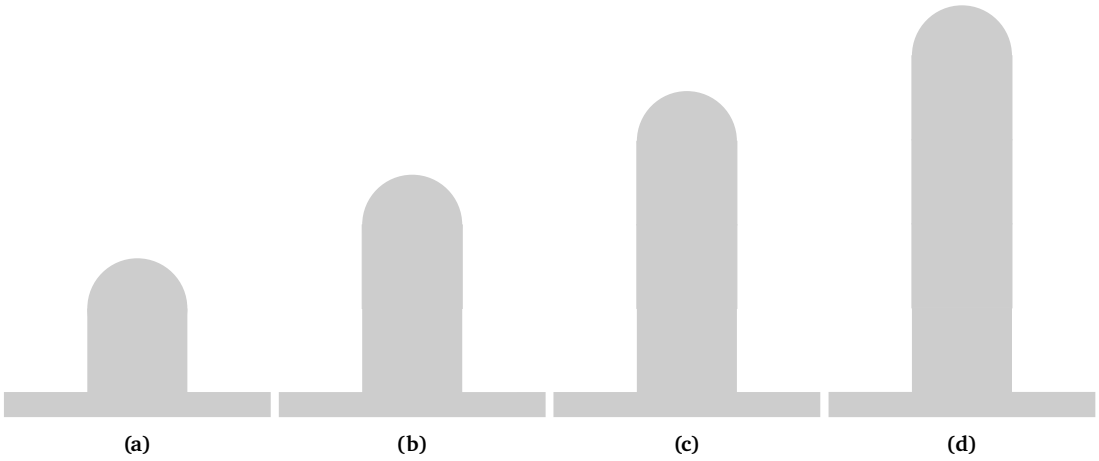

Figure 3.1: 2D schematics of the rounded cylinders with aspect ratios from 1:2 (a) to 1:5 (d)

Smallest Feature in Hot Forming

In the second set of experiments, blocks are hot formed since they represent the smallest features that can be printed. This is done to determine whether it is feasible to hot form the smallest printable feature using the setups employed in this research.

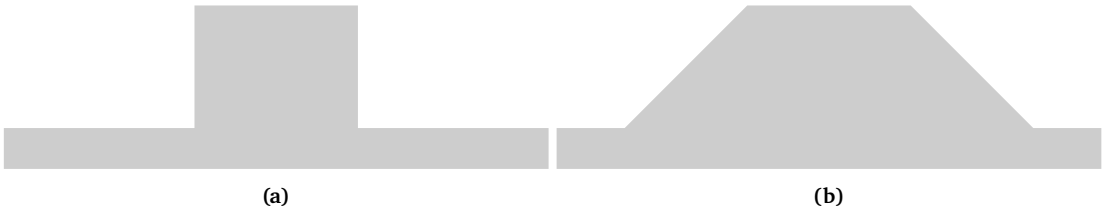

Figure 3.2: Schematic view of features with a block shape (a) and the trapezoid shape (b)

Hot Forming of Trapezoids

Various trapezoidal features are hot formed to estimate whether hot forming is suitable for the manufacturing of the MECOMOS metamaterial. Trapezoids are chosen as they can be considered a simplified design of the MECOMOS metamaterial shown in Fig. 3.3. Different variations of the trapezoids will be analysed. First trapezoids with a 2x2 mm top area, as they are the current limit of the joining method [15]. Next, the smallest printable trapezoids are hot formed, as a long-term objective is to reduce the size of a unit cell in the metamaterial. Subsequently, trapezoids with non-uniform thickness are hot formed, since in the final operational metamaterial, the sides of the unit cells will likely need to buckle. This process can be facilitated by making the sides thinner than the top and bottom sections. an example of a metamaterial with thin beam elements that buckle is shown in Fig. 3.3. To achieve the non-uniform thickness, Eq. (2.1) is used to adjust Δx, which is visualised in Fig. 3.4. And finally, trapezoids with open geometry are hot formed as they resemble the prototype of the metamaterial the most. The open geometries are achieved by first laser cutting the substrate sheets, before hot forming those sheets. This results in features with beam elements.

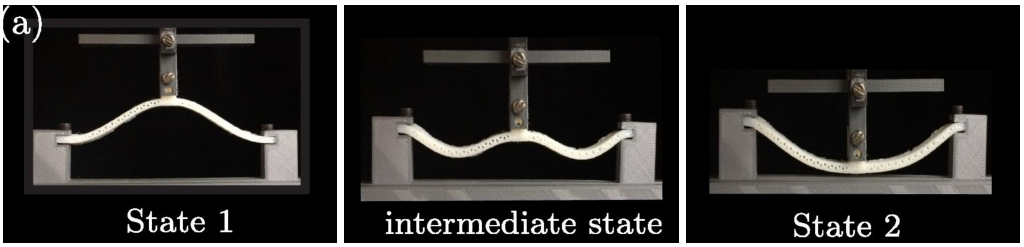

Figure 3.3: Snapshots of a hierarchical beam during the un-axial loading, from [20]

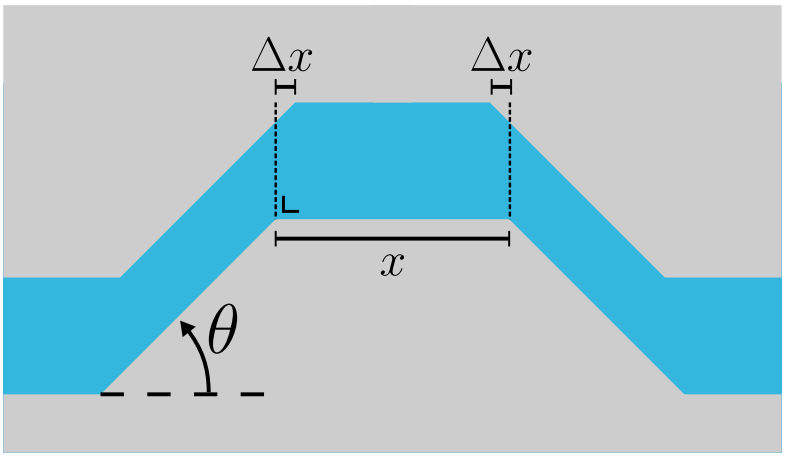

Figure 3.4: Non-uniform thickness of a trapezoid.

Mold lifetime

The life time of the molds is researched by visually inspecting the molds before hot forming, and after 25 and 50 hot forming cycles. Furthermore the maximum load is analysed that the mold can handle.

Stress relaxation

Stress relaxation in polymers is observed when a material, subjected to constant deformation under stable temperature and humidity, shows a decrease in the stress required to sustain the deformation over time. This reduction in stress is attributed to the reorientation of the polymer's long molecular chains, which move towards a more relaxed, lower-energy configuration. Initially, these chains are stretched and aligned in the direction of the applied force, however over time, they gradually return to a more stable state, reducing internal stress while maintaining constant strain. Temperature significantly impacts this process, as elevated temperatures increase the mobility of the polymer chains, facilitating quicker reorientation and therefore accelerating the stress relaxation process [21–24].

To find the effect of stress relaxation on the hot forming parameters, the different components of the hot forming setup are pressed separately and in different combinations to analyse the main source of the stress relaxation that is observed in the hot forming process. The same mold is tested with increasing pressing force, to find the relation between the pressing force and stress relaxation.

PEEK tensile tests

Tensile tests are performed on the PEEK sheets to analyse the PEEK material properties during and after the hot forming process. For the PEEK tensile tests, the PEEK sheets were cut into 2 x 5 cm rectangles. Three different tensile tests are performed to analyse the effect of hot forming on the material properties of PEEK.

The first tensile tests are performed at elevated temperatures ranging from room temperature to 175°C, these tests should provide more information about the material properties during the hot forming process. The second tensile tests are performed at room temperature and the PEEK sheets are heat treated beforehand at 143°C for a duration ranging from 2 minutes to 20 minutes. This should provide a better understanding of the differences between the setup using heating plates and the one using a heating chamber, particularly since the PEEK sheets are exposed to heat for a longer period in the heating chamber compared to the heating plates. The third tensile tests are performed at 143°C, with settling times ranging from 2 minutes to 20 minutes. Providing deeper insight into the changes in material properties during the hot forming process in both the setup with heating plates and the setup with the heating chamber Furthermore tensile tests performed by [15] are analysed to find out if the PEEK material properties are affected by the hot forming process.

3.2.5. Setups

Two setups are used to perform the hot forming experiments.

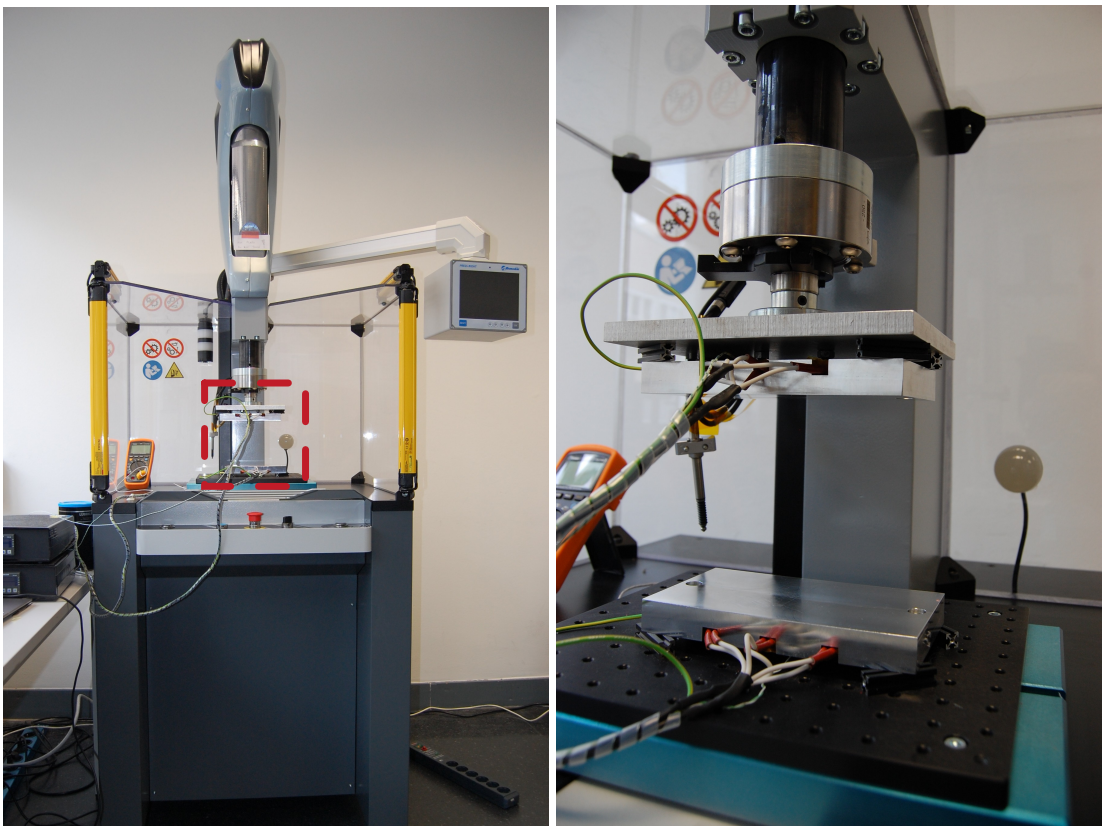

(a) **(b)**

Figure 3.5: Setup of the Alfamatic machine: (a) the complete setup (b) close-up of the indicated region.

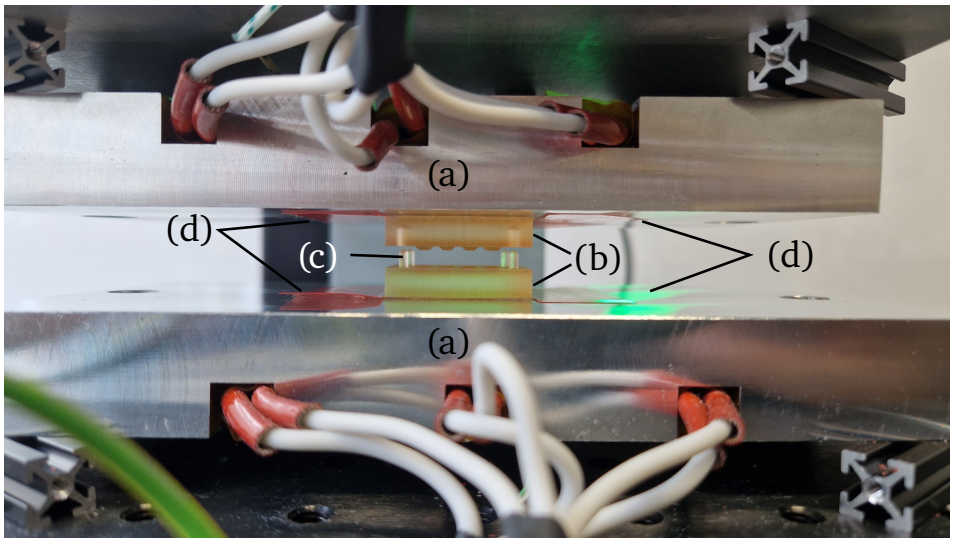

Figure 3.6: Hot forming setup: (a) heating elements, (b) upper- and lower molds, (c) location of substrate and (d) tape.

For the experiments with the heating plates the Alfamatic Electric Press is used.

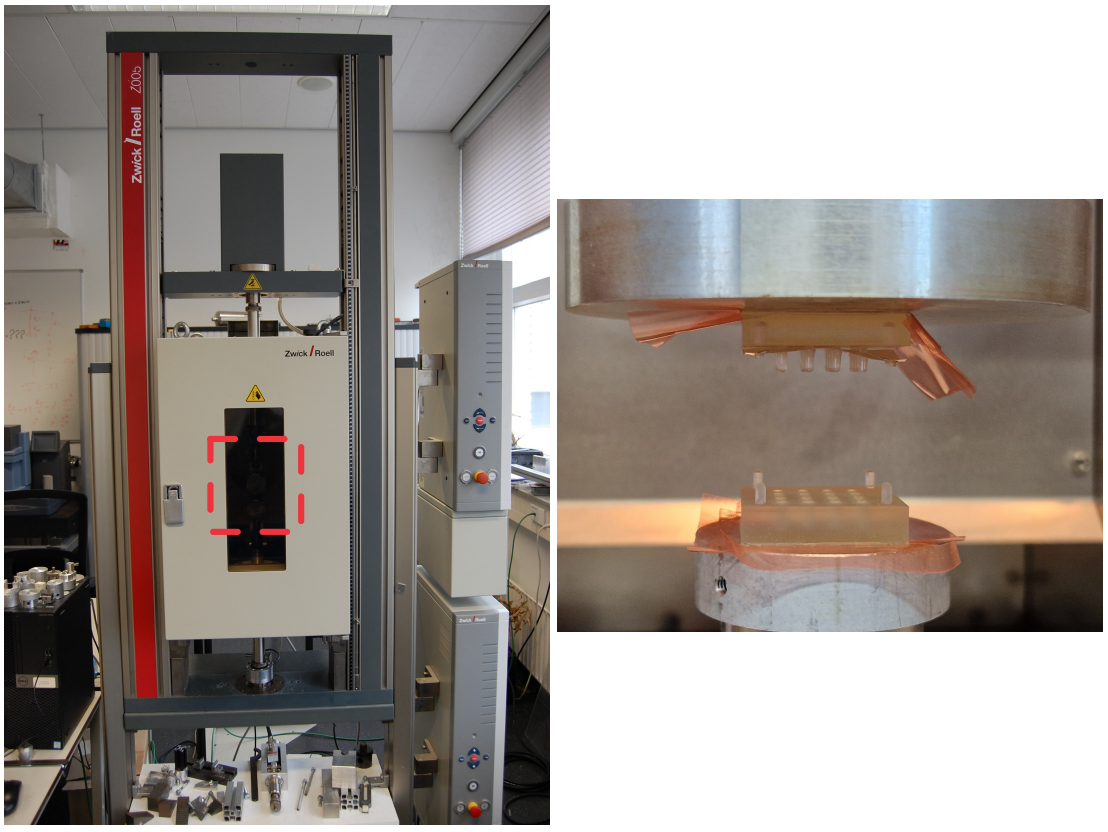

Figure 3.7: Setup of the Zwick machine: (a) the complete setup (b) close-up of the indicated region.

For the experiments with the heating chamber the Zwick Roell 005 press is used. This setup is used to find out whether a closed heating chamber can achieve a higher stretch during hot forming. Therefore this setup is only used for hot forming with the cylindrical features.

3.2.6. Imaging

Due to the flimsy nature of the thin substrates, the dimensions of the formed substrates won't be measured as these measurements would be very unreliable. The replication quality is therefore solely determined by visually analysing images taken with the Keyence microscope and a regular camera. To research the effect of hot forming on the material properties of the PEEK sheets, tensile tests are performed with the Zwick Roell 005. And lastly, to analyse the heat distribution and heat conductivity, thermal images are captured with a the FLIR E75 IR Camera.

3.3. Results and Discussion

This section shows the hot forming results. First the process parameters are discussed, followed by the hot forming results for each of the geometries. Lastly, the results of the heat measurements and the results of the tensile tests of the PEEK samples are presented.

3.3.1. Process Parameters

In this section the process parameters of hot forming are discussed.

Variable	Heating plates setup	Heating chamber setup
Forming temperature (°C)	100 - 150	140 - 150
Force (N)	1000 & 3000	700 - 800
Settling time (s)	-	120
Approach speed (mm/s)	6	2
Pressing time (s)	60	60
Demolding temperature (°C)	100 - 150	80 - 100

Table 3.2: Parameters used during hot forming.

The forming temperature proves to be very forgiving, suitable forming temperatures span from 100 to 150°C. Especially the setup with the heating plates has a large range for the forming temperature. The heat distribution within the molds was suboptimal, resulting in a significant temperature disparity between the top and bottom of the molds. While the bottom, in direct contact with the heating plate, reached temperatures between 140 and 150°C, the top portions only attained temperatures between 100 and 110°C. When the molds were pressed together, the increased conductivity allowed the substrate to reach temperatures above 110°C, as it eventually made full contact with the negative features, which were as hot as the bottom of the molds. However, this effect diminished with very thin features, as the negative features did not extend deep enough, maintaining temperatures between 100 and 110°C.

With the open setup 1 kN was used for the larger features and 3 kN was used for the smaller features, as more force was required to press the substrate into the small details of the negative molds. For the closed setup the force was set to 750 N, the maximum force that the machine would allow, which proved to be well within the hot forming limits showing that hot forming is a very forgivable manufacturing method.

The speed at with the molds move towards each other is set to 6 and 2 mm/s, for the open and closed setups respectively. 6mm/s is the lowest setting in the open setup, while for the closed setup 2 mm/s was chosen to reduce the risk of substrate tearing due to stress concentrations. For both setups the pressing time was set to 60 seconds. In the closed setup a settling time of 2 minutes was used, while a settling time isn't part of the process in the open setup.

3.3.2. Maximum Stretch in Hot Forming

By hot forming features with increasing aspect ratios, we can find the largest stretch that can be applied to a PEEK substrate.

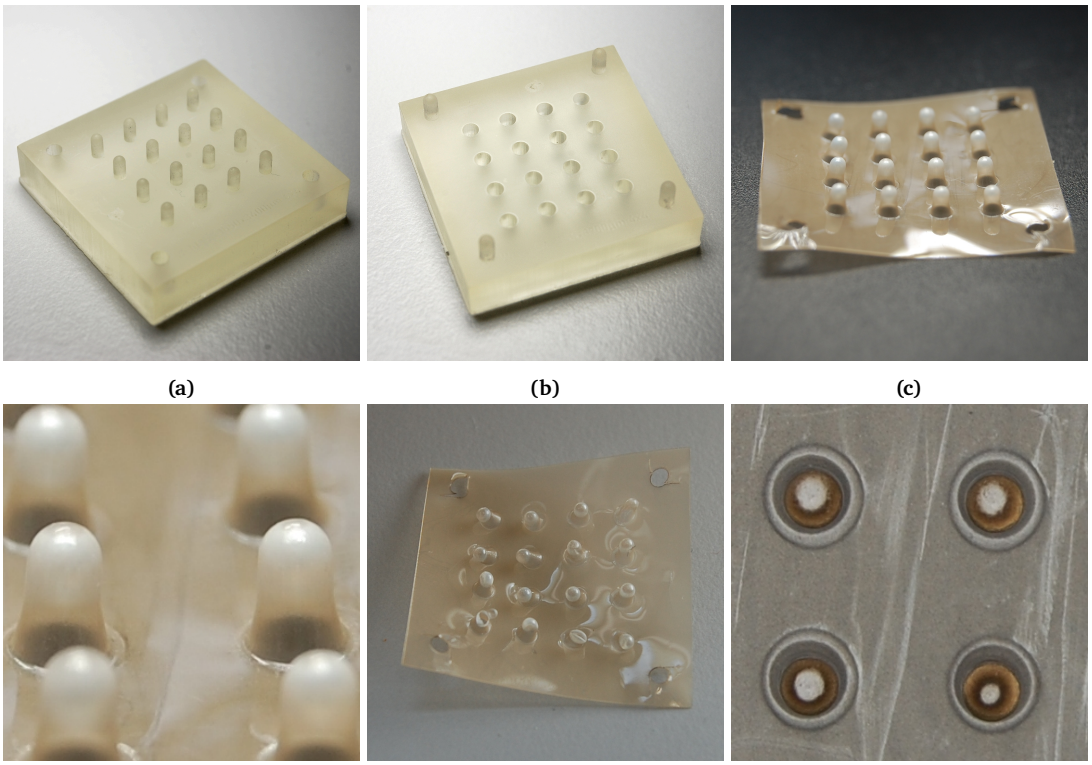

Figure 3.8: Mold and substrate belonging to aspect ratio 1:2: (a) positive mold, (b) negative mold, (c) subtrate, (d) substrate detail, (e) example of demolding issues and (f) substrate detail of flow.

Fig. 3.8 shows the result of hot forming the 1:2 aspect ratio in the open setup. The features are replicated well. In Fig. 3.8c formed substrate with high replication quality is shown, achieved by wiggling carefully to prevent deformations during demolding. Fig. 3.8e shows the deformation introduced by high demolding forces. White tips are seen at the top of each feature caused by the large stretch for each feature. Next to the white tips, light circles are visible at the base of each feature. This indicates thinning of the area directly surrounding the features, indicating the direction of the flow of the substrate material. The material is initially present at these thin areas, and flows towards the features to allow for the stretch.

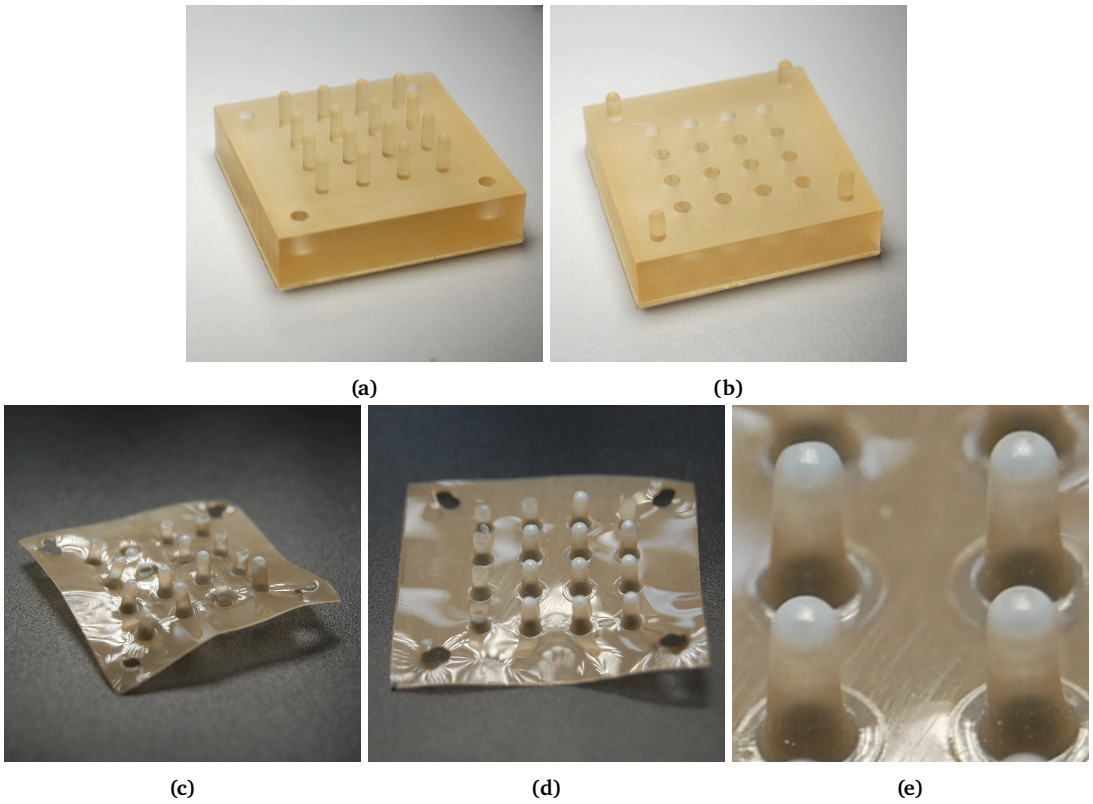

(a) (b)

(c) (d) (e)

Figure 3.9: Positive (a) and negative (b) molds belonging to aspect ratio 1:3, with corresponding substrates of the setup with heating plates (c) and the heating chamber (d), (e) shows a close-up of the features of the heating chamber.

With the setup with the heating plates it is possible to replicate a 1:3 aspect ratio, but demolding problems are inevitable in that case. Some tears at the tips are visible together with large feature deformations Fig. 3.9c. The setup with the heating chamber didn't encounter any problems with the 1:3 aspect ratio, during demolding however large stress concentrations also caused some outer features to tear Fig. 3.9d. The thin circles surrounding the features are larger for the 1:3 features as opposed to the 1:2 ratio, indicating that more material flow is required to allow for the stretch Fig. 3.9e.

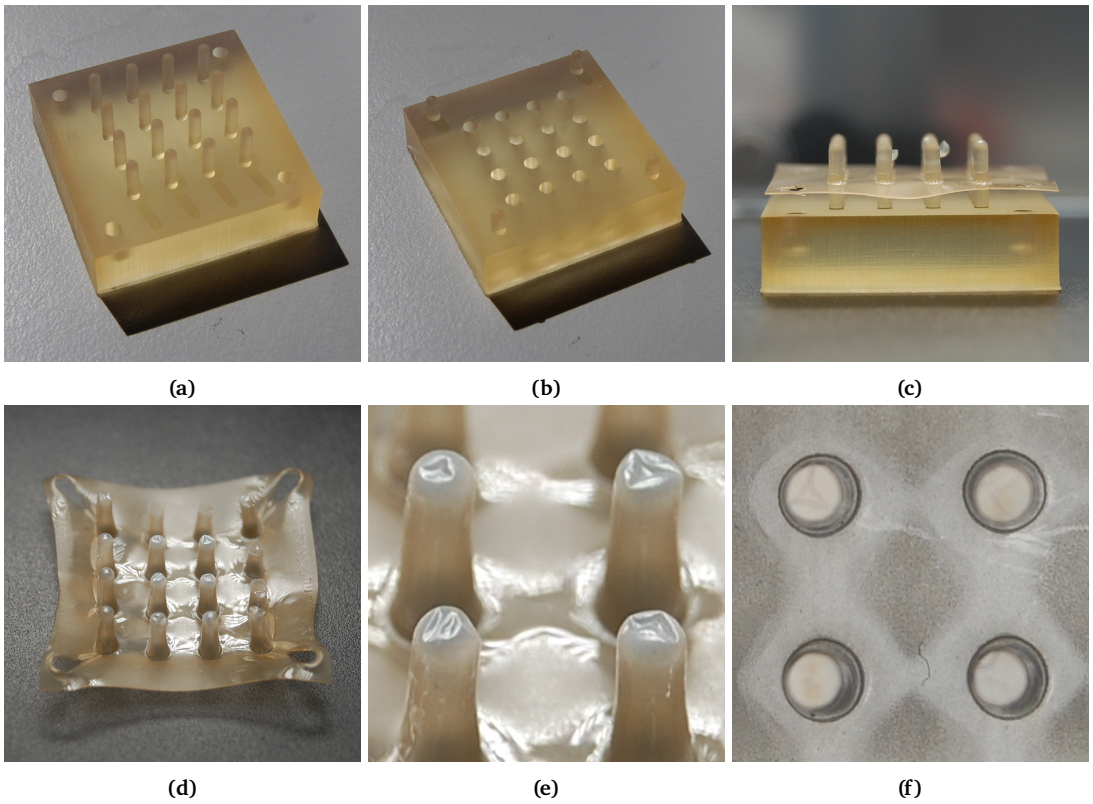

Figure 3.10: Positive (a) and negative (b) molds belonging to aspect ratio 1:4, with corresponding substrates of the setup with heating plates (c) and the heating chamber (d), with close-ups (e,f)

For the Alfamatic setup, the substrate can't be stretched completely over the 1:4 features, as seen in Fig. 3.10c. This is caused by the non-uniform heat distribution in this setup, resulting in the tips of the pins being significantly colder than the base of the molds. When the substrate is in full contact with those pins, its temperature will drop to below its forming temperature, not allowing for any further forming. Fig. 3.10d shows that the 1:4 molds aren't a problem for the Zwick configuration, however wrinkling is visible at the tops of the features, This indicates that wrinkling only occurs for large stretches when the substrate is maintained at the forming temperature, while tearing indicates a high stress concentration for temperatures below the forming temperature. Moreover, due to the large stretch more material will flow in the substrate, resulting in diamond shaped thinning of the substrate instead of the perfect circles that we have seen with the 1:2 and 1:3 features. This is caused by the fact that the stretch is so large that the circles merge into each other Fig. 3.10f. Since both methods fail to properly replicate this shape, hot forming of higher aspect ratios is not performed.

3.3.3. Smallest Feature in Hot Forming

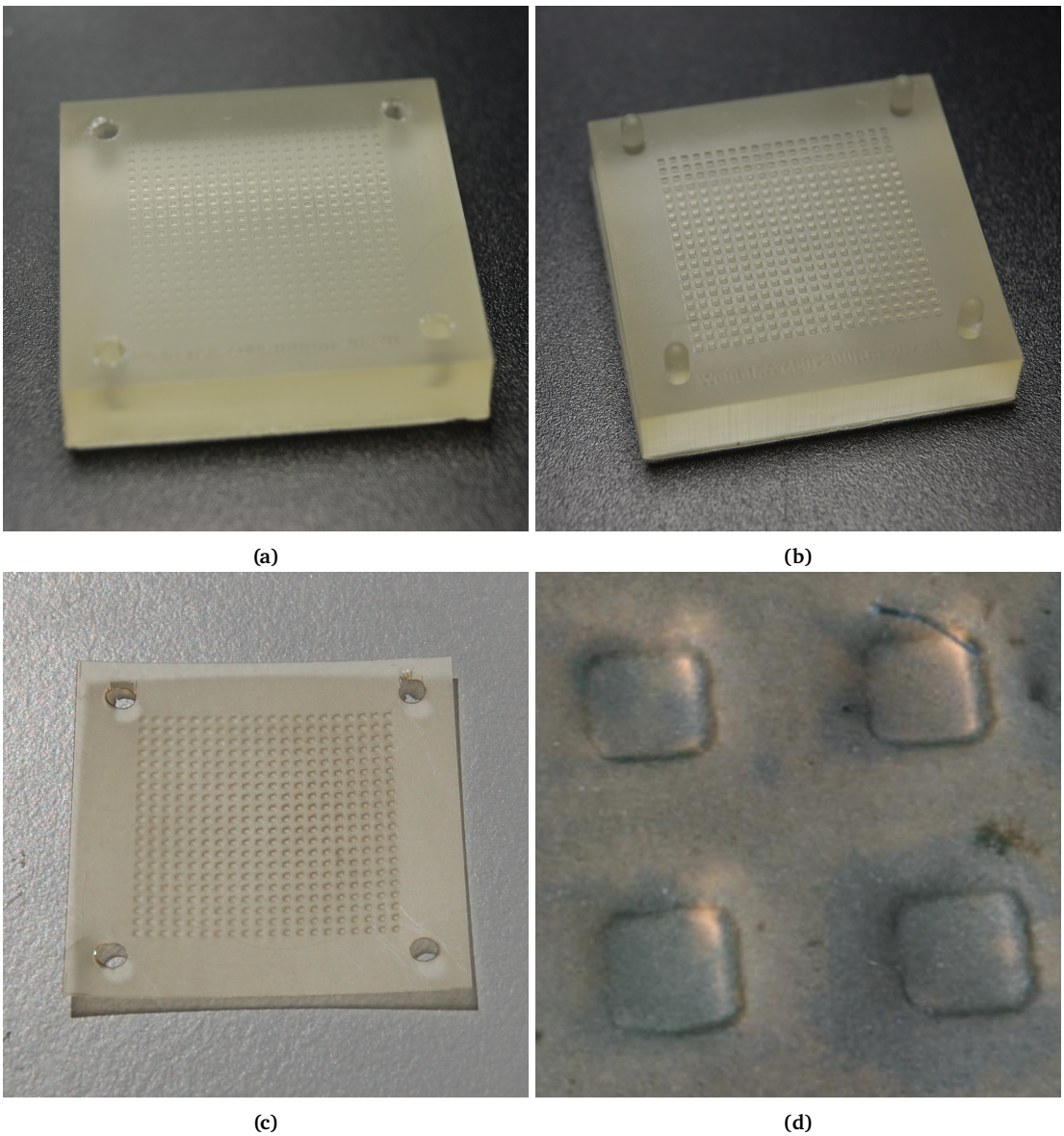

Figure 3.11: (a) positive and (b) negative mold of the rectangular features, with (c) corresponding substrate. (d) shows a microscope close-up of the substrate.

The replication quality is high for the 400x400x100 µm blocks, however a larger force was required to push the substrate into the molds, 3000 N over the previously used 1000 N. Moreover, the demolding process proceeded without any issues, and since the sheet is 125 µm thick and the features are only 100 µm tall, the resulting stretch remains well below the threshold where demolding issues occur. Thus indicating that the feature size of this proof of concept is limited by the resin printing of the molds and not by the hot forming process.

3.3.4. Trapezoids 2x2x1 mm

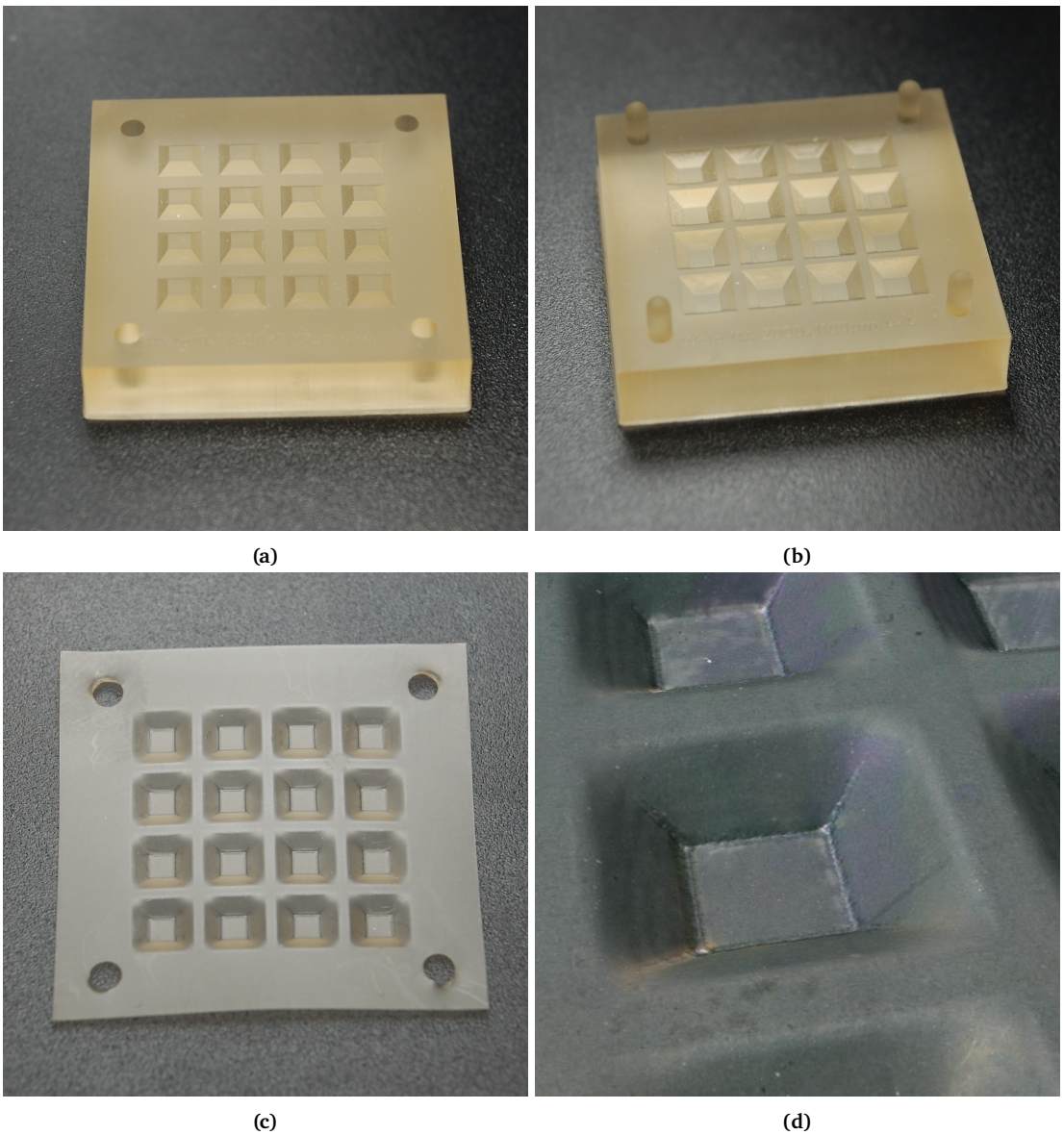

Figure 3.12: 2x2x1 mm trapezoid positive (a) and negative (b) molds, with resulting substrate (c) and microscope close-up of the substrate (d)

Currently, an area of 2x2 mm represents the lower limit of suitable joining methods for constructing the metamaterial. Therefore trapezoids with a top area of 2x2 mm are hot formed to assess the replication of such features. In future research, these features will be joined to form the metamaterial. The replication process yielded high replication quality without encountering any demolding issues. However, slight curvature at the corners suggests that there was some residual space when the molds were pressed together. Suggesting that the molds didn't fit perfectly onto each other, thus indicating that further optimization in mold manufacturing is necessary.

3.3.5. Smallest trapezoids in Hot Forming

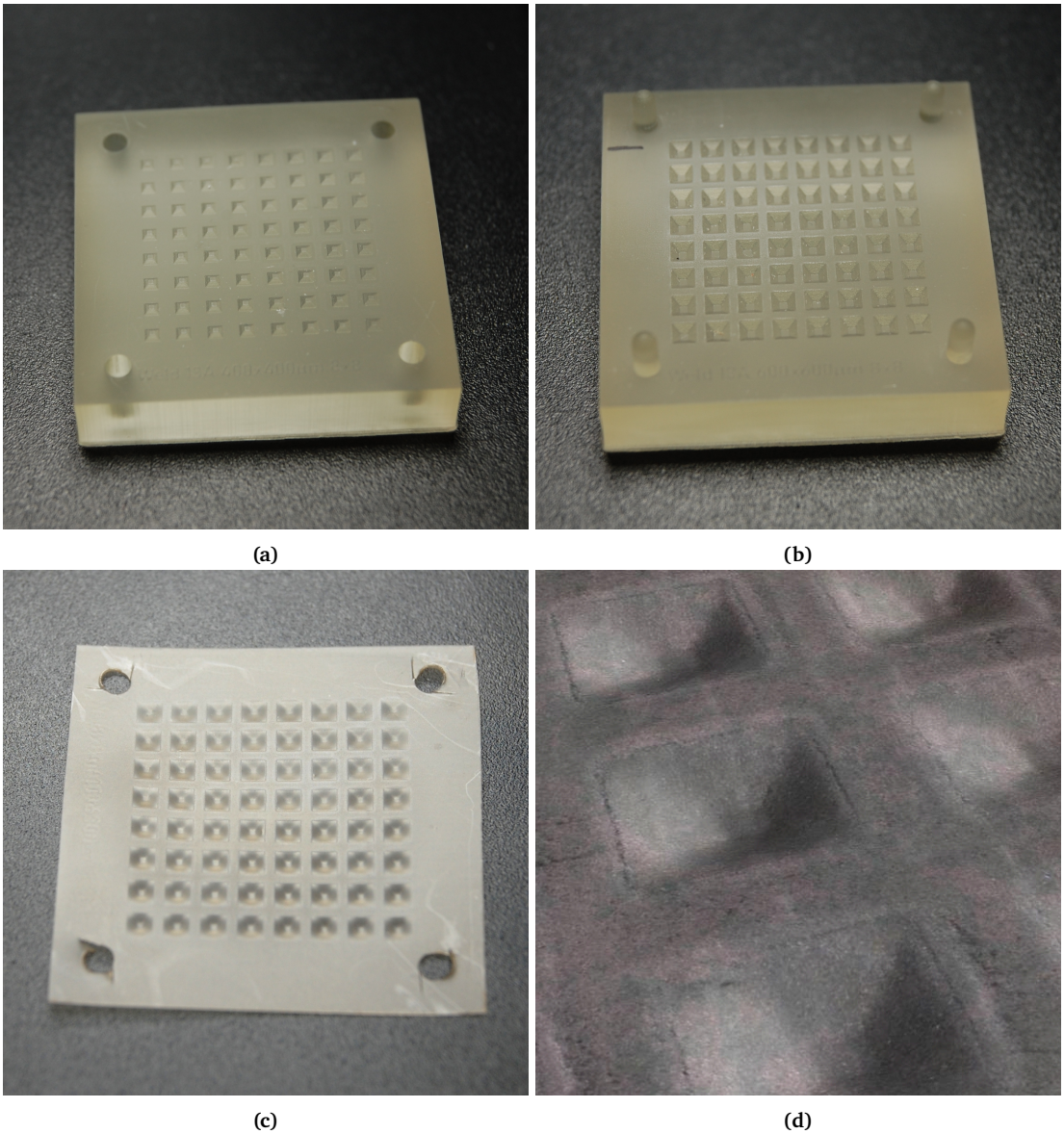

Figure 3.13: 400x400 µm trapezoid positive (a) and negative (b) molds, with resulting substrate (c) and microscope close-up of the substrate (d)

The details of the trapezoidal features weren't replicated perfectly in the substrate. This is probably caused by the molds not fitting well onto each other, due to the angle discrepancy found in Fig. 2.24c. Due to time limitations no additional hot forming experiments have been performed with dimensional adjusted molds. However, with adjusted negative molds, it should be possible to replicate these features, just as well as the smallest blocks.

3.3.6. Trapezoids with non-uniform thickness

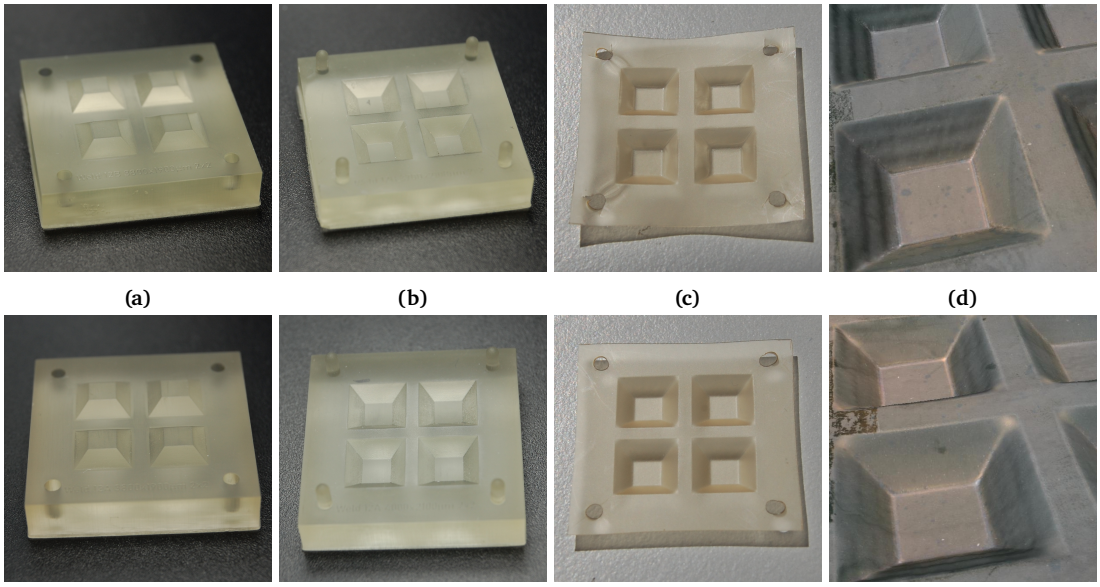

Figure 3.14: Trapezoid mold with non-uniform thickness (top) and control mold with uniform thickness (bottom): (a,e) positive molds, (b,f) negative molds, (c,g) substrate and (e,h) microscope close-up of the substrates.

To facilitate the buckling required to obtain the multi-stable metamaterial shown in Fig. 1.1 an attempt was made to hot form features with a non-uniform thickness. This should result in a decrease of the thickness of the side walls, while maintaining the thicknesses at the top and bottom of the features. This non-uniform thickness is achieved by decreasing the Δx shown in Fig. 3.4. For a Δx of 75 µm, the results are shown in Figs. 3.14c and 3.14d. The formed substrates however didn't show any thickness variations, only the edges and corners were sharper than with a uniform thickness as shown in the control feature shown in Figs. 3.14g and 3.14h.

The reason why this approach doesn't lead to a non-uniform thickness is because the non-uniformity is attempted by squeezing the substrate in a narrow space instead of stretching it further similar to the features with increasing aspect ratios. Increasing the compression will cause the material to flow more effectively into the finer details; however, the substrate will not thin out since the material cannot escape to somewhere else. To achieve non-uniform thickness, a multiple step forming process is required where the substrate is first thinned out, before hot forming it.

3.3.7. Trapezoids with open geometries

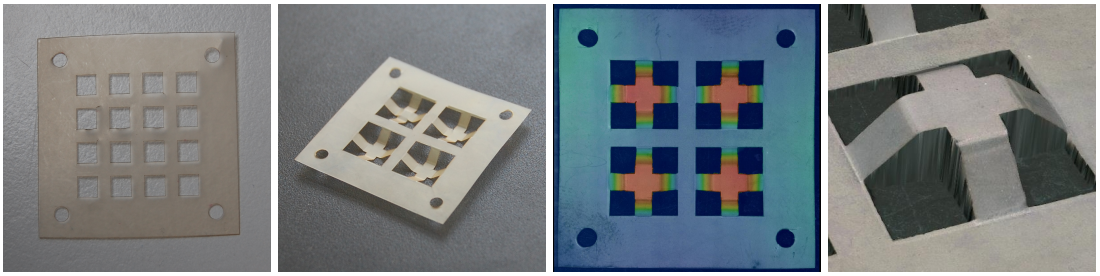

(a) (b) (c) (d)

Figure 3.15: Unformed (a) and formed (b) laser-cut substrate to create open trapezoidal features, (c) height map of the formed substrate, (d) microscope close-up of a feature.

To achieve a multi-stable unit cells, the eventual design most likely will be an open geometry. To find out if it is possible to hot form open geometries, the 4 mm molds are used to form a PEEK sheet that has been laser cut, to create the open geometry. The features are replicated adequately, however a slight evidence of necking is visible along the edges.

3.3.8. Heat distribution and conductivity to the PEEK sheets

In these experiments the heat distribution in the molds and heat conductivity to the PEEK sheets are investigated. Two molds are placed onto a heating plate and analysed with a thermal camera.

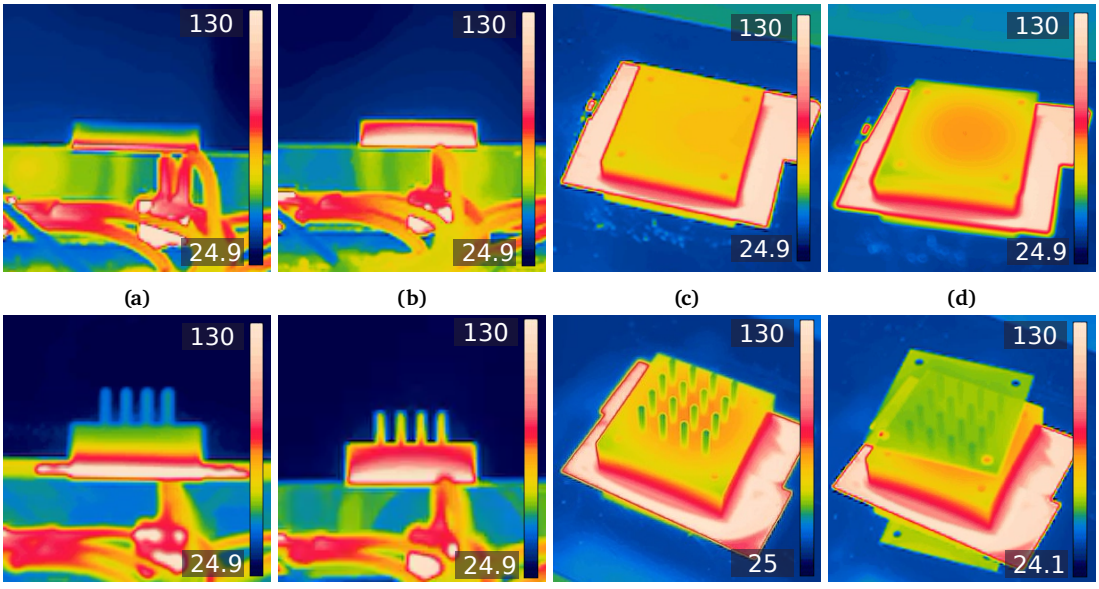

(a) (b) (c) (d)

(e) (f) (g) (h)

Figure 3.16: Thermal images of the molds with the 400x400x100 µm blocks and 1:5 cylindrical features: side image of the mold during initial heating (a,e), side image in thermal equilibrium (b,f), top view of the mold in equilibrium (c,g) and with a PEEK sheet op top of the mold (d,h)

In Fig. 3.16 the thermal images of the mold with the 400x400x100 µm blocks and 1:5 cylindrical features are displayed. At thermal equilibrium, the in-plane heat distribution

of the mold with the small blocks is more uniform, than the other mold, where the outer edge is colder than the center point. Furthermore, the heat distribution over the z-axis is more constant for the molds with the block features. Whereas for the pins the tops are cooler compared to the base of the molds. This is caused by the fact that the pins behave like cooling fins. As the surface area increases compared to its volume, reducing its thermal capacity.

The PEEK sheets almost instantly take on the mold temperature, when they are in full contact with the molds, as is the case for the molds with the small blocks. When the PEEK sheets are placed over the cylindrical features, it is visible that the peek sheets remain at a lower temperature than the mold. This phenomenon can be attributed to two factors: firstly, the limited contact area when the sheet is positioned over the cylinders, and secondly, the significantly cooler temperatures at the tops of the cylinders compared to the bases of the molds.

Region	Temperature (°C)
Base (bottom)	>130
Base (top)	99.3
Base (corner)	65.7
Tips of pins	59
PEEK sheet	57.6

(a)

Region	Temperature (°C)
Base (bottom)	>130
Base (top)	111
Base (corner)	96.3
PEEK sheet (center)	103
PEEK sheet (edge)	88.7

(b)

Table 3.3: Results of the heat measurements of the mold with 1:4 pins (a) and 400 µm blocks (b). The measurements can be found in Appendix D.

3.3.9. Lifetime Molds

In this experiment the lifetime of the molds is researched by visually inspecting molds before hot forming, and after both 25 and 50 hot forming cycles. Furthermore the maximum load is determined that the mold can withstand.

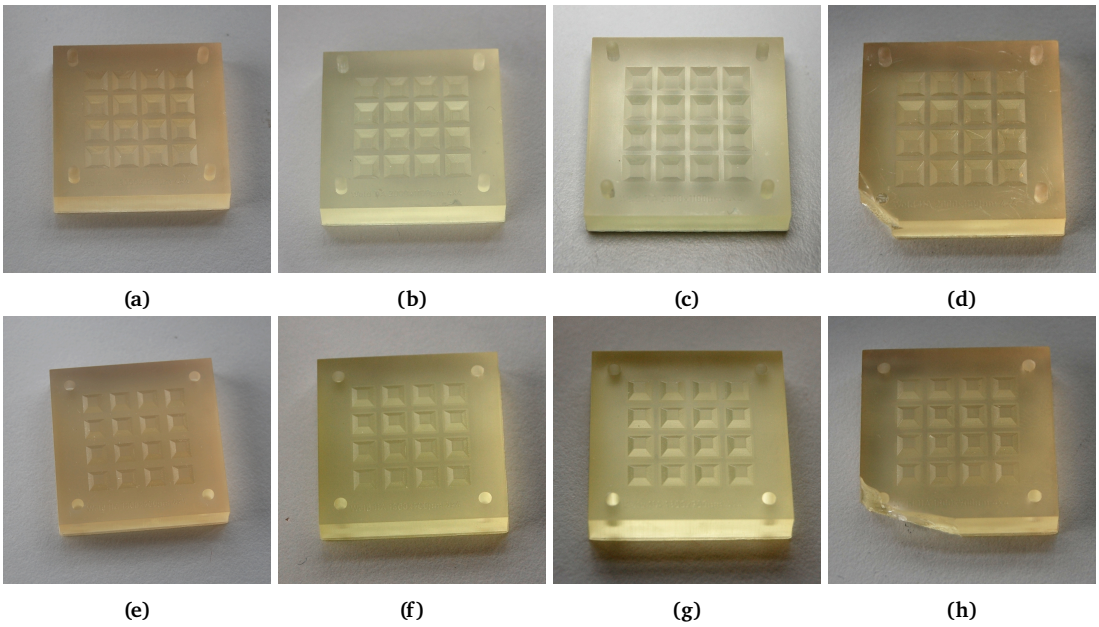

Figure 3.17: Negative (top) and positive (bottom) molds after different lifetime experiments: (a,e) unused, (b,f) after 25 cycles, (c,g) after 50 cycles and (d,h) after applying the maximum load.

Fig. 3.17 shows that the hot forming process doesn't affect the molds at all. No deformations or damages are visible after the hot forming cycles. Furthermore, it is found that the molds fail at 7000 N. However, only a small part at the corner is chipped off, meaning that this could also be caused by non-uniform pressing or an impurity in the molds.

3.3.10. Stress relaxation

Stress relaxation in polymers is observed when a material, subjected to constant deformation under stable temperature and humidity, shows a decrease in the stress needed to sustain that deformation over time [21].

The results of the stress relaxation experiment demonstrate that the tape is mostly responsible for the force drop, as shown in Fig. 3.18. The stress relaxation experiment with

	Max. force (N)	End force (N)	Drop (N)	Drop, rel. (%)
Complete setup, preformed substrate	1020.00	830.00	190.00	18.63
Complete setup, new substrate	1010.00	830.00	180.00	17.82
Molds only	1060.00	990.00	70.00	6.60
Molds with substrate	1010.00	910.00	100.00	9.90
Substrate only	1040.00	1020.00	20.00	1.92
Tape only	1010.00	850.00	160.00	15.84
1000 N	1020.00	840.00	180.00	17.65
2000 N	2040.00	1570.00	470.00	23.04
3000 N	3010.00	2280.00	730.00	24.25
4000 N	4040.00	2980.00	1060.00	26.24
5000 N	5020.00	3550.00	1470.00	29.28

Table 3.4: Values from the measurements in Figs. 3.18 and 3.19

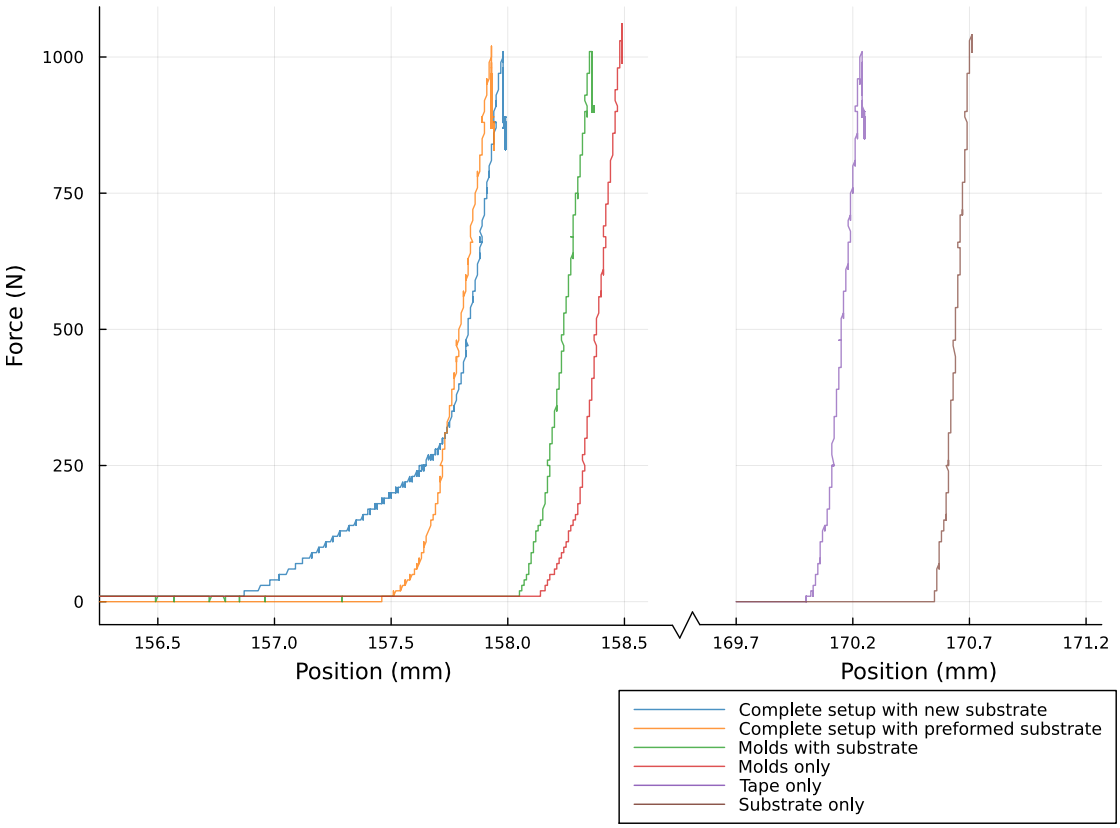

Figure 3.18: Comparison of stress relaxation for all the components.

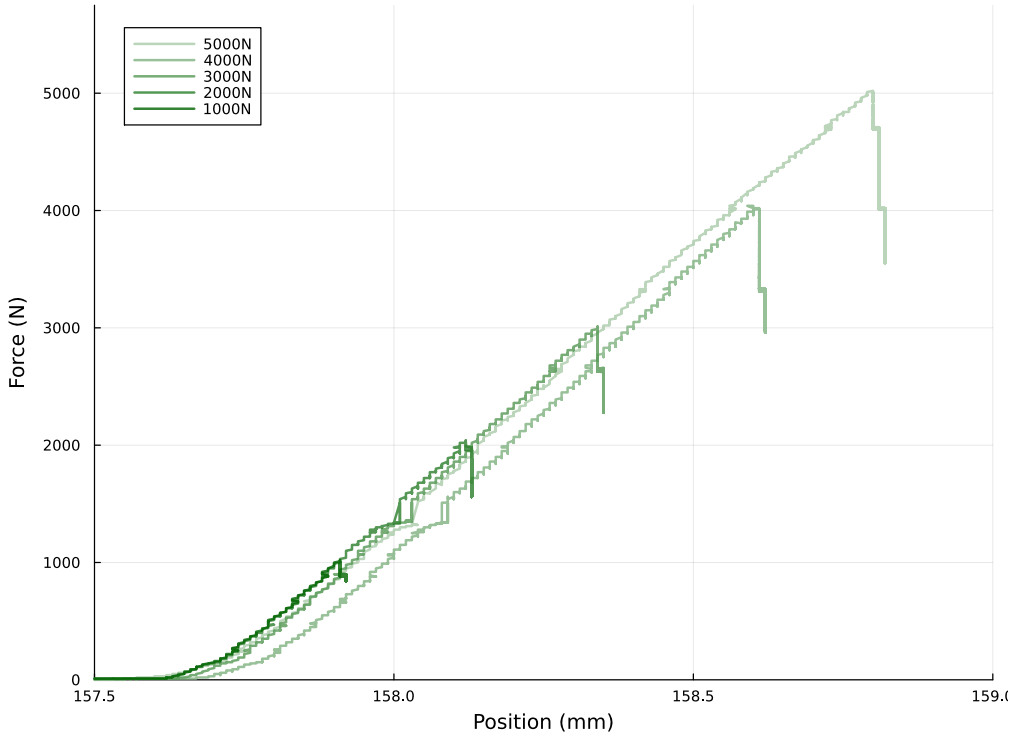

Figure 3.19: Comparison stress relaxation for peak forces ranging from 1000 to 5000N.

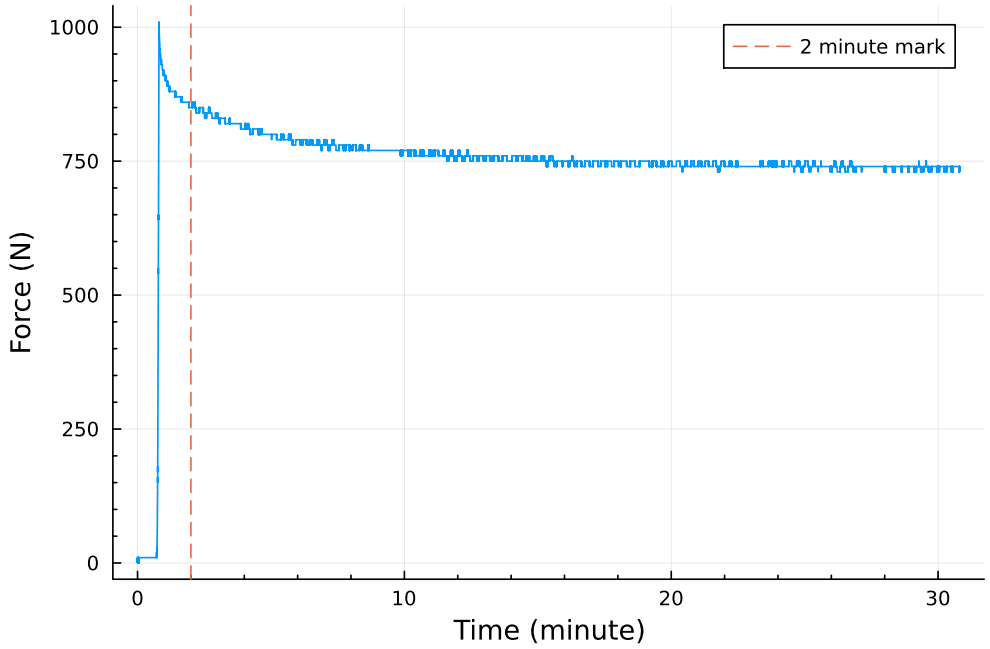

Figure 3.20: Stress relaxation over the span of 30 minutes.

only the tape shows almost the same drop as the complete setup, 15.84% and 18.63% respectively. The results for just the molds with the substrate also show a significant drop of 9.90 %, while the lines for the molds and substrate separately show a much smaller drop. It is assumed that this is caused by the fact the the substrate has to shape itself to the molds, leaving more space for rearrangement of the molecular chains, compared to the flat sheets used for the substrate only line. The molds will never fit onto each other as well as the two flat platforms. This leaves more room for the rearrangement of the molecular chains.

Placing a preformed substrate between the molds changes the shape of the first part of the force displacement line, however it doesn't affect the force drop.

In Fig. 3.19 it is shown how the force affects the force drop. It is seen that the force drop slightly increases for increasing forces, ranging from 17.65% to 29.28%.

Fig. 3.20 shows that the drop in force decreases exponentially over time. After around 10 minutes the force doesn't drop any further. This indicates that after 10 minutes the molecular chains have readjusted to their new orientation at the lower stress state. Where they remain for the remaining time for when the stress is loaded.

3.3.11. Tensile strength PEEK

Four different tensile tests are performed in this section to analyse the PEEK material properties during and after the hot forming process. For the tensile tests, the PEEK sheets were cut into 2 x 5 cm rectangles.

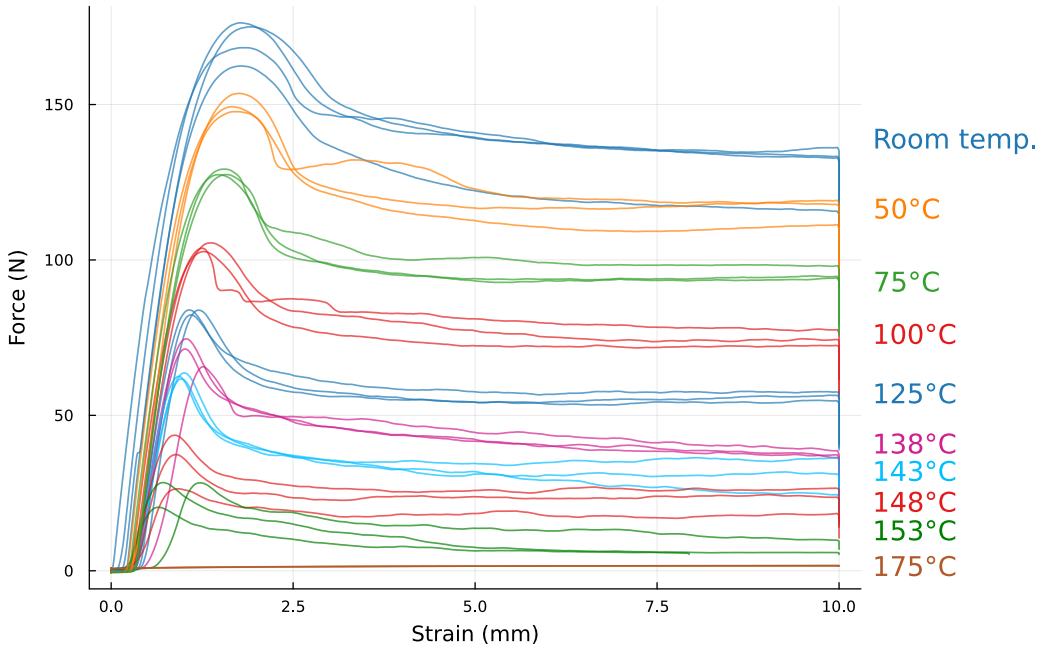

Figure 3.21: Results of the PEEK tensile tests performed at elevated temperatures.

The tensile tests at elevated temperatures are used to find the PEEK material behaviour during the hot forming process. The tests are performed at elevated temperatures ranging from room temperature to 175°C Fig. 3.21. From the graph can be concluded that the tensile strength decreases for increasing temperatures. Consequently, this sugggests that it would require less force to deform the PEEK sheets if the hot forming temperature is increased.

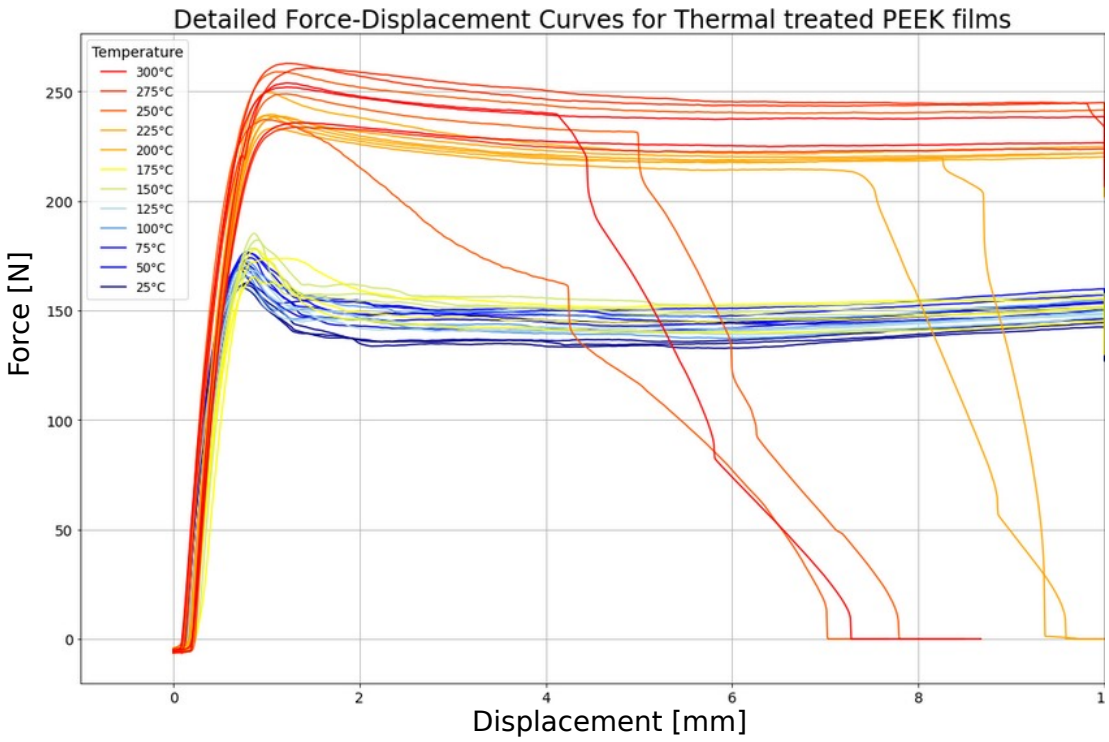

Figure 3.22: Results of the tensile test of heat treated PEEK sheets, performed at room temperature [15].

As the tensile strength decreases for increasing temperatures, it would be theoretically beneficial to increase the operating temperature of hot forming. However this operating temperature is limited by the temperature after which PEEK changes from semi-crystalline to an amorphous molecule structure. In the tensile tests performed by [15] it was determined that after heating the PEEK sheets above a temperature of 175°C, the PEEK changes to an amorphous molecule structure. At the conventional operating temperature of 143°C, the PEEK molecule chains won't be altered.

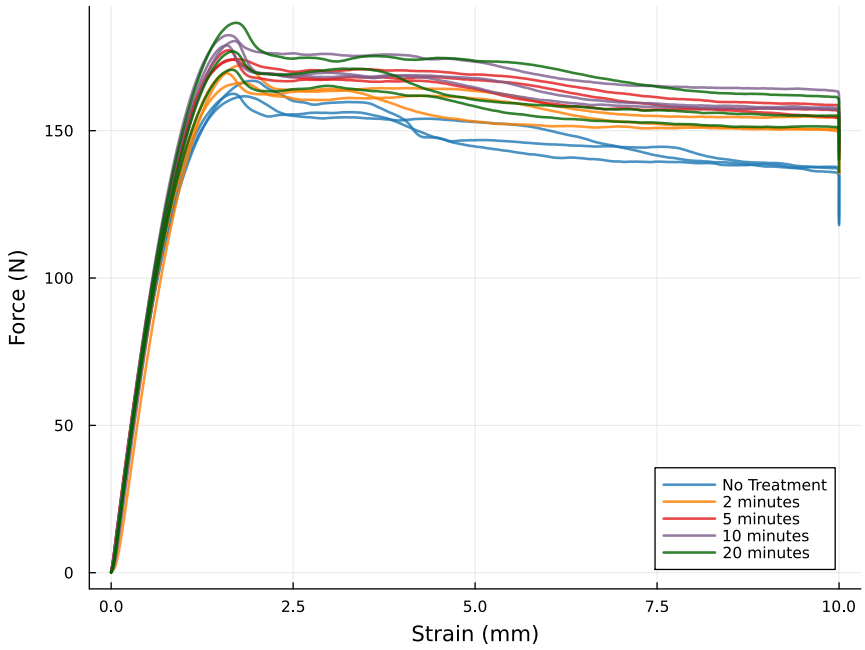

Figure 3.23: Tensile tests of heat treated PEEK sheets, performed at room temperature.

The tensile tests are performed at room temperature, to find how the PEEK material properties are affected by both of the setup. For these tensile tests, the peek sheets had undergone heat treatments at 143°C for a duration ranging from 0 minutes to 20 minutes Fig. 3.23. A small increase in tensile strength is visible for increasing heating times, but the PEEK seems to remain semi-crystalline. Since the molecular structure of the PEEK sheets remains unaffected, it can be concluded that the heat chamber process does not affect the PEEK material properties.

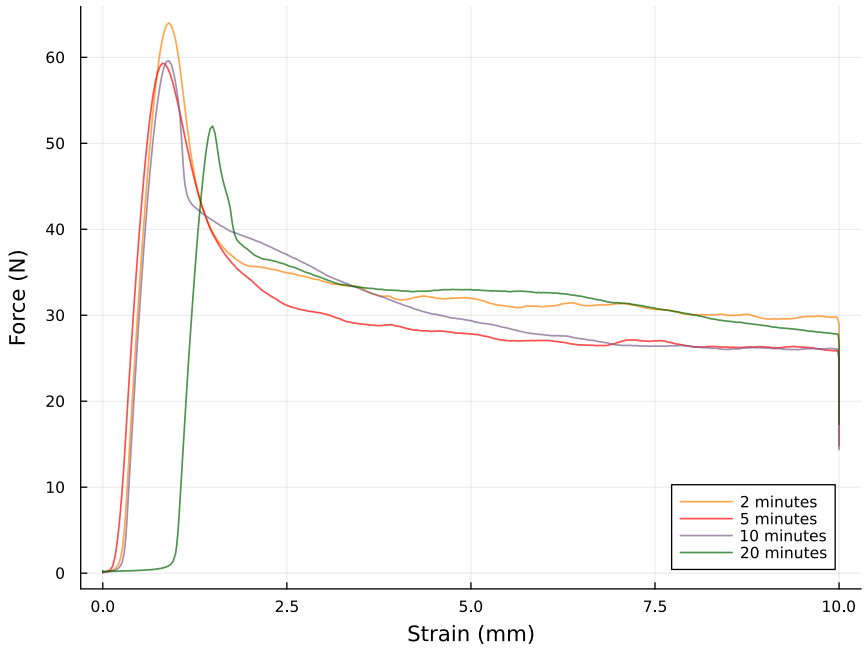

Figure 3.24: Tensile tests of PEEK sheets, performed at 143°C with settling times ranging from 2 minutes to 20 minutes.

These tensile test were performed at an elevated temperature of 143°C with a settling time ranging from 2 minutes to 20 minutes, to compare how the PEEK properties change during the hot forming process for both setups. The results indicate that the tensile strength is quite consistent, meaning that the rubbery state of peek doesn't change for the heating times used in the hot forming processed discussed in this research Fig. 3.24.

3.4. Conclusion Hot Forming

This chapter developed a proof of concept for the hot forming process. PEEK sheets were successfully formed using various resin printed molds. Two different setups have been tested, one using heating plates and another using a heating chamber for more uniform heat distribution across the molds and substrate. The forming parameters proved to be highly forgiving, with a broad range of process parameters still yielding high replication quality. The suitable forming temperature spanned from 100 to 150°C, and pressing forces between 750 and 3000 N proved effective.

The substrates closely replicated the 2x2x1 mm trapezoidal molds, with the only deviations occurring at the bottom edges due to imperfect matching of the molds. This highlights the critical importance of mold quality in the hot forming process. No limitations were identified concerning the shape or minimum size of the features, as all printed features were replicated accurately. For the 400x400x400 µm trapezoids, which were the smallest printable trapezoids, the substrate however did not closely replicate the mold design, primarily due to poor mold matching. It is expected that for matching molds, the features can be replicated with high accuracy, as was the case for the 400x400x100 µm blocks. The largest stretch was achieved at a aspect ratio of 1:3 when performed with heating plates and 1:4 when performed with a heating chamber. The

1:4 features however started to wrinkle and tear due to the large stretch and concentrated stress. Another cause for the tearing was the demolding process. The locally high stresses caused the cylindrical features to deform and tear. While the cylindrical features exhibited non-uniform substrate thickness with thinner tops, the trapezoid features did not show this non-uniformity. Instead, the reduced space between the positive and the negative molds caused the substrate to be squeezed into all mold crevices, resulting in more precise replication. The final hot forming experiments involved open geometries designed to resemble beam elements. These features were replicated with high fidelity, with only minor necking observed at the edges of the beam elements.

The setup with heating plates demonstrated uniform heat distribution in the molds for small features. However, for features with large aspect ratios, heat distribution was uneven, with the tips of the cylinders being cooler than the bases due to the increased surface area relative to the volume. The heat transfer from the molds to the PEEK sheets was highly efficient, with the sheets almost instantly adopting the mold temperature upon full contact.

Tensile tests and visual inspections indicated a continuous decrease in tensile strength with increasing temperatures, reaching 0 MPa at 175°C, which is consistent with the maximum operating temperature provided by the supplier.

Moreover, the hot forming process did not appear to affect the material properties of the PEEK sheets. The tensile strength remained within the semi-crystalline region for PEEK sheets heat treated at temperatures up to 175°C and for sheets treated at 143°C for extended periods of time.

4

Conclusion & Future work

4.1. Conclusion

This research successfully developed a proof of concept for the hot forming of PEEK sheets with resin-printed polymer molds.

Ch. 2 successfully resin printed various molds with diverse geometries, including rounded cylinders, blocks and trapezoids, suitable for hot forming. Key variables influencing the mold output in resin printing include the cleaning procedure, post-curing, and layer thickness. Four of the most critical requirements for molds were analysed for the different feature designs, including printing accuracy, repeatability, surface roughness and tensile strength. Blocks with dimensions of 400x400x100 µm proved to be the smallest printable features, and gave a printing accuracy of 40 µm.

Overall, the error in printing accuracy, ranging from 20 to 150 µm, has proven to be for the biggest part size independent, meaning that for the features smaller than 500 µm, the errors constitute a significant portion of the dimensions. The primary source of this error was attributed to bleeding during the printing process, which caused positive features to be larger than their negative counterparts. However, in the case of the smallest features analyzed, negative features were found to be larger than positive ones due to significant edge rounding effects that caused the positive features to be smaller than designed. Although the relatively significant error in small features diminishes precision, the issue is effectively offset by the high repeatability between different prints. These findings, however, are closely linked to the printer and resin used, and variations in results may occur with different equipment and materials. The surface roughness results

exhibited a wide range, from values similar to turned parts to those of FDM 3D-printed parts, making it difficult to draw definitive conclusions about the surface roughness of resin-printed molds.

Ch. 3 developed a proof of concept for the hot forming process. PEEK sheets have been successfully formed using various resin printed molds. Two different setups have been tested, one using heating plates and another using a heating chamber for more uniform heat distribution across the molds and substrate. The forming parameters proved to be highly forgiving, with a broad range of process parameters still yielding high replication quality. The suitable forming temperature spanned from 100 to 150°C, and pressing forces between 750 and 3000 N proved effective.

No limitations were identified concerning the shape or minimum size of the features, as all printed features were replicated accurately. The largest stretch was achieved at a aspect ratio of 1:3 when performed with heating plates and 1:4 when performed with a heating chamber. The 1:4 features however started to wrinkle and tear due to the large stretch and concentrated stress. Another cause for the tearing was the demolding process, due to locally high stresses causing the cylindrical features to deform and tear. The hot forming experiments involving open geometries designed to resemble beam elements, were replicated with high fidelity, with only minor necking observed at the edges of the beam elements.

Moreover, the hot forming process did not appear to affect the material properties of the PEEK sheets. The tensile strength remained within the semi-crystalline region for PEEK sheets heat treated at temperatures up to 175°C and for sheets treated at 143°C for extended periods of time.

The proof of concept presented in this research encounters limitations primarily associated with challenges in feature size, as both excessively large and overly small features can create issues. Large features may lead to uneven temperature distribution in the molds, while small features are limited by the printing accuracy during mold fabrication. To overcome the limitations associated with small features, machined metal molds are suggested, as they provide greater precision and improved heat distribution due to their superior thermal conductivity. When hot forming of tall features is desired, the usage of a setup with a heating chamber is advisable to ensure uniform heating.

4.2. Future work

There are several directions to continue this research, which can be broadly classified into three main categories: increasing our understanding of the process, improving the process and increasing the form freedom i.e., the range of shapes that can be produced through the process.

4.2.1. Gaining insight into the process

Enhancing the understanding of the hot forming process is crucial to achieving greater control during its execution. In this research, the analysis of hot formed substrates was limited to visual inspection, which, while providing a general indication of replication quality, lacks precision and fails to reveal critical information such as internal stress distribution. Consequently, this method does not offer insight into the internal stresses generated within the substrates by the current hot forming process. To address these limitations and enhance process understanding, the following approaches may be explored:

1. Simulating the hot forming process
   Simulating the hot forming process can improve the understanding of the hot forming process, by providing detailed insights into substrate flow, stress distribution, and the optimal temperature-force combinations for effective outcomes. The latter is important for potential future applications where setups can only reach certain forces or temperatures, or in cases where the substrate or mold material should be kept under a certain force or temperature. Currently the hot forming process seems to be very forgiving, but if the simulations show that there is a small temperature bandwidth where the hot forming results prove to be even better, then a conscious next step could be to improve the setup to achieve higher precision in temperature during the process.

2. Creating a hot forming window
   By performing experiments to find the possible combinations of the pressing force and hot forming temperature, the results from the simulations can be checked.

3. Measuring the thickness across the substrate
   By continuously measuring the thickness variation across the entire substrate, the results of the simulations can be verified and more insight can be obtained of the flow of the substrate.

4.2.2. Improving the hot forming process

The hot forming process can be improved by various approaches including, improvement of the demolding process, improving the uniformity of the heat distribution in the molds and implementing machined molds into the hot forming process.

1. Improving the demolding process
   The demolding process can be improved in several ways. In this research, the substrates were removed while the molds were still hot. For the heating plates the

molds were still at the forming temperature, while in the heating chamber the molds were cooled down to 90 degrees. By actively cooling down the molds after hot forming, the chance of deformation during demolding is reduced, as the stiffness of the substrate material increases when the temperature is lowered. Also the setup could be improved upon, implementing a stamp housing removes the necessity of using tweezers to remove the substrates, reducing the potential of local stresses

2. Improving the uniformity of the heat distribution in the molds.
   Creating a more uniform temperature across the entire mold, would result in a more uniform hot forming process. This could be achieved by sputtercoating the molds with a metal, or by electroplating.

3. Implementing machined molds
   Lastly the resin printed molds can be replaced by machined metal molds. This will increase the resolution of the molds and increase the heat distribution inside the molds.

4.2.3. Increasing the form freedom

There are various ways to achieve more innovative feature designs, such as the implementation of a multi-step manufacturing process and incorporating dynamic molds into the process.

1. Multi step manufacturing process
   Pre-thinning the substrate through a process such as hot embossing prior to hot forming allows for the creation of a non-uniform thickness, while still maintaining precise control over the thickness distribution across the substrate.

2. Dynamic molds
   By implementing a dynamic mold into the hot forming process, more unconventional feature geometries can be achieved, as shown in Fig. 4.1.

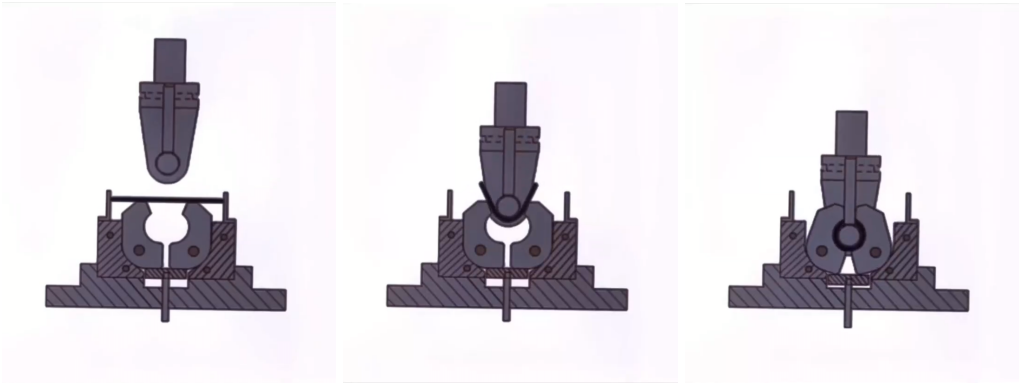

Figure 4.1: Traceless metal bending [25].

A

Test print results

A.1. Cylinders with Varying Aspect Ratios

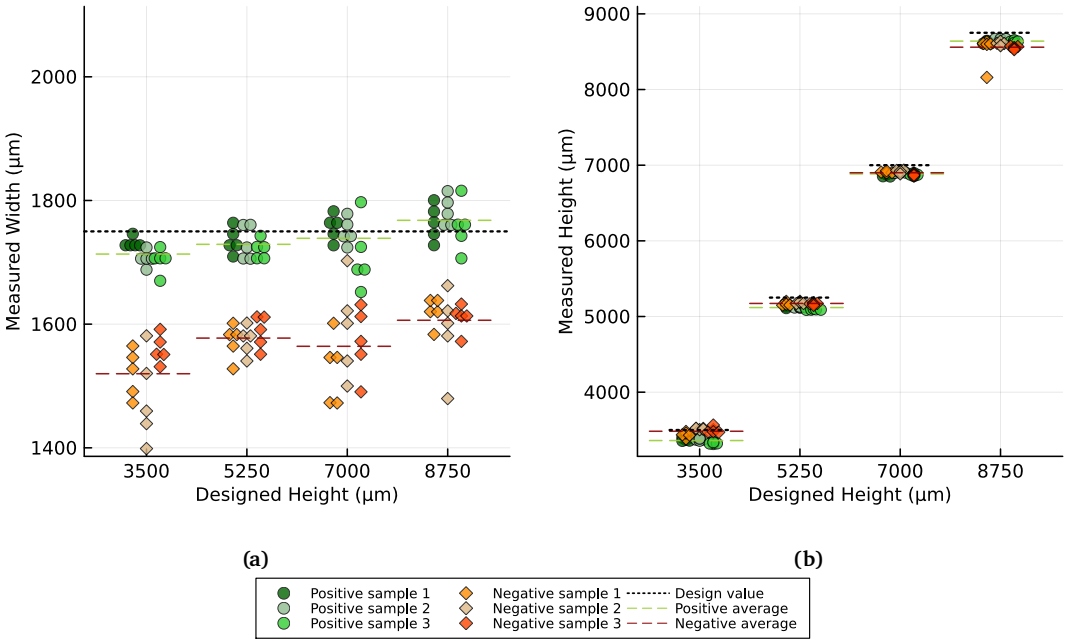

Figure A.1: Height and width measurements for the cylindrical features.

B

Hot Forming Molds

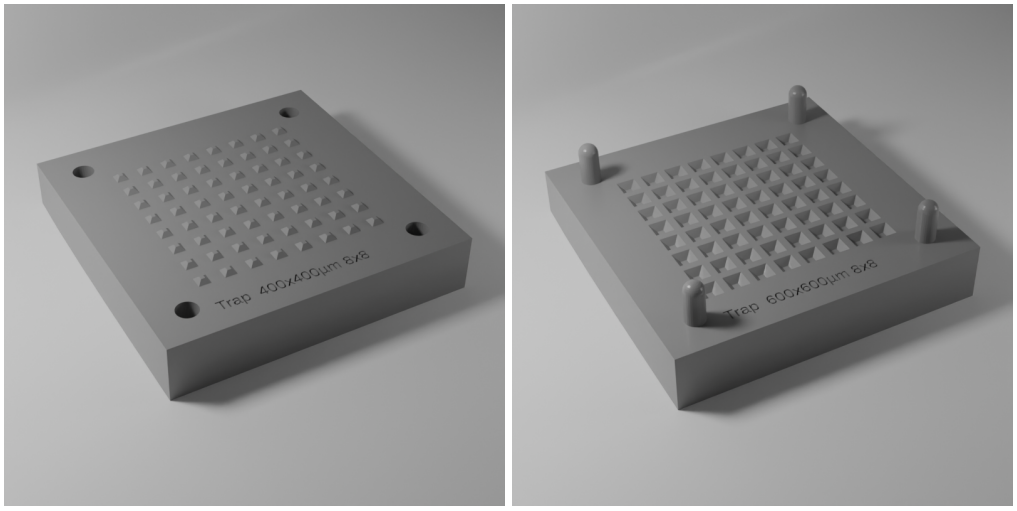

(a) **(b)**

Figure B.1: Positive (a) and negative (b) molds for the smallest trapezoidal features.

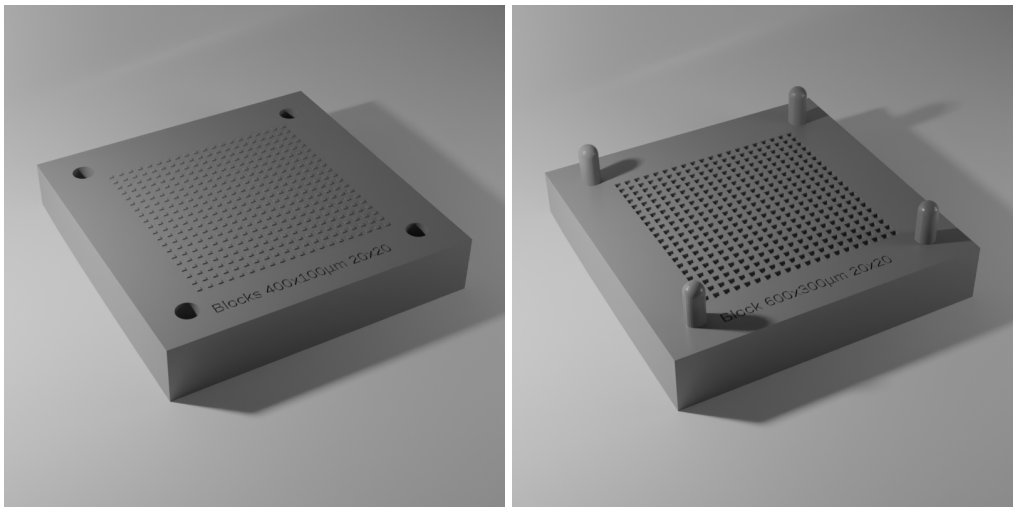

(a) **(b)**

Figure B.2: Positive (a) and negative (b) molds for the smallest blocks.

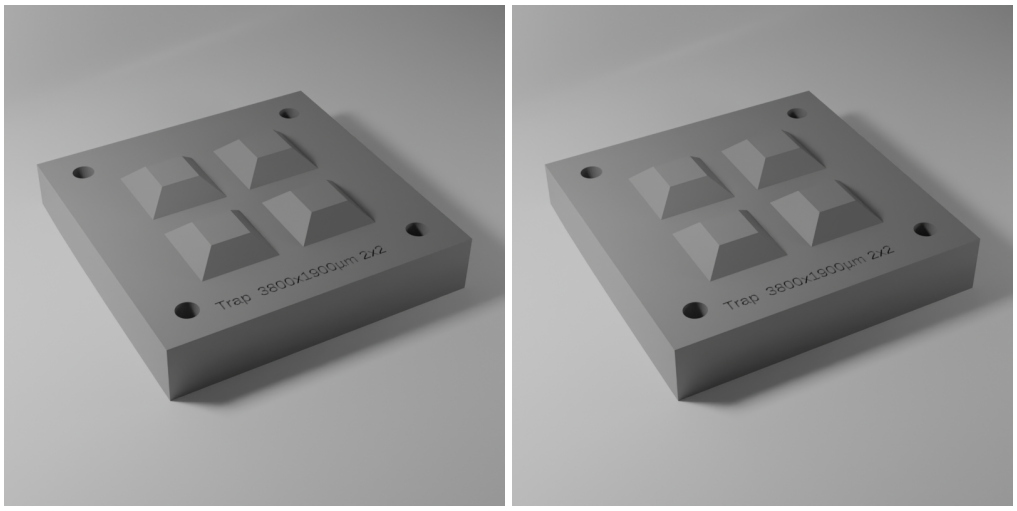

(a) **(b)**

Figure B.3: Positive (a) and negative (b) molds for the non-uniform trapezoidal features.

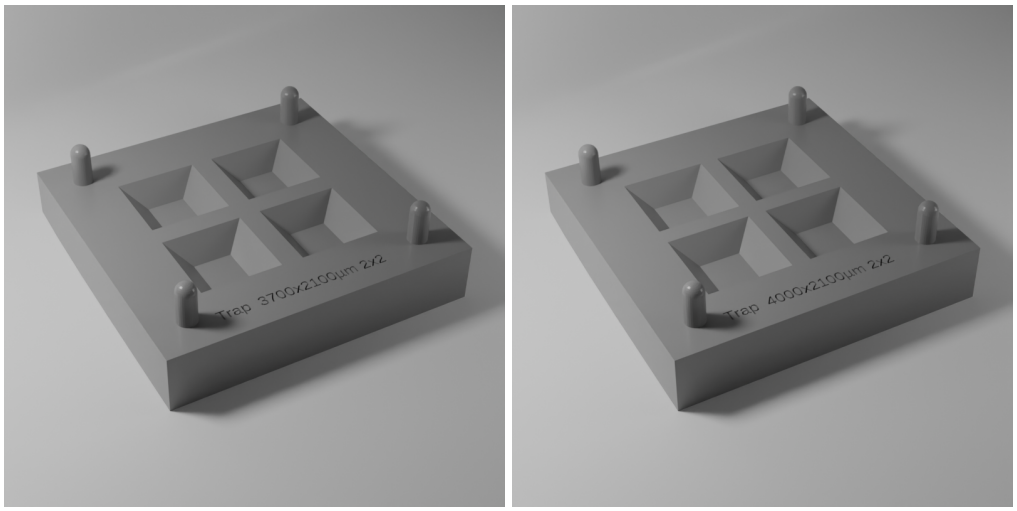

(a) **(b)**

Figure B.4: Positive (a) and negative (b) molds for the uniform trapezoidal features (4x4 mm).

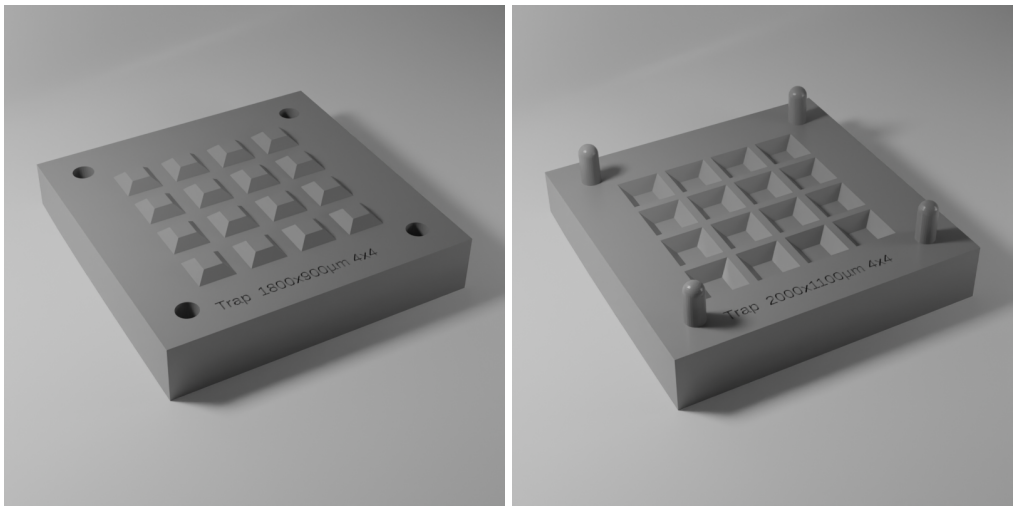

(a) **(b)**

Figure B.5: Positive (a) and negative (b) molds for the 2x2 mm trapezoidal features.

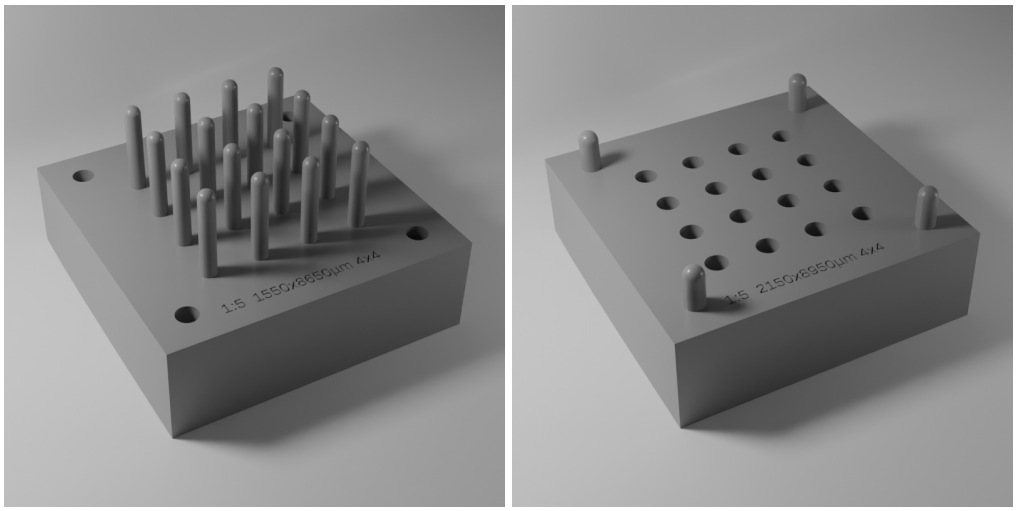

(a) **(b)**

Figure B.6: Positive (a) and negative (b) molds for the 1:5 cylindrical features.

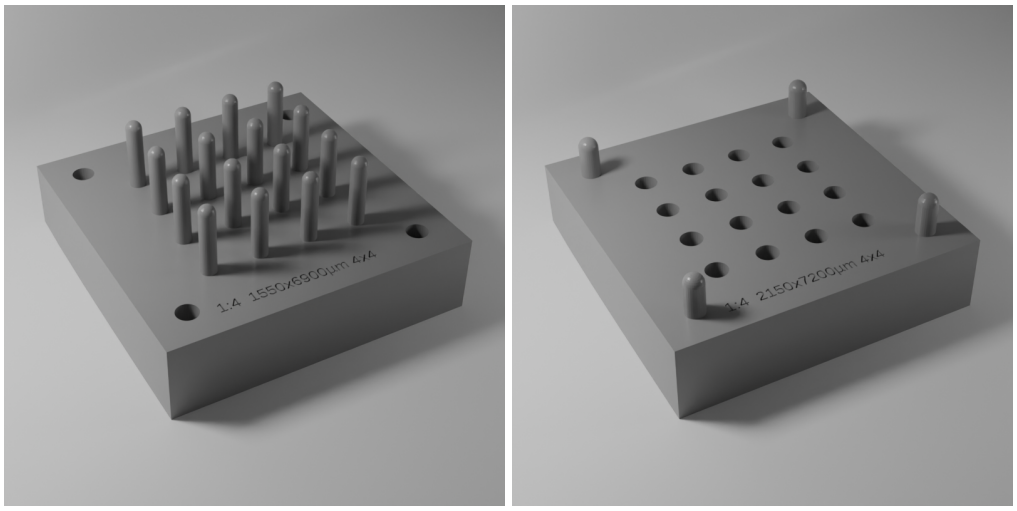

(a) **(b)**

Figure B.7: Positive (a) and negative (b) molds for the 1:4 cylindrical features.

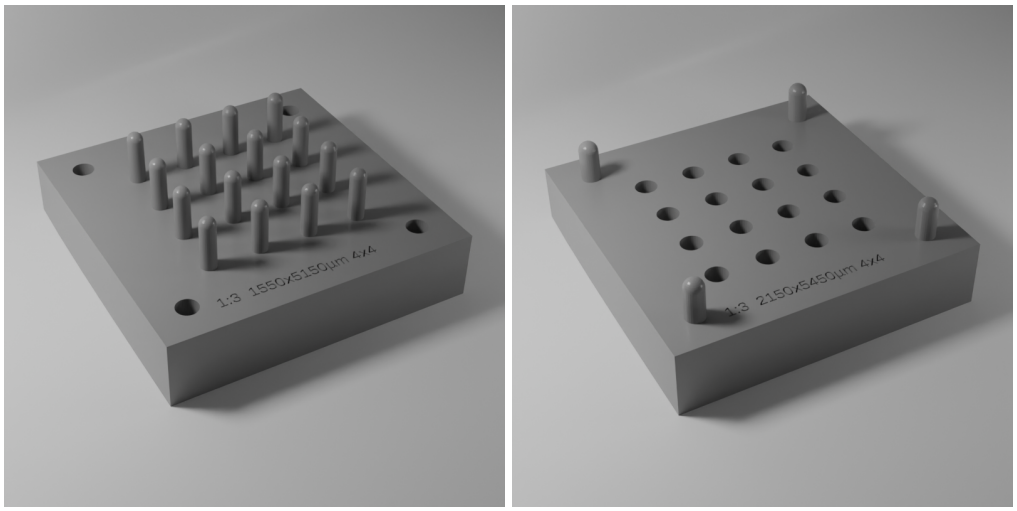

(a) **(b)**

Figure B.8: Positive (a) and negative (b) molds for the 1:3 cylindrical features.

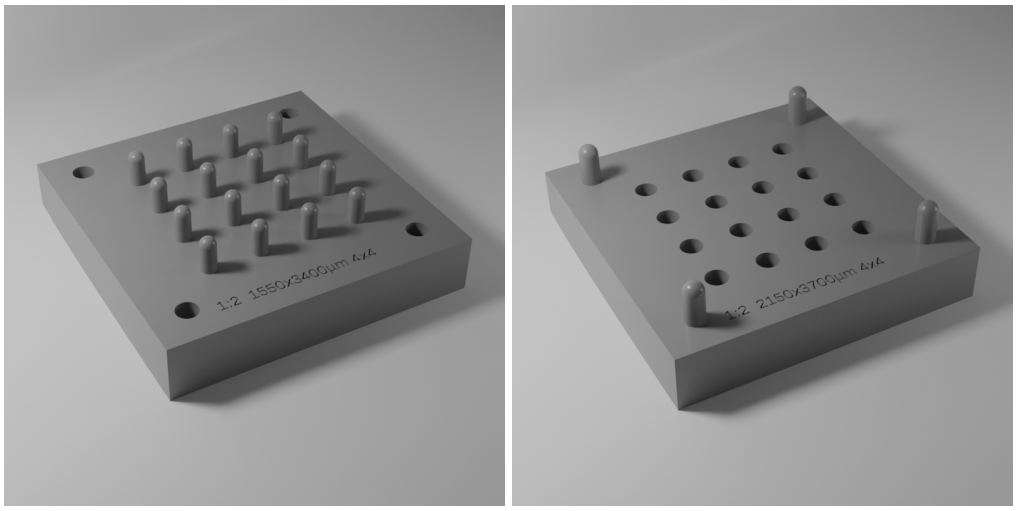

(a) **(b)**

Figure B.9: Positive (a) and negative (b) molds for the 1:2 cylindrical features.

C

OpenSCAD code

C.1. Test Prints

This code is used to generate test prints from Section 2.3.

Listing C.1: `test_print.scad`

```
// Configuration
// All dimension in micron listed below are in micron, final image is rendered in
    mm
// Size of the base block
base_block_x = 20000;
base_block_y = 20000;
base_block_z = 6000;

// Width of the features. Each element in this array is a seperate row
feature_width =   [
    1750,
    1750,
    1750,
    1750
];

// Height of features
feature_height =  [
    3500,
    5250,
    7000,
    8750
```

```
];

// Space between discrete features
feature_spacing = 1250;

// Shape of the features
feature_shape = "discrete_cylinder_rounded";
// Chose one of:
// cube
// triangle
// semicircle
// trapezium
// cylinder_rounded
// discrete_pyramid
// discrete_hemisphere
// discrete_cube
// discrete_trapezium
// discrete_cylinder_rounded

// Positive or negative print?
inverse = false;

// Angle for sloped side of trapezium, measured from bottom
feature_trap_angle = 45;


// Reference area
// The reference area is a small area next to the features where information is printed
// Included two rows of text and a triangle to indicate the middle position of the features

// text in the top row. Will automatically hide if no room is available
reference_text_top = [
    for (c = feature_width) str(c/1000) // This prints the feature width in mm for each feature
];

// Size of the top row text
reference_text_top_size = 1200;

// text in the bottom row
reference_text_bottom = [
for (c = feature_height) str(c/1000) // Prints feature height in mm
];

// Size of the bottom row text
reference_text_bottom_size = 1200;

// Font used for numbers/text. Recommended fonts: Bahnschrift or Consolas
text_reference_font = "Bahnschrift";

// Distance between triangle and text
reference_triangle_distance = 500;

// Space around text
reference_text_margin = 600;
```

```
76
77  // Depth of the text and midline indicator
78  ref_depth = 1000;
79
80  // smooth factor for circles
81  $fn = 32;
82
83  debug_size = false ; // Put transparent boxes around features to check size
84
85  // ---- CODE ----
86  no_features = len(feature_width); // Number of features to generate
87  feature_area_width = base_block_y/no_features; // Divide available area for each
        feature
88
89  assert(len(feature_width) == len(feature_height), "Feature size vectors are not
        the same length");
90
91  feature_midpoints = [ for (i = [0:no_features-1]) (i+0.5) * feature_area_width];
92
93  // Size of the triangle to indicate the feature middle
94  tri_size = min(0.9*feature_area_width, 1000);
95
96  // Total refereance area size
97  reference_area_y_size = tri_size + reference_text_margin + reference_text_top_size
         + reference_text_bottom_size;
98
99  // length available for the features
100 feature_length = base_block_y - reference_area_y_size;
101
102 // Following modules create one column of features
103 // Some are a single extruded shape, others repeat discrete objects
104
105 module feature_cube(width, height){
106     translate([-width/2,0,  0])
107         cube([width, feature_length, height]);
108 }
109
110 module feature_cylinder_rounded(width,height){
111     let( cyl_height = height - 0.5*width ){
112         feature_cube(width, cyl_height);
113         translate([0,0,cyl_height]) feature_semicircle(width,height);
114     }
115 }
116
117
118 module pyramid(size, height){
119     scale([size/2, size/2, height])
120     polyhedron(
121       points=[ [1,1,0],[1,-1,0],[-1,-1,0],[-1,1,0], // the four points at base
122                [0,0,1]  ],                                  // the apex point
123       faces=[ [0,1,4],[1,2,4],[2,3,4],[3,0,4],              // each triangle side
124                   [1,0,3],[2,1,3] ]                        // two triangles for
        square base
125      );
126 }
127
128 module feature_discrete_trapezium(width, height){
```

```
    let (amount_traps = floor(feature_length/(width+feature_spacing)))
    {
    for (i = [1:amount_traps]){
        translate([0, (i-1)*(width+feature_spacing), 0])
            feature_trapezium(width, height, depth=width);
        }
    }

}

module feature_trapezium(width, height, angle=feature_trap_angle, depth=
    feature_length){
    let (
        w = width/2,
        w_top = w-(height/tan(angle))
    ){
    assert(w_top > 0, "Angle too high for trapezium");
    rotate([90,0,180]) linear_extrude(depth) polygon([
        [-w, 0],
        [-w_top, height],
        [w_top, height],
        [w, 0],
    ]);
    }
}
module feature_triangle(width, height){
    rotate([90,0,180])
    linear_extrude(feature_length) polygon([
        [-width/2, 0],
        [0, height],
        [width/2, 0]
    ]);
}

module feature_semicircle(width, height){
    rotate([90,0,180])
    linear_extrude(feature_length) circle(d = width);
}

module feature_discrete_pyramid(width, height){
    let (amount_pyramids = floor(feature_length/(width+feature_spacing)))
    {
    for (i = [1:amount_pyramids]){
        translate([0, (i-0.5)*width+(i-1)*feature_spacing, 0]) pyramid(width,
    height);
        }
    }
}

module feature_discrete_cube(width, height){
    let (amount = floor(feature_length/(width+feature_spacing)))
    {
    for (i = [1:amount]){
        translate([0, (i-1)*(width+feature_spacing), 0])  translate([-width/2,0,
    0]) cube([width,width, height]);
        }
    }
```

```
}

module feature_discrete_hemisphere(width, height){
    let (amount = floor(feature_length/(width+feature_spacing)))
    {
    for (i = [1:amount]){
        translate([0, (i-0.5)*width+(i-1)*feature_spacing, 0]) scale([width,width,
     2*height])
          sphere(d = 1);
        }
    }
}

module feature_discrete_cylinder_rounded(width, height){
    let( cyl_height = height - 0.5*width,
    amount = floor(feature_length/(width+feature_spacing))
    ){

 for (i = [1:amount]){
        translate([0, (i-0.5)*width+(i-1)*feature_spacing, 0]){
        cylinder(h = cyl_height, d = width);
        translate([0,0,cyl_height]){
        sphere(d = width);
        }
    }
    }
    }
}

// Place the feature that is currently configured
module feature(width,height){
    if (feature_shape == "cube"){
        feature_cube(width, height);
    } else if (feature_shape == "triangle"){
        feature_triangle(width, height);
    } else if (feature_shape == "semicircle"){
        feature_semicircle(width, height);
    } else if (feature_shape == "trapezium") {
        feature_trapezium(width,height);
    } else if (feature_shape == "cylinder_rounded") {
        feature_cylinder_rounded(width,height);
    } else if (feature_shape == "discrete_pyramid"){
        feature_discrete_pyramid(width, height);
    } else if (feature_shape == "discrete_hemisphere"){
        feature_discrete_hemisphere(width, height);
    } else if (feature_shape == "discrete_cube"){
        feature_discrete_cube(width, height);
    } else if (feature_shape == "discrete_cylinder_rounded"){
        feature_discrete_cylinder_rounded(width, height);
    } else if (feature_shape == "discrete_trapezium") {
       feature_discrete_trapezium(width,height);
    }
}

// Generate reference area
module reference_area(ref_text_top, ref_text_bottom, depth) {
    let(
```

```
        area_y = reference_area_y_size,
        sep_y = reference_text_margin,
        text_size_top = reference_text_top_size,
        text_size_bottom = reference_text_bottom_size,
    ){
    translate([0, area_y-reference_triangle_distance, 0])
    linear_extrude(depth) polygon([
        [-tri_size/2, -tri_size/2],
        [0, 0],
        [tri_size/2, -tri_size/2]
    ]);

    translate([0,sep_y*0.5,0])
    linear_extrude(depth) text(ref_text_bottom, font = text_reference_font, valign
    ="bottom", size = text_size_bottom, halign = "center");

    translate([0,sep_y*0.5+text_size_bottom,0])
    linear_extrude(depth) text(ref_text_top, font = text_reference_font, valign="
    bottom", size = text_size_top, halign = "center");

    }
}

// Place all features on the block
module generate_features(inverse){
    rot_y = inverse ? 180 :0;
    move_up = inverse ? 1 : 0;

    for(i = [0:no_features-1]){
    translate([0,0,move_up]) {
        translate([feature_midpoints[i], reference_area_y_size, base_block_z])
        rotate([0, rot_y, 0]) {
            feature(feature_width[i], feature_height[i]);
            if (debug_size) %feature_cube(feature_width[i], feature_height[i]);
            }
        }
    }
}


scale([0.001, 0.001, 0.001]){ // scale to mm
    difference(){
        cube([base_block_x, base_block_y, base_block_z]);
        for (i = [0:no_features-1]){
            translate([feature_midpoints[i], 0, base_block_z-ref_depth+10])
            reference_area(reference_text_top[i], reference_text_bottom[i],
    ref_depth);
        }
        if (inverse) generate_features(true);
    }
    if (!inverse) generate_features(false);
}
```

C.2. Mold generation

The following code was used to generate the molds in Section 3.3, and shown in Appendix B.

Listing C.2: `mold_generate.scad`

```
// Configuration
// All dimension in micron listed below are in micron, final image is rendered in mm
// Size of the base block
base_block_x = 30000;
base_block_y = 30000;
base_block_z = 6000;

// Title of the figure, is displayed below features
mold_title = "  1:2  ";

// Single feature dimensions. Text below below features includes this information
feature_width = 2150;
feature_height = 3700;

// Distance between features, measured from center to center
feature_distance = 5000;

// Number of feature to place in grid, format: [x,y]. Will be included as text in information area
feature_matrix_size = [4,4];

// Feature shape
feature_shape = "discrete_cylinder_rounded"; //[cube, triangle, semicircle, trapezium, cylinder_rounded, discrete_pyramid, discrete_hemisphere, discrete_cube, discrete_trapezium, discrete_cylinder_rounded]

// Trapezoid angle, note that width in case of trapezoid refers to the top part. This angle determines width of the bottom part
feature_trap_angle = 45;

// Dimensions of the pins on the corners of the mold
pin_diameter = 1900;
pin_height = 4000;

// Extrude or inverse the pins/features? (positive of negative mold)
pin_inverse = false;
inverse = true;


// dimensions of the inner area with features
inner_dimensions = [20000, 20000];

// [x,y] coordinate of the first pin, others use same offsets from other edges
pin_location = [3500,3500];
//pin_location = ([base_block_x, base_block_y] - inner_dimensions)/4;


// Text in reference area
// The value below combines information from above
reference_text = str(mold_title, feature_width, "x", feature_height,
```

```
                    "µm ", feature_matrix_size.x, "x", feature_matrix_size.y);
;
// Font for text
text_reference_font = "Bahnschrift";
// Text size
text_size = 1100;
// Depth of reference text
ref_depth = 800;

// smooth factor for circles
$fn = 32;

// ---- CODE ----

assert (feature_width < feature_distance, "Distance too low, features will overlap
    ");

// Following modules create different (single) feature shapes

// 2D extruded rectangle
module feature_cube(width, height, feature_length) {
  translate([ -width / 2, -feature_length/2, 0 ]) cube([ width, feature_length,
    height ]);
}

// 2D extruded triangle
module feature_triangle(width, height, feature_length) {
  translate([0,-feature_length/2,0]) rotate([ 90, 0, 180 ])
    linear_extrude(feature_length)
      polygon([ [ -width / 2, 0 ], [ 0, height ], [ width / 2, 0 ] ]);
}

// 2D extruded upper half of a circle
module feature_semicircle(width, height, feature_length) {
  translate([0,-feature_length/2,0]) rotate([ 90, 0, 180 ]) linear_extrude(
    feature_length) circle(d = width);
}

// 2D extruded rounded cylinder, essentially cube + semicircle
module feature_cylinder_rounded(width,height, feature_length){
     let( cyl_height = height - 0.5*width ){
    feature_cube(width, cyl_height, feature_length);
    translate([0,0,cyl_height]) feature_semicircle(width,height, feature_length);
    }
}

// Seperate trapezoids shapes
module feature_discrete_trapezium(width, height, angle=feature_trap_angle){
    let (
        w = width/2 + (height/tan(angle)) ,
        w_top = width/2,
    ){
        rotate([0,0,45])
        cylinder(h=height, r1 = w*sqrt(2), r2 = w_top*(sqrt(2)),$fn=4);
    }
}

```

```
// 2D extruded trapezoid
module feature_trapezium(width, height, depth, angle=feature_trap_angle, ){
    let (
        w = width/2 + (height/tan(angle)),
        w_top = w
    ){
    translate([0,-feature_length/2,0]) rotate([90,0,180]) linear_extrude(depth)
    polygon([
        [-w, 0],
        [-w_top, height],
        [w_top, height],
        [w, 0],
    ]);
    }
}

// Discrete pyramids
module pyramid(size, height) {
  scale([ size / 2, size / 2, height ])
      polyhedron(points =
                      [
                        [ 1, 1, 0 ], [ 1, -1, 0 ], [ -1, -1, 0 ],
                        [ -1, 1, 0 ], // the four points at base
                        [ 0, 0, 1 ]
                      ], // the apex point
                  faces =
                      [
                        [ 0, 1, 4 ], [ 1, 2, 4 ], [ 2, 3, 4 ],
                        [ 3, 0, 4 ], // each triangle side
                        [ 1, 0, 3 ], [ 2, 1, 3 ]
                      ] // two triangles for square base
      );
}
// Discrete pyramids helper function
module feature_discrete_pyramid(width, height) {
    pyramid(width, height);
}

// Discrete blocks
// Note width is used as length and depth
module feature_discrete_cube(width, height) {
          translate([ -width/2, -width/2, 0 ]) cube([ width, width, height ]);

}

// Discrete half spheres
module feature_discrete_hemisphere(width, height) {
       scale([width,width, 2*height])
          sphere(d = 1);
}

// Discrete cylinders, with rounded top
module feature_discrete_cylinder_rounded(width, height){
    let( cyl_height = height - 0.5*width ){
        cylinder(h = cyl_height, d = width);
        translate([0,0,cyl_height]){
            sphere(d = width);
```

```
            }
    }
}

// Create single feature, depending on the configured value above
module feature(width, height, depth=feature_length) {
  if (feature_shape == "cube") {
    feature_cube(width, height, depth);
  } else if (feature_shape == "triangle") {
    feature_triangle(width, height, depth);
  } else if (feature_shape == "semicircle") {
    feature_semicircle(width, height, depth);
  } else if (feature_shape == "trapezium") {
    feature_trapezium(width,height, depth);
  } else if (feature_shape == "cylinder_rounded") {
    feature_cylinder_rounded(width,height, depth);
  } else if (feature_shape == "discrete_pyramid") {
    feature_discrete_pyramid(width, height);
  } else if (feature_shape == "discrete_hemisphere") {
    feature_discrete_hemisphere(width, height);
  } else if (feature_shape == "discrete_cube") {
    feature_discrete_cube(width, height);
  } else if (feature_shape == "discrete_cylinder_rounded"){
    feature_discrete_cylinder_rounded(width, height);
  } else if (feature_shape == "discrete_trapezium") {
       feature_discrete_trapezium(width,height);
  } else {
    assert(false, "unknown feature type");
  }
}

// Create the information area with text about this mold
// ll and ur are the lower left and upper right coordinates for the area
module reference_area(ll, ur, ref_text, depth) {
  let(  h = (ur.y-ll.y), // calculate height of the area
        w = (ur.x-ll.x), // calculate width
        text_size = text_size ? min(text_size,h) : h,  // Try to find a proper
    text (font) size.
        )
    {
        translate([ll.x, ll.y, base_block_z+1]) mirror([0,0,1]) {
        translate([ 0, h/2, 0 ]) linear_extrude(depth)
            text(ref_text, font = text_reference_font, valign = "center",
                 size = text_size, halign = "left");
        }
    }
}

// Module to place the features
module generate_features(inverse) {
  rot_y = inverse ? 180 : 0;
  move_up = inverse ? 1 : 0;

  // Generate matrix of x by y dots, with "feature_spacing" distance between each
    dot
  // If we want to center this matrix around (0,0), we need to substract the (size
    +1)/2, in case we use 1-based counting
```

```
  x_offset = (feature_matrix_size.x+1)/2;
  y_offset = (feature_matrix_size.y+1)/2;

  mid = base_block_x/2;
  translate([base_block_x/2, base_block_y/2, base_block_z]) intersection() {
  cube([inner_dimensions.x, inner_dimensions.y, 4*feature_height], center= true);
  for (x = [1:feature_matrix_size.x], y = [1:feature_matrix_size.y])
  let (
        x_coor = (x-x_offset)*feature_distance,
        y_coor = (y-y_offset)*feature_distance)
  {
    translate([ 0, 0, move_up ]) {
      translate(
          [x_coor, y_coor, 0 ])
     rotate([ 0, rot_y, 0 ]) feature(feature_width, feature_height,
    inner_dimensions.y);
    }
  }
  }
}

// Module to place the four pins
module place_pins(pin_loc, diameter, height, inverse = false ){
    let(rot_y = pin_inverse ? 180 : 0,
        move_up = pin_inverse ? 1 : 0)
    for(x = [0:1], y = [0:1]){
        let(loc_x = abs(x*base_block_x - pin_loc.x),
            loc_y = abs(y*base_block_y - pin_loc.y),
            cyl_height = height-0.5*diameter,
            )
            translate([loc_x, loc_y, base_block_z+move_up]) rotate([0,rot_y,0]) {
                cylinder(h = cyl_height, d = diameter);
                translate([0,0,cyl_height]){
                    sphere(d = diameter);
                }
                }
    }
}

feature_length = inner_dimensions.y;

ref_ll = [(base_block_x - inner_dimensions.x)/2, 0];
ref_ur = [(base_block_x - inner_dimensions.x)/2 + inner_dimensions.x,  (
    base_block_y - inner_dimensions.y)/2];

scale([ 0.001, 0.001, 0.001 ]) { // Scale from um to mm
  difference() {
    cube([ base_block_x, base_block_y, base_block_z ]); // Create base block
    reference_area(ref_ll, ref_ur, reference_text, ref_depth);
    if (inverse) generate_features(true);
    if(pin_inverse) place_pins(pin_location, pin_diameter, pin_height, pin_inverse
    );
  }
  if (!inverse)
    generate_features(false);
  if(!pin_inverse) place_pins(pin_location, pin_diameter, pin_height);
}
```

D

Thermal Measurements Heat Distribution and Conductivity

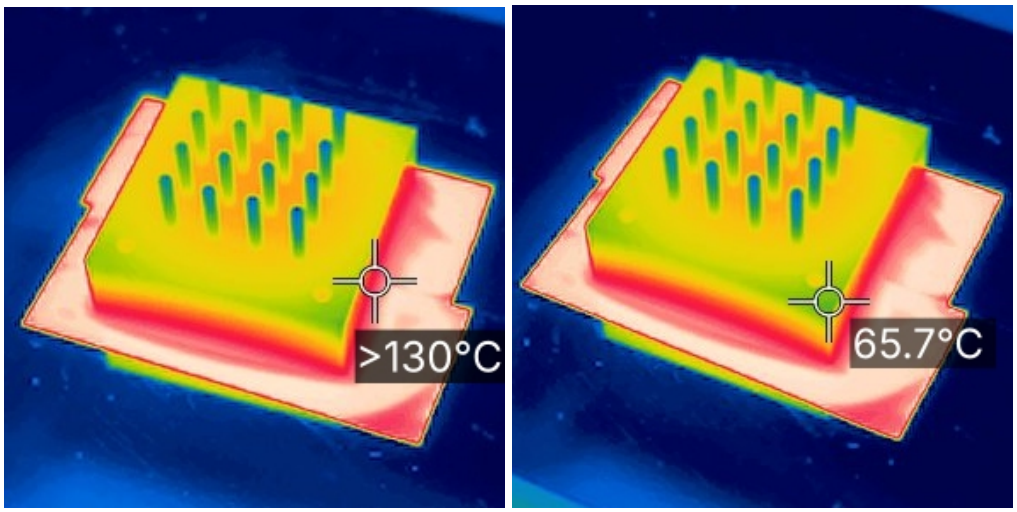

(a) (b)

Figure D.1

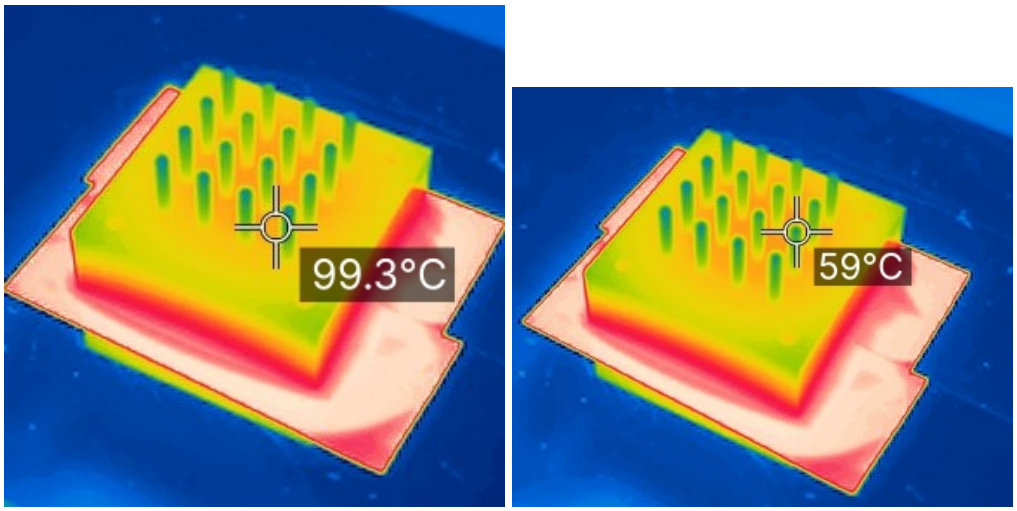

(a) (b)

Figure D.2

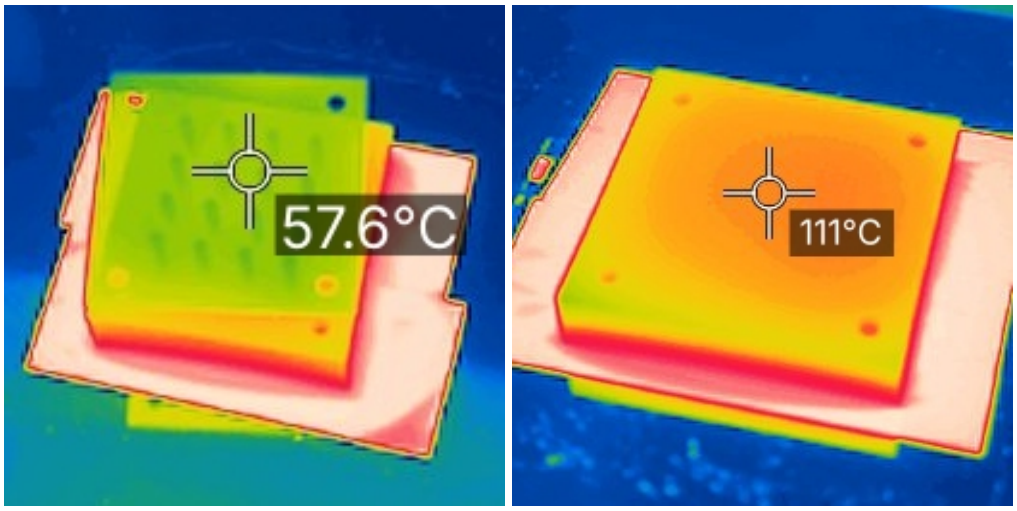

(a) (b)

Figure D.3

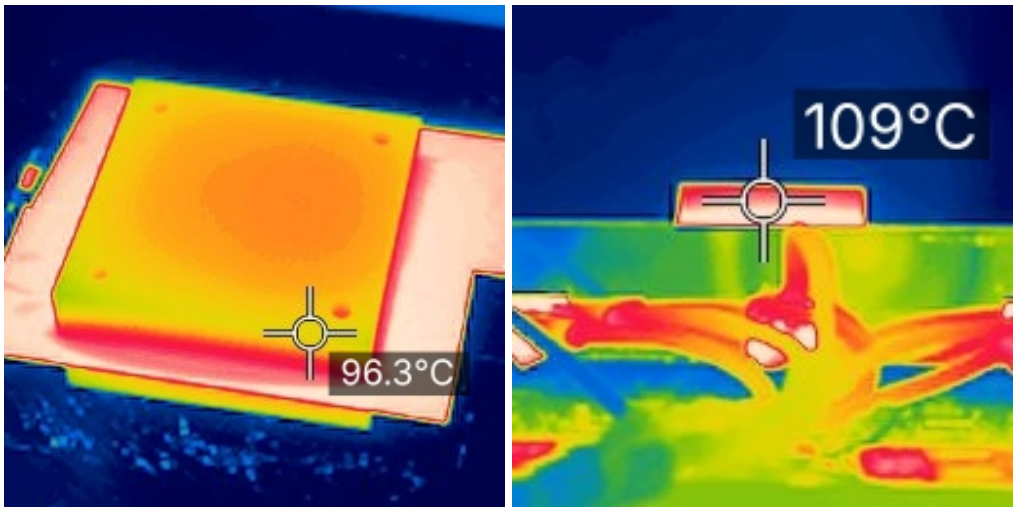

(a) (b)

Figure D.4

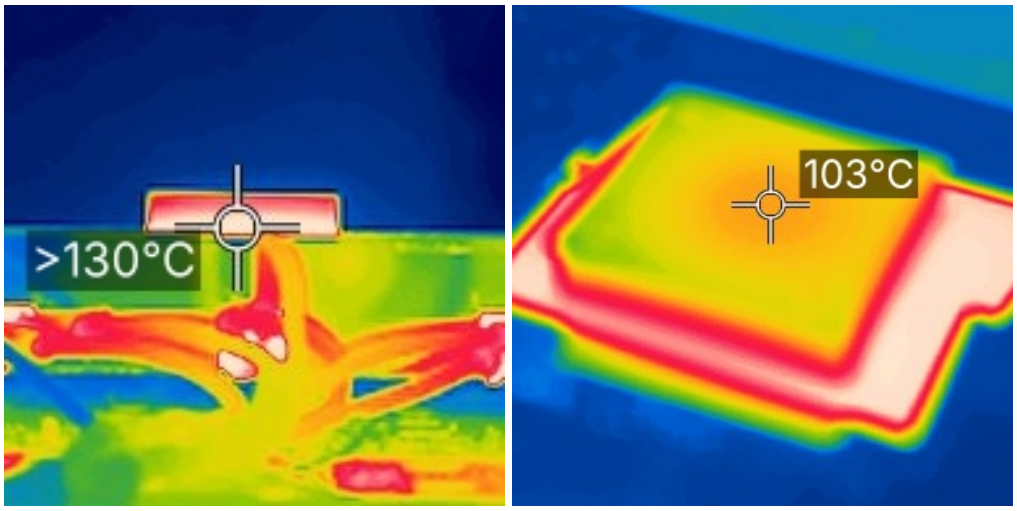

(a) (b)

Figure D.5

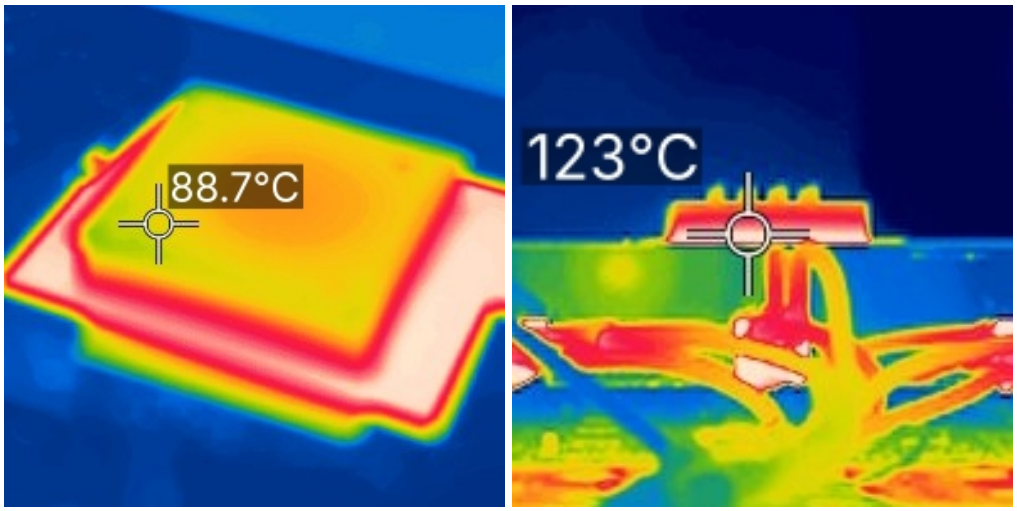

(a) (b)

Figure D.6

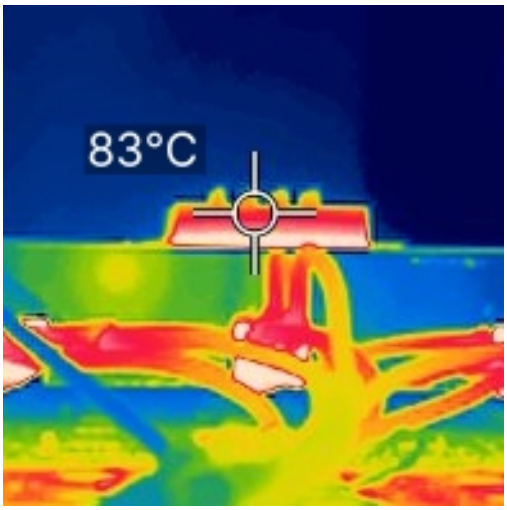

(a)

Figure D.7

Bibliography

[1] J. Herder, M. Tichem, H. Goosen, H. Bilyalova, and P. Roberjot. "Mechanical metamaterials for compact motion systems (MECOMOS)." (2023), [Online]. Available: https://www.tudelft.nl/3me/over/afdelingen/precision-and-microsystems-engineering-pme/research/mechatronic-system-design-msd/msd-research/mechanical-metamaterials-for-compact-motion-systems-mecomos.

[2] R. Kumar, M. Kumar, J. S. Chohan, and S. Kumar, "Overview on metamaterial: History, types and applications," *Materials Today: Proceedings*, vol. 56, pp. 3016–3024, 2022, 3rd International Conference on Contemporary Advances in Mechanical Engineering, ISSN: 2214-7853. DOI: https://doi.org/10.1016/j.matpr.2021.11.423. [Online]. Available: https://www.sciencedirect.com/science/article/pii/S2214785321074435.

[3] Y. Zhang, Q. Wang, M. Tichem, and F. van Keulen, "Design and characterization of multi-stable mechanical metastructures with level and tilted stable configurations," *Extreme Mechanics Letters*, vol. 34, p. 100 593, 2020, ISSN: 2352-4316. DOI: https://doi.org/10.1016/j.eml.2019.100593. [Online]. Available: https://www.sciencedirect.com/science/article/pii/S2352431619302615.

[4] M. C. Sobieraj and C. M. Rimnac, "Fracture, fatigue, and notch behavior of PEEK," in Elsevier, Jan. 2019, pp. 67–82, ISBN: 9780128125243. DOI: 10.1016/B978-0-12-812524-3.00005-3.

[5] Z. El-Qoubaa and R. Othman, "Characterization and modeling of the strain rate sensitivity of polyetheretherketone's compressive yield stress," *Materials and Design*, vol. 66, pp. 336–345, PA Feb. 2015, ISSN: 18734197. DOI: 10.1016/j.matdes.2014.10.080.

[6] P. Martin, "12 - thermoforming of polymers," in *Advances in Polymer Processing*, S. Thomas and Y. Weimin, Eds., Woodhead Publishing, 2009, pp. 352–383, ISBN: 978-1-84569-396-1. DOI: https://doi.org/10.1533/9781845696429.3.352. [Online]. Available: https://www.sciencedirect.com/science/article/pii/B9781845693961500126.

[7] J. Throne, "Thermoforming," in Elsevier Inc., 2017, pp. 345–375, ISBN: 9780323390408. DOI: 10.1016/B978-0-323-39040-8.00016-X.

[8] S. Giselbrecht *et al.*, "Microthermoforming as a novel technique for manufacturing scaffolds in tissue engineering (CellChips)," vol. 151, Aug. 2004, pp. 151–157. DOI: 10.1049/ip-nbt:20040824.

[9] P. Sridhar, S. S. Bahga, and J. P. Khatait, "Design of precision hot embossing machine for micropatterning on PMMA," *Journal of Micro and Nano-Manufacturing*, vol. 9, 3 Sep. 2021, ISSN: 21660476. DOI: 10.1115/1.4051770.

[10] L. Peng, Y. Deng, P. Yi, and X. Lai, *Micro hot embossing of thermoplastic polymers: A review*, Jan. 2014. DOI: 10.1088/0960-1317/24/1/013001.

[11] D. Patil, A. Sharma, S. Aravindan, and P. V. Rao, "Development of hot embossing setup and fabrication of ordered nanostructures on large area of polymer surface for antibiofouling application," *Micro and Nano Letters*, vol. 14, pp. 191–195, 2 Feb. 2019, ISSN: 17500443. DOI: 10.1049/mnl.2018.5462.

[12] Y. J. Kim, H. N. Kim, and D. Y. Kim, "A study on effects of curing and machining conditions in post-processing of sla additive manufactured polymer," *Journal of Manufacturing Processes*, vol. 119, pp. 511–519, Jun. 2024, ISSN: 15266125. DOI: 10.1016/j.jmapro.2024.03.112.

[13] R. Melentiev, M. Melentieva, and N. Yu, *Top 10 directions in lithography 3d printing*, Jul. 2024. DOI: 10.1016/j.bprint.2024.e00343.

[14] V. J. Kharat *et al.*, "Additive manufacturing (3d printing): A review of materials, methods, applications and challenges," *Materials Today: Proceedings*, Nov. 2023, ISSN: 22147853. DOI: 10.1016/j.matpr.2023.11.033.

[15] W. Dijkman, "Laser transmission welding of thin peek films," M.S. thesis, Delft University of Technology, 2024.

[16] "Astm d638-22 standard test method for tensile properties of plastics," ASTM International. (2022), [Online]. Available: https://www.astm.org/d0638-22.html.

[17] "Sa (arithmetical mean height) - area roughness parameters," Machining Doctor. (2024), [Online]. Available: https://www.keyence.com/ss/products/microscope/roughness/surface/parameters.jsp.

[18] "Surface finish chart by machining technology," Machining Doctor. (2024), [Online]. Available: https://www.machiningdoctor.com/calculators/surface-finish-calculator/#surface-finish-chart-by-machining-technology.

[19] "RS Pro PEEK Thermal Insulating Film, 200mm x 305mm x 0.125mm," RS Components. (2024), [Online]. Available: https://nl.rs-online.com/web/p/plastic-film/7648725.

[20] Y. Zhang, M. Tichem, and F. van Keulen, "A novel design of multi-stable metastructures for energy dissipation," *Materials and Design*, vol. 212, Dec. 2021, ISSN: 18734197. DOI: 10.1016/j.matdes.2021.110234.

[21] D. D. Magura, M. A. Sozen, and C. P. Siess, "A study of stress relaxation in prestressing reinforcement," *Civil Engineering Studies SRS-237*, 1962.

[22] G. Papanicolaou and S. Zaoutsos, "1 - viscoelastic constitutive modeling of creep and stress relaxation in polymers and polymer matrix composites," in *Creep and Fatigue in Polymer Matrix Composites (Second Edition)*, ser. Woodhead Publishing Series in Composites Science and Engineering, R. M. Guedes, Ed., Second Edition, Woodhead Publishing, 2019, pp. 3–59, ISBN: 978-0-08-102601-4. DOI: https://doi.org/10.1016/B978-0-08-102601-4.00001-1. [Online]. Available: https://www.sciencedirect.com/science/article/pii/B9780081026014000011.

[23] J. André and J. Cruz Pinto, "Modeling nonlinear stress relaxation of polymers," *Polymer Engineering & Science*, vol. 54, no. 2, pp. 404–416, 2014. DOI: https://doi.org/10.1002/pen.23581. eprint: https://4spepublications.onlinelibrary.wiley.com/doi/pdf/10.1002/pen.23581. [Online]. Available: https://4spepublications.onlinelibrary.wiley.com/doi/abs/10.1002/pen.23581.

[24] S. Abramowitch and D. Easley, "Introduction to classical mechanics," in Elsevier Inc., Mar. 2016, pp. 89–107, ISBN: 9780128032299. DOI: 10.1016/B978-0-12-803228-2.00004-0.

[25] "Press brake," Nanjing Harsle Machine Tool Co. (2024), [Online]. Available: https://www.harsle.com/press-brake.html.